TECHNICAL REPORT H-71-6

# HOWELL-BUNGER VALVE VIBRATION SUMMERSVILLE DAM PROTOTYPE TESTS

by

F. M. Neilson

September 1971

Sponsored by U. S. Army Engineer District, Huntington

Conducted by U. S. Army Engineer Waterways Experiment Station, Vicksburg, Mississippi

TECHNICAL REPORT H-71-6

# HOWELL-BUNGER VALVE VIBRATION SUMMERSVILLE DAM PROTOTYPE TESTS

by

F. M. Neilson

September 1971

Sponsored by U. S. Army Engineer District, Huntington

Conducted by U. S. Army Engineer Waterways Experiment Station, Vicksburg, Mississippi

ARMY-MRC VICKSBURG, MISS

# FOREWORD

The tests reported herein were authorized initially on 28 March 1967 and performed under the sponsorship of the U. S. Army Engineer District, Huntington. The tests were accomplished by the Prototype Section, Hydraulic Analysis Branch, of the Hydraulics Division, U. S. Army Engineer Waterways Experiment Station, during March 1968 by Messrs. E. B. Pickett, E. D. Hart, L. M. Duke, H. C. Greer, and J. W. Beasley. Messrs. J. Herman and J. A. Wheeler of the Huntington District and personnel on the Summersville Project assisted with the tests. Initial data reduction and analysis were made under the supervision of Mr. Pickett with the assistance of Messrs. E. D. Hart and D. F. Bastian. Messrs. Herman and Wheeler participated in this initial analysis. Dr. F. M. Neilson supervised the final data reduction, analysis, and report under the general supervision of Mr. Pickett, Chief of the Hydraulic Analysis Branch, and Mr. E. P. Fortson, Jr., Chief of the Hydraulics Division.

Directors of the Waterways Experiment Station during the conduct of the tests and the preparation and publication of this report were COL John R. Oswalt, Jr., CE, COL Levi A. Brown, CE, and COL Ernest D. Peixotto, CE. Technical Directors were Messrs. J. B. Tiffany and F. R. Brown.

CONTENTS

## NOTATION

| Symbol | Definition | Dimensions (F-L-T) |
|---|---|---|
| $A_o$ | Conduit cross-sectional area (95.03 $ft^2$) at location US | $L^2$ |
| $A_v$ | Howell-Bunger valve cross-sectional area (62.16 $ft^2$) including vanes and hub | $L^2$ |
| c | Distance from neutral axis | L |
| $C_D$ | Howell-Bunger valve discharge coefficient | -- |
| $C_Q$ | Butterfly valve flow coefficient | -- |
| D | (1) Howell-Bunger valve inside diameter (106.75 in.)<br>(2) Flexural rigidity of a vibrating elastic plate | L<br>FL |
| $D_o$ | Conduit diameter (11.0 ft) at location US | L |
| E | Young's modulus of elasticity ($30 \times 10^6$ psi in all computations) | $FL^{-2}$ |
| $\mathbb{E}$ | Euler number | -- |
| $\mathbb{E}_1$ | Euler number (equation 10) | -- |
| f | Frequency in Hz | $T^{-1}$ |
| $f_1$ | Fundamental natural frequency of transverse vibration of the Howell-Bunger valve vane | $T^{-1}$ |
| $f_2$ | Fundamental natural frequency of transverse vibration of the Howell-Bunger valve structure | $T^{-1}$ |
| $f_3$ | Fundamental natural frequency of torsional vibration of the Howell-Bunger valve cone | $T^{-1}$ |
| g | Gravitational acceleration (32.2 $ft/sec^2$ in all computations) | $LT^{-2}$ |
| G | Bulk modulus of elasticity in shear ($12 \times 10^6$ psi in all computations) | $FL^{-2}$ |
| H | Total head in the flow | L |
| $H_L$ | Difference in total head | L |
| $H_o$ | Total head at location US | L |

| Symbol | Definition | Dimensions (F-L-T) |
|---|---|---|
| $H_v$ | Total head at the Howell-Bunger valve entrance | L |
| I | Moment of inertia of an area | $L^4$ |
| $I_p$ | Polar moment of inertia of a mass | $L^4$ |
| k | Transfer coefficient | -- |
| K | Added mass coefficient | -- |
| $K_c$ | Loss coefficient (11-ft conduit) | -- |
| $K_e$ | Loss coefficient (entrance) | -- |
| $K_f$ | Loss coefficient (main tunnel) | -- |
| $K_t$ | Loss coefficient (trifurcation) | -- |
| $K_t$ | Torsional stiffness | FL |
| $K_L$ | Loss coefficient for the upstream flow passage | -- |
| L | Length dimension | L |
| L' | Distance (8.7 ft) from valve mounting flange to the apex of the cone | L |
| $L_v$ | Width (50.375 in.) of the Howell-Bunger valve vane | L |
| M | Bending moment | FL |
| P | Pressure | $FL^{-2}$ |
| P' | Fluctuation (rms value) of static pressure | $FL^{-2}$ |
| $P_{max} - P_{min}$ | Extreme pressure fluctuation (peak-to-peak) | $FL^{-2}$ |
| $P_o$ | Wall pressure at location US | $FL^{-2}$ |
| $P_v$ | Vapor pressure | $FL^{-2}$ |
| Q | Discharge from the Howell-Bunger valve | $L^3T^{-1}$ |
| $Q_T$ | Total flow rate in the upstream conduit | $L^3T^{-1}$ |
| S | Valve gate travel | L |
| $S_t$ | Strouhal number | -- |
| t | Thickness of a vane or plate | L |
| $t_o$ | Reference thickness | L |
| u',v',w' | Orthogonal components (rms values) of the velocity fluctuations in turbulent flow | $LT^{-1}$ |
| V | Velocity of flow | $LT^{-1}$ |
| $V_o$ | Mainstream velocity at location US | $LT^{-1}$ |
| $V_{VN}$ | Velocity of flow within the Howell-Bunger valve shell | $LT^{-1}$ |

| Symbol | Definition | Dimensions (F-L-T) |
|---|---|---|
| $w$ | Weight per unit length | $FL^{-1}$ |
| $W$ | Weight | $F$ |
| $Z$ | Elevation | $L$ |
| $Z_R$ | Water-surface elevation in the reservoir | $L$ |
| $\gamma$ | Specific weight of water | $FL^{-3}$ |
| $\Delta L$ | Change in length with regard to strain | $L$ |
| $\Delta P$ | Pressure differential | $FL^{-2}$ |
| $\Delta\sigma_f$ | Flexural stress fluctuation | $FL^{-2}$ |
| $\lambda_b, \lambda_p, \lambda_t$ | Coefficients in expressions for valve natural frequencies | -- |
| $\mu$ | Mass undergoing vibratory motion per unit area of plate | $FL^{-5}T^2$ |
| $\nu$ | (1) Kinematic viscosity of water<br>(2) Poisson's ratio | $L^2T^{-1}$<br>-- |
| $\pi$ | 3.1415. . . | -- |
| $\rho$ | Mass density of water | $FL^{-4}T^2$ |
| $\rho_s$ | Mass density of plate material | $FL^{-4}T^2$ |
| $\sigma$ | Stress | $FL^{-2}$ |
| $\sigma_c$ | Cavitation index | -- |
| $\sigma_{fmax} - \sigma_{fmin}$ | Extreme flexural stress fluctuation (peak-to-peak) | $FL^{-2}$ |
| $\bar{\sigma}_f$ | Time-averaged flexural stress | $FL^{-2}$ |
| $\bar{\sigma}_{f_o}$ | Reference value of $\bar{\sigma}_f$ | $FL^{-2}$ |

## CONVERSION FACTORS, BRITISH TO METRIC UNITS OF MEASUREMENT

British units of measurement used in this report can be converted to metric units as follows:

| Multiply | By | To Obtain |
|---|---|---|
| inches | 2.54 | centimeters |
| feet | 0.3048 | meters |
| miles (U. S. statute) | 1.609344 | kilometers |
| square feet | 0.092903 | square meters |
| acre-feet | 1233.482 | cubic meters |
| inches per second | 2.54 | centimeters per second |
| feet per second | 0.3048 | meters per second |
| cubic feet per second | 0.02831685 | cubic meters per second |
| feet per second per second | 0.3048 | meters per second per second |
| pounds | 0.45359237 | kilograms |
| pounds per square inch | 0.070307 | kilograms per square centimeter |
| pounds per cubic foot | 16.0185 | kilograms per cubic meter |
| microinches per inch | 0.001 | microns per millimeter |
| Fahrenheit degrees | 5/9* | Celsius or Kelvin degrees |

---

* To obtain Celsius (C) temperature readings from Fahrenheit (F) readings, use the following formula: $C = (5/9)(F - 32)$. To obtain Kelvin (K) readings, use $K = (5/9)(F - 32) + 273.15$.

## SUMMARY

This report presents data obtained during prototype tests concerned with the vibration of a 106-3/4-in.-diam Howell-Bunger valve at Summersville Dam, Gauley River, W. Va. Prototype measurements include both dynamic and time-averaged values of pressures in the flow and strain at locations on the valve structure. Transverse, vertical, and peripheral accelerations were measured at the downstream end of the valve cone. The data were recorded simultaneously on analog magnetic tape and on oscillograph charts. Data reduction was by scaling the oscillograph traces and by using electronic analog equipment to perform linear spectral density, amplitude density, and cross-correlation analyses on the magnetic tape data. The results include information on (a) discharge characteristics of the Summersville outlet works, (b) evaluation of the nature of the pressure fluctuations in the flow, and (c) evaluation of the nature of the vibration (including approximate natural frequency values) of the valve at the strain gage and accelerometer locations. The primary conclusion regarding the vibration is that the significant strain fluctuations are caused by low-frequency pressure fluctuations buffeting the valve. These frequencies are well below the natural frequencies of the structure.

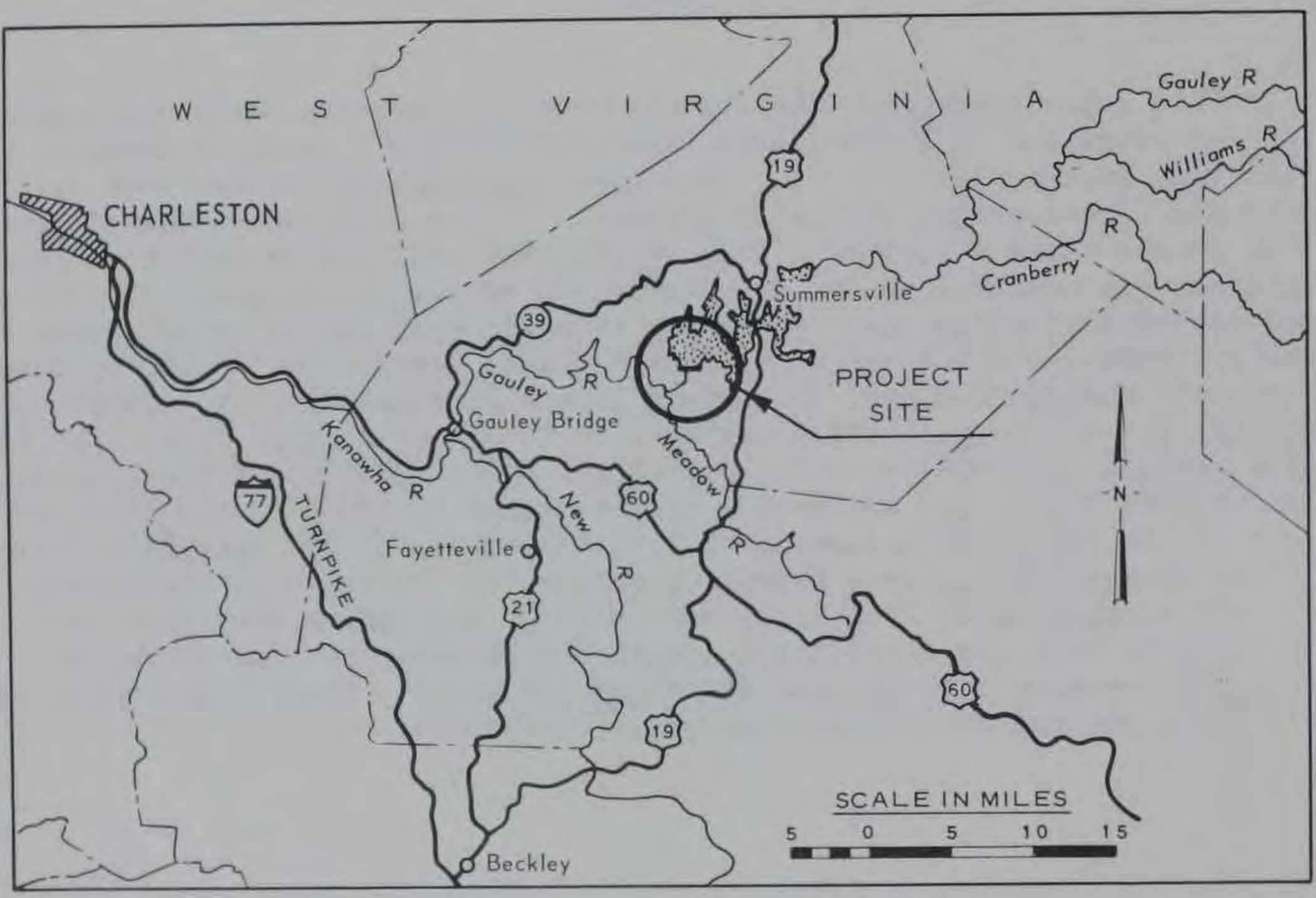


Fig. 1. Vicinity map

# HOWELL-BUNGER VALVE VIBRATION
# SUMMERSVILLE DAM PROTOTYPE TESTS

## PART I: INTRODUCTION

### Pertinent Features of the Project

1. Summersville Dam is located in Nicholas County, W. Va., 34.5 miles* above the mouth of the Gauley River and about 5 miles southwest from the town of Summersville as shown in fig. 1. The dam is a rock-fill structure, 2280 ft long and 390 ft high. Total storage capacity of the reservoir is 413,525 acre-ft, of which 390,611 acre-ft is reserved for flood-control storage above minimum pool (el 1520.0**). Water is normally released through the flood-control conduits. A 1250-ft uncontrolled spillway with a crest elevation of 1710.0 is provided for emergency releases.

2. The flood-control outlet works as shown in plate 1 consist of a 29-ft-diam tunnel about 1700 ft long discharging through a manifold system of three 11-ft-diam conduits averaging about 210 ft long. Two hydraulically operated, bulkhead-type closure gates are provided in the intake. The water passes initially through the two rectangular gate passages that converge into the 29-ft circular tunnel 65 ft downstream from the gates. Outflow is controlled by a 9-ft, six-vane Howell-Bunger valve at the downstream end of each 11-ft conduit. A 3-ft-diam bypass pipe with a 2-1/2-ft Howell-Bunger valve branches from the upstream 11-ft conduit to discharge low flows. A butterfly valve is located about two diameters upstream from each Howell-Bunger valve. Spray dispersion from the Howell-Bunger valves is controlled by steel-lined hoods approximately twice the diameter of the valves. The general nature of the flow from the test conduit discharging with the subject Howell-Bunger valve in the 80 percent open position is illustrated in figs. 2a and b. The backsplash deflector shown in fig. 2b prevents reverse flow (i.e. flow in the upstream direction along the

---

* A table of factors for converting British units of measurements to metric units is presented on page xiii.

** All elevations (el) cited herein are in feet referred to mean sea level.

a. From downstream

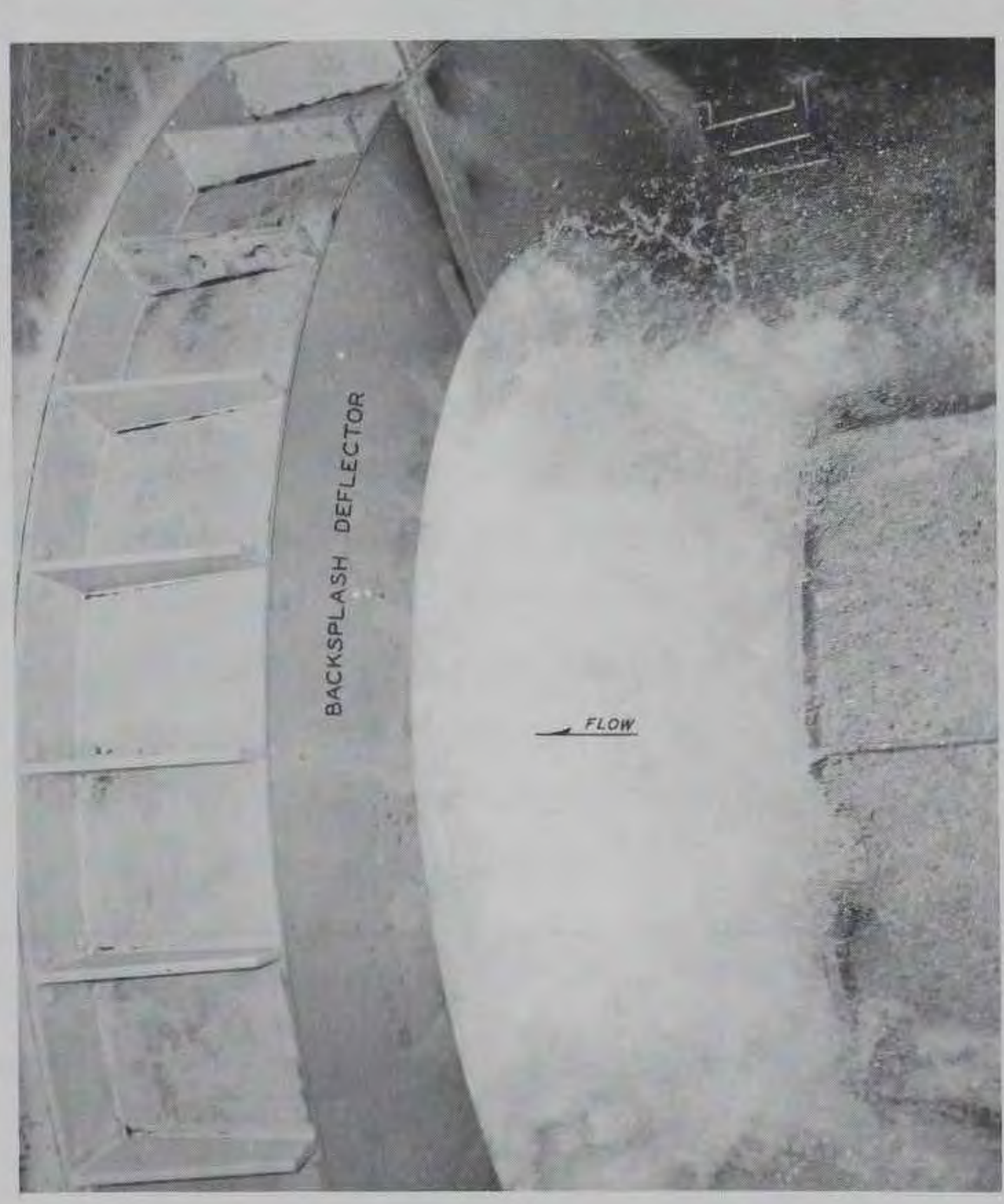


b. In the valve chamber

Fig. 2. Efflux from the test conduit

periphery of the hood) from entering the valve chamber. The configuration of the deflector was selected by model testing at the U. S. Army Engineer Waterways Experiment Station.*

## Howell-Bunger Type Valves

3. A Howell-Bunger, or fixed-cone dispersion type, valve is commonly used to regulate flows from high-head hydraulic structures. This type of valve has proven to be a satisfactory regulatory device at many prototype installations. However, at some installations these valves have undergone a fatigue-type failure and concern has arisen pertaining to the reasons for the failures.

4. Two of three large Howell-Bunger valves originally installed in the outlet works at Summersville Dam, W. Va., suffered fatigue-type failures. These valves were replaced with new Howell-Bunger valves of the same general design but containing stronger (thicker) structural components. This report is concerned with prototype measurements taken during operation of one of the new valves.

## Purpose of Investigation

5. The purpose of the investigation and the main objectives of the tests were, first, to determine whether or not the new Howell-Bunger valve would undergo a fatigue-type failure during prolonged operation, and second, to obtain some basic data pertaining to the dynamic response of a prototype Howell-Bunger valve. Of secondary consideration was the evaluation of hydraulic characteristics of the outlet conduit.

---

* B. P. Fletcher, Memorandum for Record (unpublished), U. S. Army Engineer Waterways Experiment Station, CE, Vicksburg, Miss., 15 January 1969.

## PART II: PROTOTYPE VALVE AND INSTRUMENTATION

### Background Information, Howell-Bunger Valve

#### Description

6. The basic arrangement of a Howell-Bunger valve is shown in fig. 3. The valve is made up of a movable cylindrical gate a, and a stationary valve body. The valve body is made up of a large cylindrical shell b, a small cylindrical hub c, a system of radial vanes d, a conical head e, and a ring-type seal f; the items b-f are rigidly connected (welded). Also shown are a ring seal g attached to the lip of the gate, a ring seal h between the gate and valve shell, and an operating drive mechanism i. The commonly used screw-type operating mechanism is indicated in fig. 3 although in some installations, usually involving smaller valves, a lever device is used to move the gate. During a closing operation the gate is moved forward (downstream) over the valve shell until, in the fully closed position, the gate seal g impinges against the stationary seal f. Conversely, during an opening operation the gate is withdrawn from the cone and a series of discharge ports are formed around the periphery of the

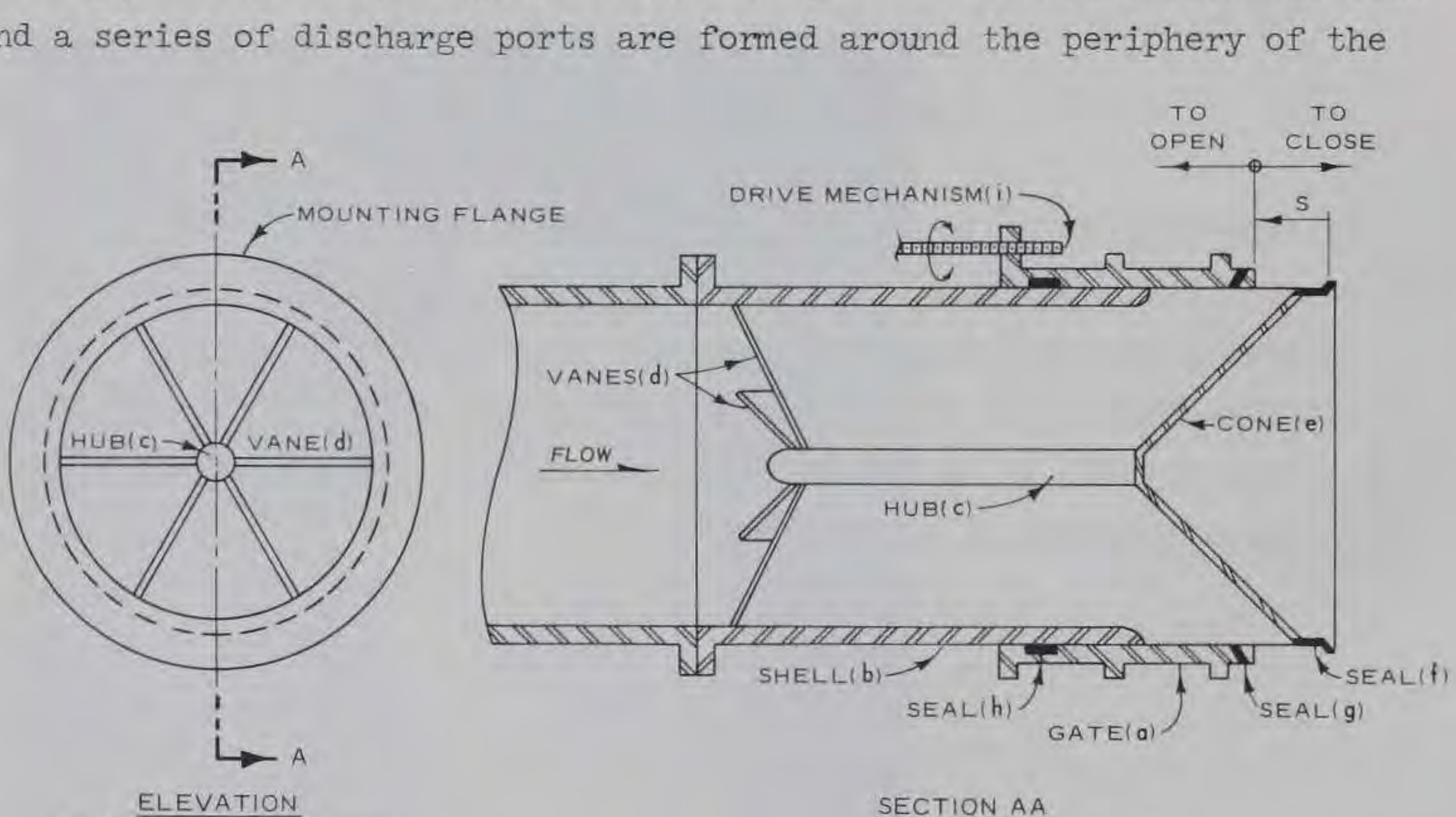


Fig. 3. Six-vane Howell-Bunger valve

valve body. Each discharge port is bounded on the downstream by the seal f, on the upstream by the gate seal g, and on each side by a radial vane. The flow rate is regulated by positioning the gate at intermediate locations, that is, by adjusting the size of the discharge ports. The measurement S shown in fig. 3 is termed the sleeve travel and is a measure of the gate opening. The valve is fully open when the gate has been withdrawn to the extent that flow is controlled by the downstream lip of the cylindrical shell.

7. The main advantages of the Howell-Bunger valve for high-pressure outlets are: first, only a relatively small force is required to move the gate, and second, excellent flow regulation over a wide range of discharges can be easily attained. Howell-Bunger type installations are generally designed in such a way that effective energy dissipation can be obtained with nominal or even no stilling basin appurtenances. The character of the hollow jet is conducive to air entrainment, which in some installations is a design criterion. Extensive information concerning operational characteristics of this type of valve are given by Elder and Dougherty[1] and in the subsequent discussions of that paper. Additional information is available in hydraulic engineering handbooks.[2] As stated by Kohler and Ball,[3] Howell-Bunger valves range in size from 8 to 108 in. in diameter and have been installed for heads up to about 900 ft.

Dynamic response

8. The Howell-Bunger valve is a complex structure and an elastic analysis of its vibration characteristics, as either a closed-form solution or numerical solution, is not available to date. Some aspects of the vibration of Howell-Bunger valves are discussed by Campbell.[4] The general theory of vibration is available in many texts, such as Thomson,[5] Timoshenko,[6] Robson,[7] and in handbooks such as Flügge.[8] Currently, there is a lack of available information concerning the three basic ways by which a flow condition can induce the valve structure to vibrate to failure. First, permissible values of magnitudes of low-frequency pressure fluctuations in the flow entering the valve have not been established; that is, over the range of frequencies in which the magnification factor is near unity (when the frequencies of the pressure pulses are well below all

structural resonance frequencies), the valve will be damaged only if the magnitude of the pressure pulses is extremely large. However, the tolerable magnitude of these pulses, which could be determined by means of an analysis of the stresses caused by various static nonsymmetrical pressure-type loadings, is not known. Second, the natural frequencies and modes of vibration of the valve structure are not known. Since a low-damped structure is susceptible to resonant excitation[5] whenever loadings are applied at a structural natural frequency, the evaluation of the free vibration characteristics of the valve is an important design consideration. And third, interactions between the flow parameters and the response of the valve elastic system have not been investigated. General features of the hydroelastic aspect of flow-induced vibration problems are described by Toebes[9] and Heller.[10] In particular, for certain flow characteristics a submerged elastic system (such as the Howell-Bunger valve) may be susceptible to self-excited vibration even when there are no pressure pulses created in the flow upstream from the system.

## Prototype Valve

9. Pertinent details of the valve are shown in plate 2. The terminology used herein when referring to a particular vane in the valve is also defined in plate 2. For example, vane 3 is located in the 3 o'clock position when viewing the valve from upstream; outlet port 3-5 refers to the flow passage area between vanes 3 and 5. Four particular items that are detailed in plate 2 are illustrated in figs. 4, 5, and 6. The valve inside diameter, 106-3/4 in., is less than the 108-in. diameter of the conduit and original valves. The short beveled reducer that accommodates this change is shown in fig. 4. Part of the leading edge of vane 3 is also apparent in fig. 4. The six 2-1/3-in.-thick vanes and the 6-in.-diam hub are all streamlined. Flow separation surfaces in outlet port 5-7 along the downstream edge of the shell and gate are illustrated in fig. 5. The new Howell-Bunger valve is mounted in a position for which there are no vertical vanes, i.e. there are no vanes numbered 6 and 12. This particular mounting position was selected since it avoids having any vane located in

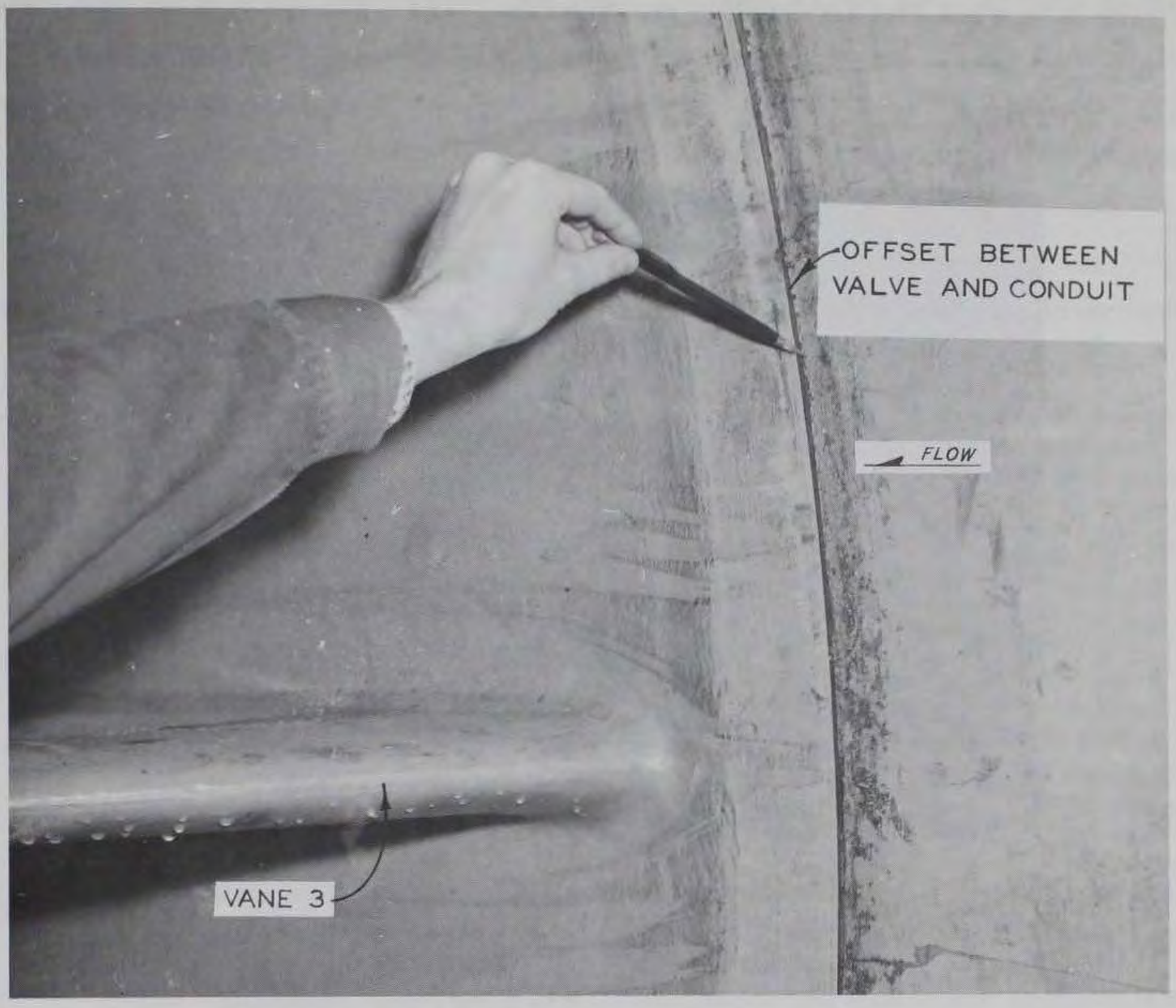


Fig. 4. Bevel at valve inlet

Fig. 5. Flow separation points at valve outlet

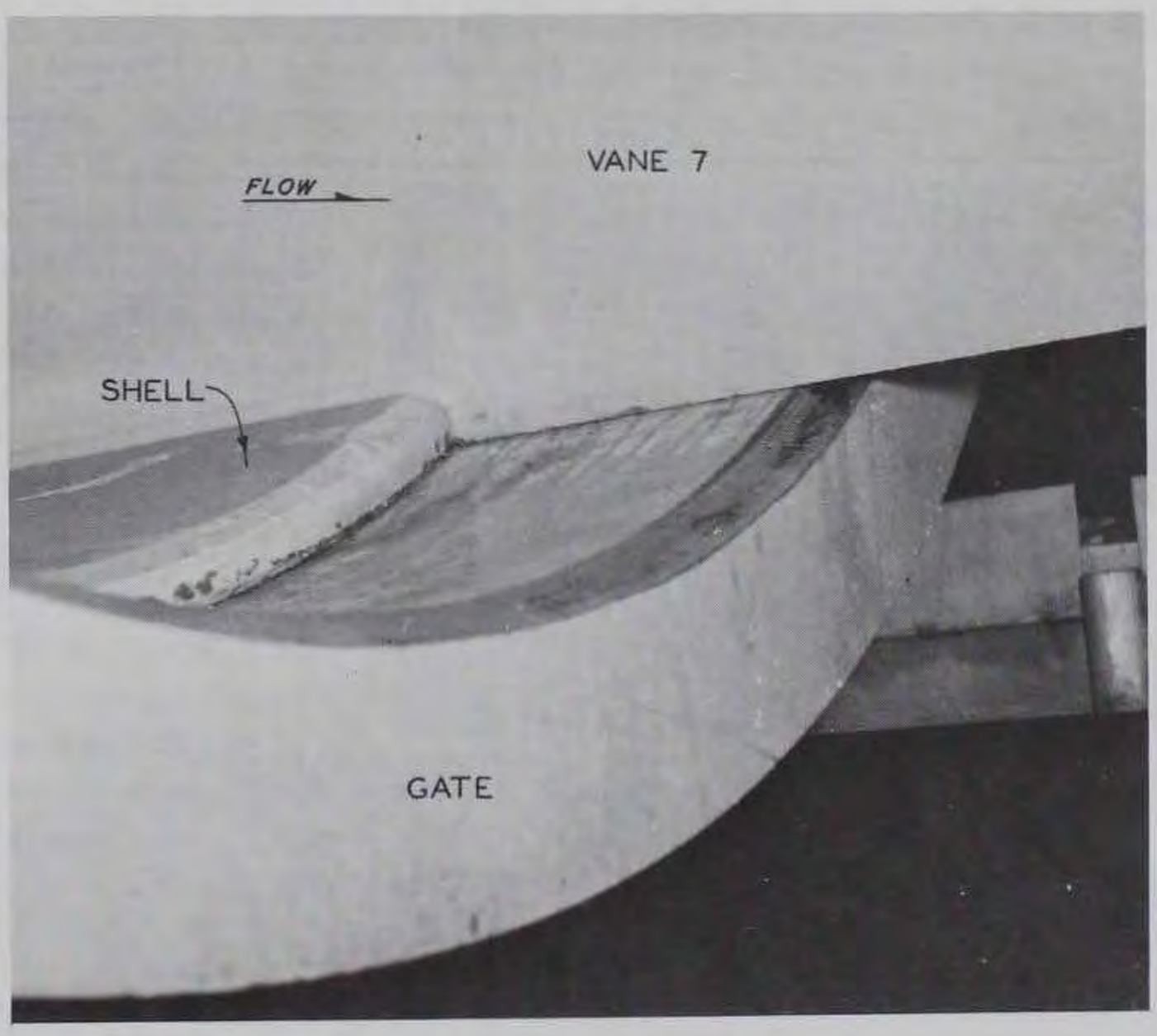

the same plane as the butterfly valve axis. The orientation of the butterfly valve relative to the original Howell-Bunger valve, which contained vanes 2, 4, 6, 8, 10, and 12, is shown in fig. 6. The valve dimensions and

Fig. 6. Looking downstream at the fully open butterfly valve. Note the original 108-in.-diam Howell-Bunger valve in the background

weights most often referred to in this report are listed below for the new valve and for the original valve.

| Item | Dimensions | |
|---|---|---|
| | New Valve | Old Valve |
| Number of vanes | 6 | 6 |
| Vane thickness, in. | 2.33 | 1 |
| Hub diameter, in. | 6.00 | 3 |
| Valve inside diameter, in. | 106.75 | 108.00 |
| Shell thickness, in. | 2.00 | 1.375 |
| Overall length of valve, ft | 13.208 | 13.208 |
| Estimated weight of valve, lb | 69,500 | 35,000 |
| Estimated weight of gate, lb | 20,000 | 20,000 |
| Estimated weight of drive mechanism, lb | 2,000 | 2,000 |

## Instrumentation

10. The instrumentation system was operable on 27 March and a

preliminary series of tests was performed. During the preliminary tests some transducers became inoperable and were either replaced or eliminated from the regular test program performed on 29 March. Three upstream pressure sensing locations (US, PUB, PUT) are shown in plate 1; the majority of the transducers are located on the Howell-Bunger valve and are shown in plate 3. The valve gate opening was the controlled variable during the tests and instrumentation was provided to obtain the following data (subparagraphs a-f) as a function of gate opening.

a. Mean pressures. The average total pressure in the valve was measured with a 150-psia transducer on a small diameter tap at PDT with a 160-psia Bourdon gage connected to the piezometer hole at VG. Conduit pressures upstream of the butterfly valve were measured utilizing piezometer US in conjunction with the Bourdon gage.

b. Mean and fluctuating pressures in the reducer. Two 1000-psi pressure transducers were flush-mounted at the top (PUT) and bottom (PUB) of the reducer (downstream from the butterfly valve) as shown in plate 1. The main purposes of these transducers were to investigate possible cavitation in the reducer and to locate sources of excessive pressure fluctuations in the flow upstream from the Howell-Bunger valve.

c. Fluctuating pressures in the Howell-Bunger valve. Pressure fluctuations on the sides of two vanes (P7L, P7R and P5L, P5R) and on the inner side of the shell (PS4, PS6, PS8) were measured with 25-psid, flush-mounted pressure transducers. These locations are shown in plate 3; the PS4 transducer and adaptor are illustrated in fig. 7. The pressures at these locations range from about 110 psi when the Howell-Bunger valve is closed to about 25 psi at large valve openings. To prevent overranging the transducers, a system designed to maintain a backup pressure against each transducer diaphragm was installed. This system, which uses a manually regulated compressed nitrogen supply, is shown schematically in plate 3. At each tested flow condition the backup pressure was adjusted using commercial regulators, and measured by means

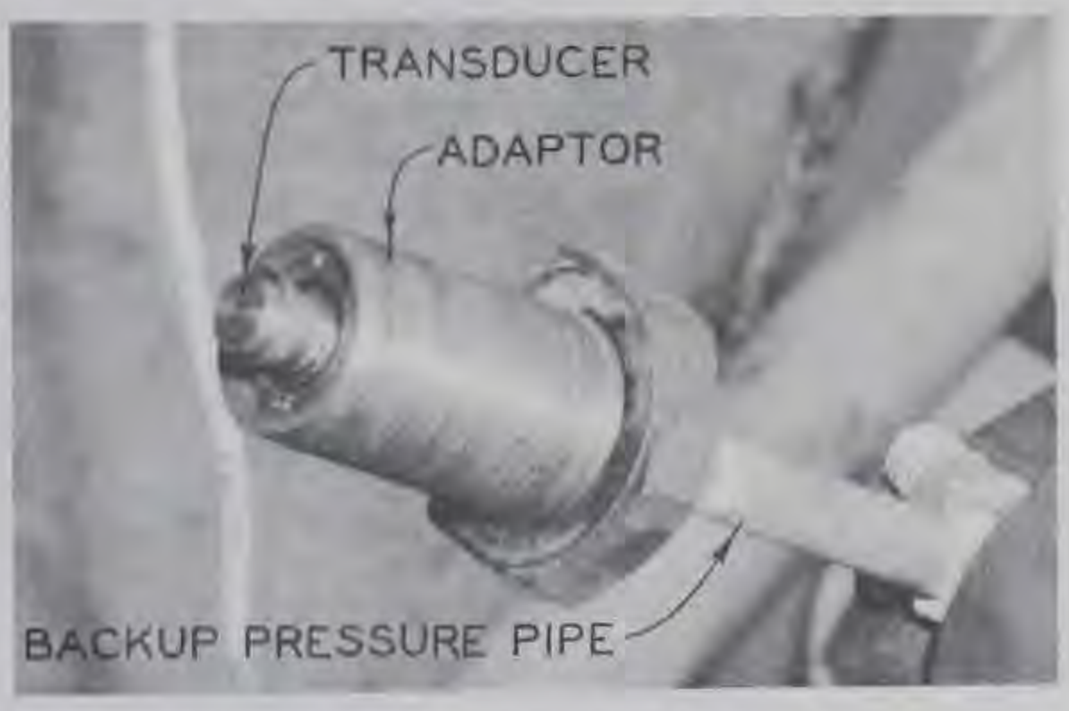


Fig. 7. Pressure transducer PS4 (flange not shown)

of a 160-psig Bourdon gage. Note that the pressure at a transducer location is the sum of the transducer measurement and the backup pressure. The 25-psid transducers were overranged on 27 March. P5L, P5R, PS4, and PS6 were replaced with new 25-psid transducers and P7L and P7R were replaced with 150-psia transducers for tests on 29 March. In addition, on 29 March no measurements were made at PS8 which had also been overranged during check-out. For convenience, the pressure transducers used are summarized below:

| Transducer | Range and Type | |
|---|---|---|
| | 27 Mar 1968 | 29 Mar 1968 |
| P7L | 25 psid | 150 psia |
| P7R | 25 psid | 150 psia |
| P5L | 25 psid | 25 psid |
| P5R | 25 psid | 25 psid |
| PS4 | 25 psid | 25 psid |
| PS6 | 25 psid | 25 psid |
| PS8 | 25 psid | None |
| PUT | 1000 psig* | 1000 psig* |
| PUB | 1000 psia | 1000 psia |
| PDT | 150 psia | 150 psia |

* Mounted in sealed adaptor to function similarly to 1000 psia.

d. Strain measurements. Strain gages were installed at 16 points on the Howell-Bunger valve by a WES technician at the valve fabricator's plant. The gages were placed in the key flexural stress regions associated with vanes 5 and 7 as determined by a study of the original valve failure. The gages were connected electrically in a manner that used two gages to measure flexural strain at one location; that is, the desired measurements are strains due to bending; the strains due to axial loading are not measured. The resulting eight measuring locations are shown in plate 3. Note that (a) there is a strain gage on each side of the metal plate at each measuring location, and (b) all strain gages are aligned normal to the Howell-Bunger valve axis. A more detailed explanation of the strain measurement and a description of the sign convention used in recording and reducing the data are presented in test results. For test purposes each strain measurement was related to direction of bending by mechanically applying forces to the appropriate vane or shell segment. Strain gage locations, and the adjacent pressure transducer locations, are illustrated in fig. 8.

e. Accelerations. Vertical (AV) and transverse (AT) movements

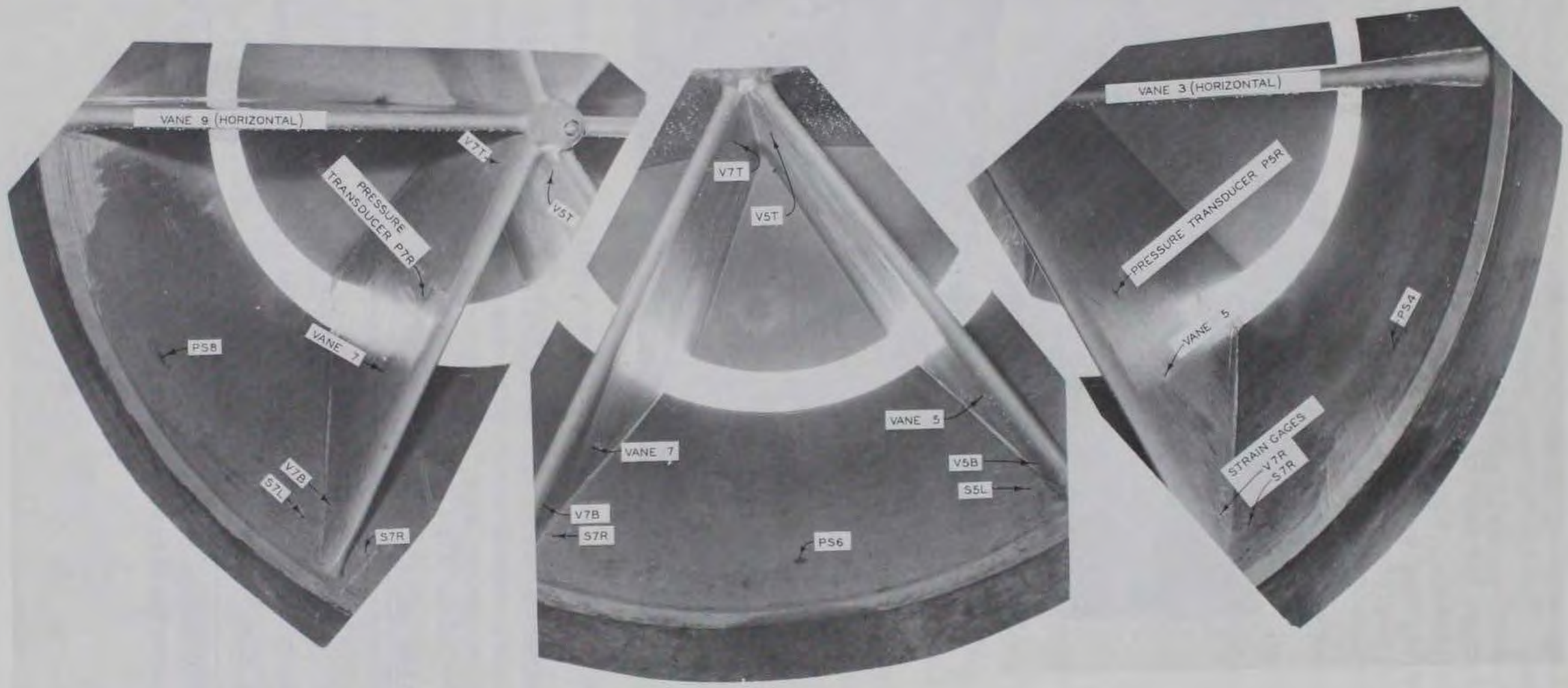


Fig. 8. Valve instrumentation (looking downstream). The strain gages are covered by epoxy and paint and are not visible

of the valve cone were detected by means of 5g* accelerometers mounted on the valve axis at the downstream end of the hub. The electrical leads from the accelerometers were installed at the valve fabricator's plant in a hole bored through the hub to its upstream end and then along slots in the leading edges of two vanes. Torsional vibration measurements were made by shifting transverse accelerometer (AT) to the periphery of the cone (AP) in a horizontal line with AV.


Fig. 9. Accelerometer locations (looking upstream)

Hence the torsional acceleration measurement was never performed concurrently with the transverse measurement. Accelerometer locations are detailed in plate 3 and illustrated in fig. 9.

f. Other data. The upper and lower pool elevations and air and water temperatures were observed during the tests. The valve gate opening, which was the controlled variable, was observed by means of calibrated dials that were provided by the manufacturer. The dial readings were confirmed by in-place measurements during the 1967 tests.[11]

---

* g is the acceleration of gravity (32.2 ft/sec$^2$) and is used throughout this report as a reference acceleration.

## PART III: TEST PROCEDURE AND RESULTS

### Test Conditions and Operations

11. During tests of 27 March, the reservoir was at el 1638.8, the average air temperature was 70 F, and the water temperature was 39 F. During tests of 29 March, the reservoir was at el 1642.7, the average air temperature was 70 F, and the water temperature was 39 F. During both series of tests, the 2-1/2-ft Howell-Bunger valve was continuously discharging a flow of about 70 cfs, and the butterfly valve and the upstream control gates were in the fully open position. The two remaining 11-ft-diam conduits (see plate 1) passed no flow during the tests.

12. Both series of tests, 27 and 29 March, were performed in the same manner. First, starting from a fully closed position, the test valve gate was opened continuously to the 70 percent dial reading position and then closed continuously to the fully closed position. Time pulse signals were made manually (by means of an electrical push-button switch) at each 10 percent change in dial reading. Second, starting from the 30 percent dial reading position, the gate was moved at 10 percent increments to 70 percent open and then at 5 percent increments to 95 percent open. The valve was then closed in a continuous operation.

### Recording

13. Both series of tests, 27 and 29 March, were recorded in the same manner. Signals from the accelerometers, strain gages, and pressure transducers were amplified and recorded simultaneously on analog magnetic tape and on oscillograph strip charts. The magnetic-tape recorder was a commercial data type and had no low-frequency limitation; that is, signal frequencies down to and including direct current were recorded. Two light-beam oscillographs, with a high-frequency limitation of about 1500 Hz, produced the strip chart records. The oscillograms were chemically developed during the test period. During the incremental gate-opening tests, the data for each valve opening were recorded for 4 min on magnetic tape and for 20 sec on oscillograph strip charts. The oscillograph speed was

10 in./sec during all incremental gate opening tests and during the continuous valve closing on 27 March. The continuous closing on 29 March was recorded at a chart speed of 1/4 in./sec. All magnetic tape runs were recorded at 7-1/2 in./sec. The recordings were made as follows:

| Recorder A | | | Recorder B | | |
|---|---|---|---|---|---|
| Tape Recorder Channel No. | Transducer Symbol | Measurement | Tape Recorder Channel No. | Transducer Symbol | Measurement |
| TA1 | AT and AP | Acceleration | TB1 | S7L | Strain |
| TA2 | AV | Acceleration | TB2 | S7R | Strain |
| TA3 | V7T | Strain | TB3 | S5L | Strain |
| TA4 | V7B* | Strain | TB4 | S5R | Strain |
| TA5 | V5T | Strain | TB5 | PUT* | Pressure |
| TA6 | V5B* | Strain | TB6 | PUB | Pressure |
| TA7 | -- | Voice | TB7 | -- | Voice |
| TA8 | P7R | Pressure | TB8 | PDT** | Pressure |
| TA9 | P7R | Pressure | TB9 | PS8** | Pressure |
| TA10 | P5L | Pressure | TB10 | PS6* | Pressure |
| TA11 | P5R | Pressure | TB11 | PS4 | Pressure |
| TA12 | PS6* | Pressure | TB12 | V7B* | Strain |
| TA13 | PUT* | Pressure | TB13 | V5B* | Strain |
| TA14 | -- | Time code | TB14 | -- | Time code |

* Duplicate recordings.

** Not recorded 29 March.

14. Duplicate recordings of V7B, V5B, PS6, and PUT on the magnetic tapes were made to permit easier and more varied correlation analyses with analog equipment. Common time signals (60 Hz, 1 Hz, and 1/60 Hz) were recorded on all oscillograms and tapes to synchronize recordings. A 12.5-kc signal also was recorded on the tapes for use in processing operations.

## Results of Tests

15. Data from the 27 and 29 March tests were scanned for content. Because of transducer failures and varied magnetic tape recording levels, the 27 March data are incomplete and inconsistent and, except for pressure data, are not presented herein; data from the 29 March tests are more nearly complete and are presented in detail. The continuous opening and closing operations were used for reference purposes during data reduction

and were not analyzed. The oscillograph data were scaled, utilizing calibration steps recorded on the charts at the time of the tests, to yield temporal mean values of pressures and strains, and approximate values of the maximum peak-to-peak amplitudes of acceleration, and pressure and strain fluctuations. The oscillograph results are described in the following paragraphs; the controlled variable is the Howell-Bunger valve dial reading. The mean magnetic tape recordings were analyzed by means of commercial electronic analog devices. The results are described and presented in paragraphs 22-25.

Oscillograph data

16. Average pressures. Temporal mean values of the pressures at six locations (US, PUT, PUB, PDT, PSB, VG) during the 27 March series of tests and similar pressures at nine locations (US, PUT, PUB, PS4, PS6, P5L, P5R, P7L, P7R) during the 29 March series of tests are listed in table 1. The pressures scaled from oscillograph data (rather than gage readings) are the average of maximum and minimum peak pressures occurring at the listed dial reading and are scaled to an accuracy of about $\pm$0.5 psi. Gage pressures (US and VG) were also observed to an accuracy of about $\pm$0.5 psi.

17. Average strains. The measurement of flexural strain at one location requires two strain gages as shown in fig. 10a. Due to loadings on the plate, two gages of equal lengths AB and CE are deformed to lengths AB' and CD'. For axial loading, fig. 10b, the measured flexural strain, $\Delta L/L$, equals $(\overline{BB'} - \overline{DD'})/AB$ or zero. For bending, fig. 10c, the measured flexural strain equals (BB' + D'D)/AB, or (BB' - DD')/AB. In the more common situation, fig. 10d, bending and axial loading occur simultaneously. The measured flexural strain is (BB' - DD')/AB which, as shown in fig. 10d, eliminates the axial strain from the measurement.

18. The convention used to differentiate positive from negative flexure at each strain gage location is depicted in fig. 11. In the sketch the concave side of a deformed vane or shell segment is in compression and the convex side is in tension. Measured temporal mean values of flexural strain at eight locations (S7L, S7R, V7B, V7T, S5L, S5R, V5B, V5T) on 29 March are listed below according to the sign convention shown in fig. 11.

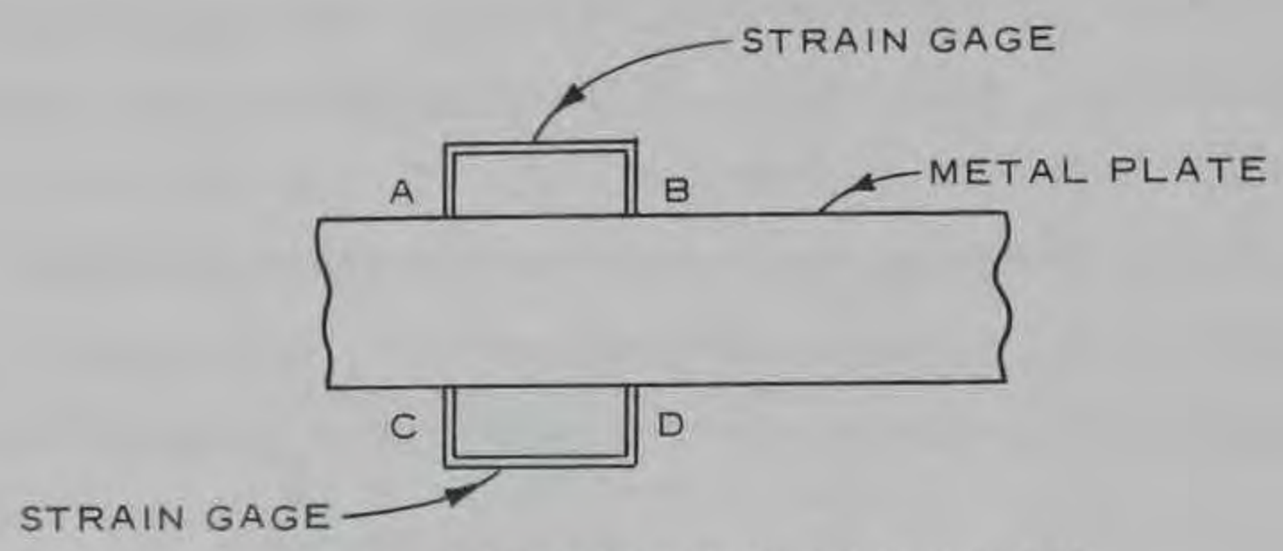


a. IDEALIZED REFERENCE SITUATION FOR ONE STRAIN GAGE PAIR.

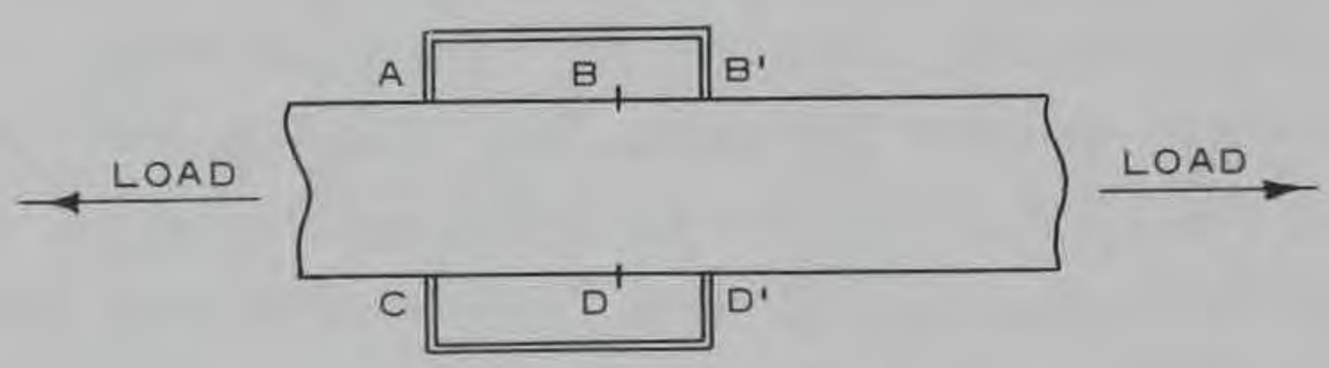


b. AXIAL LOADING.

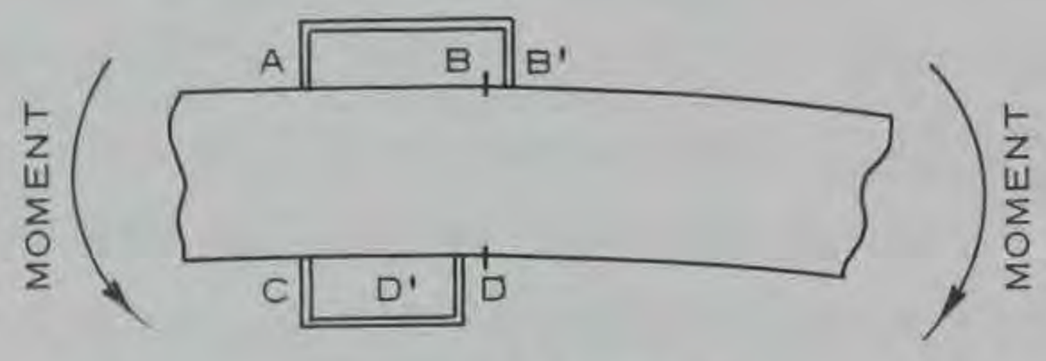


c. PURE BENDING.

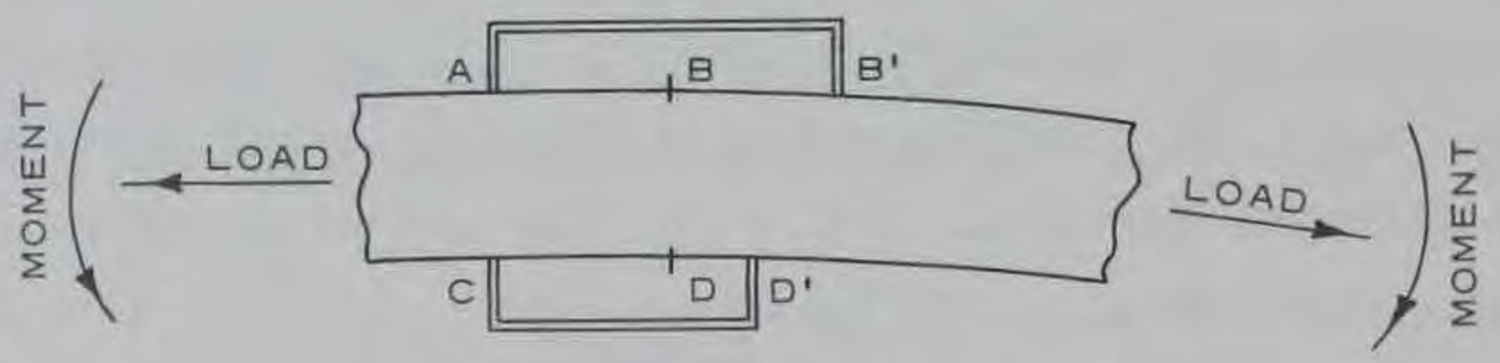


d. COMBINED BENDING AND AXIAL LOADING.

Fig. 10. Measurement of flexural strain

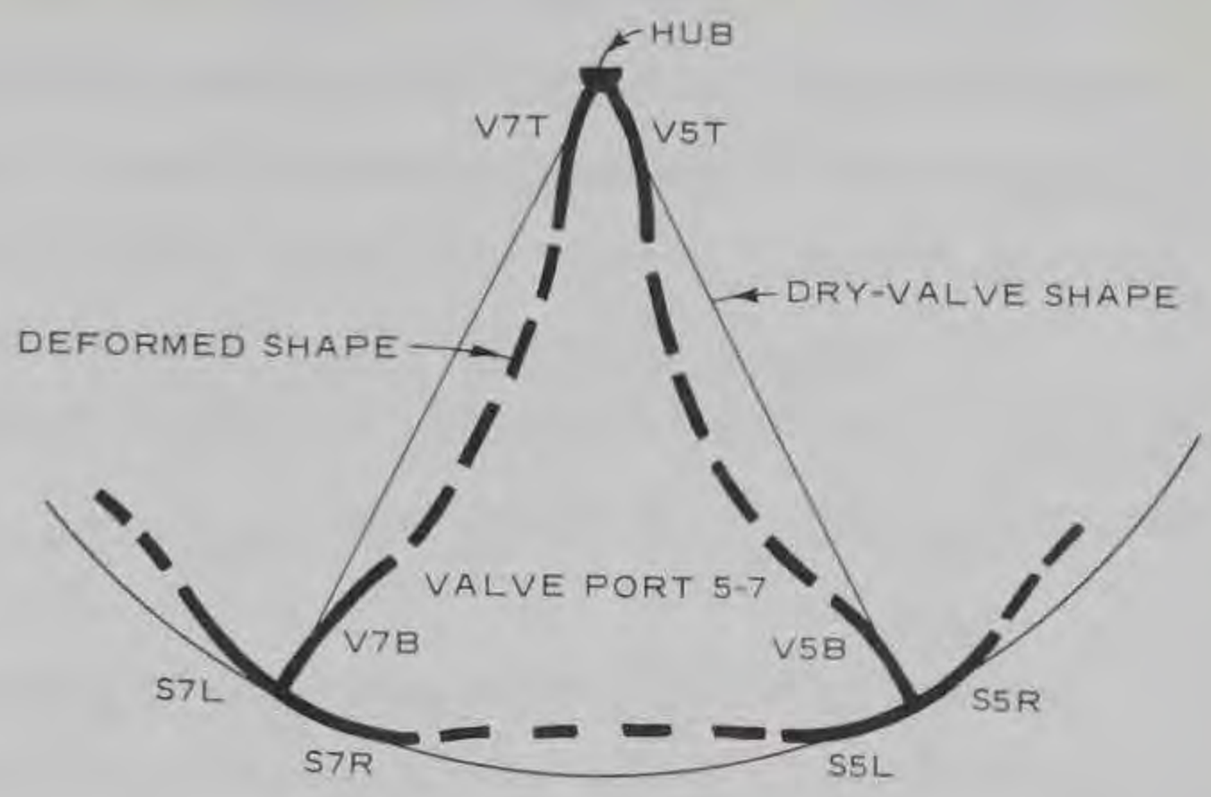


Fig. 11. Positive flexural strain; reversed bending at any of the illustrated data locations causes negative flexural strain

The tabulated values may be in error by as much as ±2 microin./in. due to scaling of the data.

| Dial Reading % | Strain, microin./in. | | | | | | | |
|---|---|---|---|---|---|---|---|---|
| | S7L | S7R | V7B | V7T | S5L | S5R | V5B | V5T |
| 0 | -80 | -60 | 6 | -2 | -75 | -75 | 8 | 8 |
| 30 | -60 | -46 | 10 | 4 | -72 | -64 | 13 | 16 |
| 40 | -48 | -38 | 5 | 2 | -57 | -53 | 13 | 10 |
| 50 | -43 | -25 | 16 | 10 | -45 | -49 | 6 | 15 |
| 60 | -27 | -33 | 3 | 5 | -43 | -33 | 13 | 13 |
| 70 | -33 | -12 | 18 | 10 | -44 | -24 | 9 | 17 |
| 75 | -29 | -10 | 11 | 0 | -51 | -12 | -17 | -7 |
| 80 | -22 | -7 | 20 | 11 | -32 | -30 | 19 | 25 |
| 85 | -23 | 0 | 15 | 2 | -33 | -12 | 1 | 11 |
| 90 | -26 | 5 | 36 | 30 | -15 | -25 | 4 | 29 |
| 95 | -31 | 16 | 31 | 21 | -16 | -20 | -6 | 28 |

19. Pressure fluctuations. The maximum peak-to-peak amplitudes of the pressure fluctuations at eight locations (PUT, PUB, PS4, PS6, P5L, P5R, P7L, P7R) on 29 March are as follow:

| Dial Reading % | Maximum Peak-to-Peak Pressure Fluctuation, psi | | | | | | | |
|---|---|---|---|---|---|---|---|---|
| | PUT | PUB | PS4 | PS6 | P5L | P5R | P7L | P7R |
| 30 | 2.5 | 2.8 | 0.7 | 0.6 | 1.0 | 1.2 | 0.0 | 0.0 |
| 40 | 3.5 | 3.3 | 0.9 | 1.3 | 1.0 | 1.0 | 0.0 | 0.0 |
| 50 | 4.0 | 3.3 | 1.2 | 1.4 | 1.8 | 1.5 | 1.4 | 1.5 |
| 60 | 5.5 | 5.7 | 2.0 | 1.7 | 2.0 | 1.9 | 2.3 | 2.9 |
| 70 | 6.5 | 7.1 | 2.7 | 2.0 | 2.3 | 2.6 | 3.2 | 2.4 |
| 75 | 10.6 | 8.0 | 2.7 | 2.2 | 2.3 | 2.3 | 3.6 | 3.9 |
| 80 | 10.6 | 9.4 | 3.1 | 3.1 | 2.9 | 4.2 | 5.0 | * |
| 85 | 11.0 | * | * | 3.0 | 4.9 | 4.5 | 4.5 | * |
| 90 | 10.1 | * | * | 3.0 | 5.1 | * | 5.0 | * |
| 95 | * | * | * | 3.4 | 5.9 | * | 5.0 | * |

* Data not recoverable.

The tabulated values were obtained by scaling the difference between the extreme maximum peak and the extreme minimum peak occurring in the oscillograph trace. The accuracy of scaling the oscillograph pressure data is about ±0.5 psi.

20. Strain fluctuations. The maximum peak-to-peak amplitudes of the flexural strain fluctuations at eight locations (S7L, S7R, V7B, V7T, S5L, S5R, V5B, V5T) on 29 March are:

| Dial Reading % | Maximum Peak-to-Peak Strain, microin./in. | | | | | | | |
|---|---|---|---|---|---|---|---|---|
| | S7L | S7R | V7B | V7T | S5L | S5R | V5B | V5T |
| 30 | 10 | 10 | 14 | 14 | 16 | 15 | 17 | 14 |
| 40 | 16 | 15 | 19 | 19 | 20 | 20 | 28 | 22 |
| 50 | 19 | 16 | 31 | 25 | 26 | 23 | 41 | 30 |
| 60 | 21 | 23 | 42 | 39 | 39 | 39 | 66 | 51 |
| 70 | 34 | 34 | 51 | 52 | 51 | 47 | 87 | 62 |
| 75 | 26 | 28 | 50 | 46 | 51 | 46 | 93 | 71 |
| 80 | 35 | 36 | 67 | 65 | 59 | 59 | 95 | 68 |
| 85 | 40 | 39 | 84 | 82 | 54 | 57 | 103 | 82 |
| 90 | 40 | 52 | 80 | 69 | 69 | 69 | 131 | 99 |
| 95 | 50 | 54 | 88 | 63 | 75 | 62 | 118 | 92 |

The tabulated values were obtained by scaling the difference between the extreme maximum peak and the extreme minimum peak occurring in the oscillograph trace. The accuracy of scaling is about ±2 microin./in. An example of oscillograph strain and pressure data is presented in plate 4.

21. Acceleration. Maximum peak-to-peak accelerations at locations AV, AT, and AP are listed below. The accuracy of scaling the data is about ±0.01 g.

| Dial Reading % | Acceleration, g's | | |
|---|---|---|---|
| | AV* | AT** | AP* |
| 30 | 0.10 | 0.13 | 0.33 |
| 40 | 0.12 | 0.17 | 0.58 |
| 50 | 0.12 | 0.28 | 0.58 |
| 60 | 0.20 | 0.33 | 0.65 |
| 70 | 0.30 | 0.39 | 0.79 |
| 75 | 0.29 | -- | 0.91 |
| 80 | 0.42 | 0.55 | 1.06 |
| 85 | 0.48 | 0.61 | 1.25 |
| 90 | 0.57 | 0.66 | 1.44 |
| 95 | 0.64 | 0.68 | 1.58 |

* 29 March data.
** 27 March data.

Magnetic tape data

22. Selected channels of the magnetic tape data of 29 March were inspected in analog form by means of the following data reduction devices.

a. Ortholog Model OR-WA/1 Wave Analyzer System (Gulton Industries).

b. Probability Density Analyzer, Model 161 (B and K Instruments).

c. Signal Correlator, Model 100 (Princeton Applied Research Corporation).

The reader is referred to manufacturers' literature for details of the electronic devices. Time compression techniques, in which the data tape is played back at a greater speed than that used during recording, were utilized to enable the wave analyzer to scan low real-time frequencies (as low as 0.5 Hz real time). The mean value of each data channel was eliminated from the analysis by capacitance coupling the signal into each analyzer.

23. The wave analyzer was used to evaluate the linear spectral density of the following 29 March data channels:

| Transducer | Measurement | Dial Readings, % |
|---|---|---|
| AP | Acceleration | 90, 80, 70, 60 |
| AV | Acceleration | 90, 80, 70, 60 |
| P7R | Pressure | 90, 80, 70, 60 |
| PUT | Pressure | 90, 80, 70, 60 |
| S7R | Strain | 90, 80, 70, 60 |
| S7L | Strain | 90, 80, 70, 60 |
| V7B | Strain | 90, 80, 70, 60 |
| V7T | Strain | 90, 80, 70, 60 |

Smoothed spectral density diagrams are presented in plates 5 and 6. Pertinent real-time parameters that describe the procedure used to obtain the diagrams are tabulated below:

| Parameter | Low Frequency | High Frequency |
|---|---|---|
| Frequency range, Hz | 0.5-20 | 10-160 |
| Effective bandwidth, Hz | 0.156 | 12.5 |
| Elapse time of data loop, sec | 200 | 200 |
| Averaging time, sec | 128 | 16 |
| Sweep time, sec | 64,000 | 14,400 |
| Time compression | 64:1 | 8:1 |

In addition, comparable linear spectral densities of strains at V7T, V5T, and V5B were obtained by means of a Nelson-Ross Model P026 plug-in wave analyzer. This analysis was performed on the magnetic tape data from the tests of 29 March in which the valve was in the 90 percent dial reading position. The output signal from the analyzer, which was displayed on an oscilloscope and photographed, is presented in plate 7. The time compression ratio during the analysis was 8:1; the sweep rate, in real-time units, was 0.17 Hz/sec; the sweep ranges were from 0 to 50 Hz and from 50 to 100 Hz. The spectra previously presented in plates 5 and 6 were smoothed from data similar to those shown in plate 7. Note that the spectrum of V7T shown in plate 7 is also shown in plate 6.

24. The amplitude density function, the cumulative amplitude density function, and the average number of zero crossings per second were obtained by means of the probability density analyzer. The above functions were observed by means of an oscilloscope whose display was photographed. The resulting diagrams are presented in plate 8. The number of zero crossings per second was obtained by using a digital counter in conjunction with the analyzer. The 29 March test channels inspected by means of the analyzer and the corresponding zero crossing rates (in real-time units) include:

| Transducer | Measurement | Dial Reading % | Zero Crossings per Second |
|---|---|---|---|
| V7T | Strain | 90 | 100.0 |
| V7B | Strain | 90 | 86.1 |
| | | 80 | 69.4 |
| | | 70 | 60.5 |
| | | 60 | 52.1 |
| V5T | Strain | 90 | 86.6 |
| V5T | Strain | 90 | 70.1 |
| | | 80 | 56.5 |
| | | 70 | 51.0 |
| | | 60 | 47.2 |
| S7L | Strain | 90 | 83.1 |
| S7R | Strain | 90 | 85.9 |
| S5L | Strain | 90 | 65.4 |
| S5R | Strain | 90 | 61.2 |

25. The correlator was used to obtain cross-correlations between

selected data channels for runs on 29 March at 90 percent dial reading. The channels investigated are as follows:

| Transducer A | Correlated with | Transducer B | Measurement A | Correlated with | Measurement B |
|---|---|---|---|---|---|
| V7B | | P7R | Strain | | Pressure |
| V7T | | P7R | Strain | | Pressure |
| V7B | | V5B | Strain | | Strain |

Correlograms (copies from direct X-Y recorder plots) are presented in plate 9. Note that in the above listing the A channel is delayed in the correlator so that a peak in the correlogram at positive time $\tau_o$ indicates that a component in the A signal <u>preceded</u> a similar component in the B signal by the time interval $\tau_o$. A negative correlation at zero time delay indicates that the two channels A and B are essentially out of phase; conversely, a positive correlation indicates that the two channels are essentially in phase.

## PART IV: ANALYSIS OF OSCILLOGRAPH AND MAGNETIC TAPE DATA

### Oscillograph Data

#### Discharge

26. Flow rates were not measured during the subject tests. The procedure used to evaluate the required discharges is as follows. First, a loss coefficient for the upstream conduit (from the reservoir to piezometer US) is calculated using current operational rating curves* in conjunction with data from piezometer US. This calculation is terminated at 70 percent dial reading, the maximum valve opening for which the rating curves have been verified. Second, the mean value of the loss coefficient is used in conjunction with piezometer US data to obtain discharges over the full range of dial readings used in the subject tests. The rating procedure is substantiated by (a) comparing the loss coefficient with values obtained during previous (1966) prototype tests,[11] (b) computing a butterfly valve discharge coefficient for comparison with Hydraulic Design Criteria[12] values, (c) computing the Howell-Bunger valve discharge coefficient for comparison with Hydraulic Design Criteria[13] values, and (d) combining items a, b, and c to obtain an analytical expression for discharge and comparing computed discharges with downstream gaging data.** These computations are described in the following paragraphs.

27. Conduit head loss. The head loss in the upstream flow passage is

$$H_L = K_L \frac{V_o^2}{2g} \qquad (1)$$

in which $H_L$ is the head loss between the reservoir and piezometer US, $K_L$ is a loss coefficient, $V_o$ is the velocity of flow in the 11-ft-diam conduit, and $g$ is the acceleration of gravity. The value of $H_L$ equals $Z_R - [(P/\gamma) + Z]_o - Q^2/2gA_o^2$ where $Z_R$ is reservoir elevation, $[(P/\gamma) + Z]_o$

---

* The operational rating curves were computed from data taken while the original valves were in place. (This information is contained in an unpublished communication from J. Herman to the author in Sept 1968.) The discharge coefficient for the earlier valve was divided by a factor of 1.075 to account for the reduced flow passage area in the new valves.

** J. A Wheeler, unpublished communication to author, Jan 1969.

is the piezometric head at the location US, $A_o$ is the cross-sectional area of the conduit (95.03 sq ft), and $Q$ is discharge. Hence, the loss coefficient may be evaluated using equation 1 in the form

$$K_L = \frac{2g\left[Z_R - \left(\frac{P}{\gamma} + Z\right)_o - \frac{Q^2}{2gA_o^2}\right]}{\left(\frac{Q}{A_o}\right)^2} \qquad (2)$$

The results are tabulated below. The value $\gamma = 62.4$ pcf (water at 39 F) is used in all computations in which the specific weight of water is required.

| Date March | Dial Reading % | $Q_T$* cfs | $H_L$** ft | $K_L$ | $\frac{V_o D_o}{\nu}$† |
|---|---|---|---|---|---|
| 27 | 30 | 2430 | 5.6 | 0.552 | 1.7 ($10^7$) |
| | 40 | 3120 | 7.1 | 0.424 | 2.1 |
| | 50 | 3930 | 11.1 | 0.419 | 2.7 |
| | 60 | 4360 | 17.7 | 0.541 | 3.0 |
| | 70 | 4870 | 23.4 | 0.575 | 3.3 |
| 29 | 30 | 2550 | 5.0 | 0.448 | 1.7 |
| | 40 | 3160 | 8.3 | 0.481 | 2.2 |
| | 50 | 3970 | 8.7 | 0.321 | 2.7 |
| | 60 | 4520 | 13.4 | 0.381 | 3.1 |
| | 70 | 4940 | 19.2 | 0.458 | 3.4 |
| | | | Mean $K_L$ | = 0.460 | |

* $Q_T$ is the rating curve value plus 70 cfs to account for the small discharge through the 2.5-ft-diam bypass valve.

** The piezometric head $[(P/\gamma) + Z]_o$ used in computing $H_L$ uses the values of pressures at location US as listed in table 1.

† Reynolds number; $\nu = 1.7 \times 10^{-5}$ ft$^2$/sec and $D_o = 11.0$ ft.

28. The large scatter in values of loss coefficient $K_L$ is due to (a) the relatively large significance of an accuracy of $\pm$0.5 psi in the Bourdon gage reading at US (equaling $\pm$1.15 ft in $[(P/\gamma) + Z]_o$), (b) errors in the project rating curve discharge values, and (c) errors in the Howell-Bunger valve dial setting. However, since the actual value

of $K_L$ is known to be essentially constant over the range of Reynolds numbers occurring during the tests, its mean value is used in subsequent computations. The loss coefficient for the upstream flow passage also was evaluated from data taken during the 1966 [11] prototype tests, using

$$K_L = K_e + K_f + K_t + K_c = 0.45 \qquad (3)$$

in which $K_e$ (0.01) is the entrance loss; $K_f$ (0.02) is the loss along the 29-ft tunnel; $K_t$ (0.16) is the trifurcation transition loss; and $K_c$ (0.26) is the loss along the 11-ft conduit.

29. Test discharges. Discharges computed by means of equation 2 with $K_L$ equal to 0.460 and using the values of Bourdon gage pressure at location US listed in table 1 are as follows:

| Date March | Dial Reading % | $[(P/\gamma) + Z]_o$ ft msl | $Q_T$ cfs | $Q^*$ cfs |
|---|---|---|---|---|
| 27 | 30 | 1623 | 2500 | 2430 |
| | 40 | 1615 | 3080 | 3010 |
| | 50 | 1601 | 3870 | 3800 |
| | 60 | 1589 | 4480 | 4410 |
| | 70 | 1575 | 5060 | 4990 |
| | 75 | 1569 | 5280 | 5210 |
| | 80 | 1564 | 5450 | 5380 |
| | 85 | 1559 | 5660 | 5590 |
| | 90 | 1552 | 5900 | 5830 |
| | 95 | 1553 | 5860 | 5790 |
| 29 | 30 | 1627 | 2540 | 2470 |
| | 40 | 1617 | 3180 | 3110 |
| | 50 | 1607 | 3780 | 3710 |
| | 60 | 1594 | 4390 | 4320 |
| | 70 | 1582 | 4940 | 4870 |
| | 75 | 1576 | 5160 | 5090 |
| | 80 | 1569 | 5420 | 5350 |
| | 85 | 1563 | 5630 | 5560 |
| | 90 | 1557 | 5830 | 5760 |

* Test valve discharge equals total discharge minus 70-cfs bypass discharge.

30. Butterfly valve discharge coefficient. Flow through a butterfly valve is expressed[12] as

$$Q = C_Q D_o^2 \sqrt{g(H_o - H_v)} \qquad (4)$$

in which $C_Q$ is a discharge coefficient, $D_o$ is the diameter (11 ft) of the butterfly valve, $H_o$ is the total head upstream of the valve at US (with flow equal to $Q_T$), and $H_v$ is the total head downstream from the valve (with flow equal to $Q$). Evaluation of equation 4, using data listed in table 1, is as follows:

| Date March | Dial Reading % | Q cfs | $[(P/\gamma) + Z]_v$* ft msl | $H_o - H_v$** | $\sqrt{2g(H_o - H_v)}$ |
|---|---|---|---|---|---|
| 27 | 30 | 2430 | 1606.0 | -0.7 | -- |
| | 40 | 3010 | 1585.2 | 2.6 | 12.9 |
| | 50 | 3800 | 1561.7 | -4.2 | -- |
| | 60 | 4410 | 1536.0 | -5.8 | -- |
| | 70 | 4990 | 1508.6 | -8.9 | -- |
| | 75 | 5210 | 1494.4 | -7.5 | -- |
| | 80 | 5380 | 1480.9 | -4.4 | -- |
| | 85 | 5590 | 1469.8 | -5.4 | -- |
| | 90 | 5830 | 1455.6 | -6.5 | -- |
| | 95 | 5790 | 1460.6 | -9.1 | -- |
| 29 | 30 | 2470 | 1608.6 | 0.1 | 2.5 |
| | 40 | 3110 | 1586.1 | 1.8 | 10.8 |
| | 50 | 3710 | 1562.2 | 3.3 | 14.6 |
| | 60 | 4320 | 1529.9 | 7.7 | 22.3 |
| | 70 | 4870 | 1500.3 | 10.0 | 25.4 |
| | 75 | 5090 | 1473.0 | 9.5 | 24.7 |
| | 80 | 5350 | 1473.0 | 9.5 | 24.7 |
| | 85 | 5560 | 1458.0 | 11.5 | 27.2 |
| | 90 | 5760 | 1445.1 | 11.5 | 27.2 |

* $[(P/\gamma) + Z]_v$ equals the average piezometric head in the Howell-Bunger valve using available channels (as listed in table 1) of PDT, PS4, PS6, PS8, P7L, P7R, P5L, P5R, and VG.

** $H_v = [(P/\gamma) + Z] + \frac{Q^2/A_{vn}^2}{2g}$ in which $A_{vn}$ is the clear flow passage area in the Howell-Bunger valve (57.07 sq ft).

31. Obviously, the negative values of $(H_o - H_v)$ shown above for data of 27 March are not physically correct. Since the maximum head loss in the flow through the butterfly valve is only about 10 times the 0.5-psi accuracy of the pressure gage readings, a large scatter in the computed value of the discharge coefficient is to be expected.

32. Values of Q are plotted against $\sqrt{2g(H_o - H_v)}$ in fig. 12, which indicates that the value of $C_Q$ is about 2.4. The Hydraulic Design Criteria[12] suggested design value of $C_Q$ for a fully open butterfly valve (located in a noncontracting pipe section) is 1.72, which is also shown in fig. 12. The higher value of $C_Q$ at Summersville is expected inasmuch as

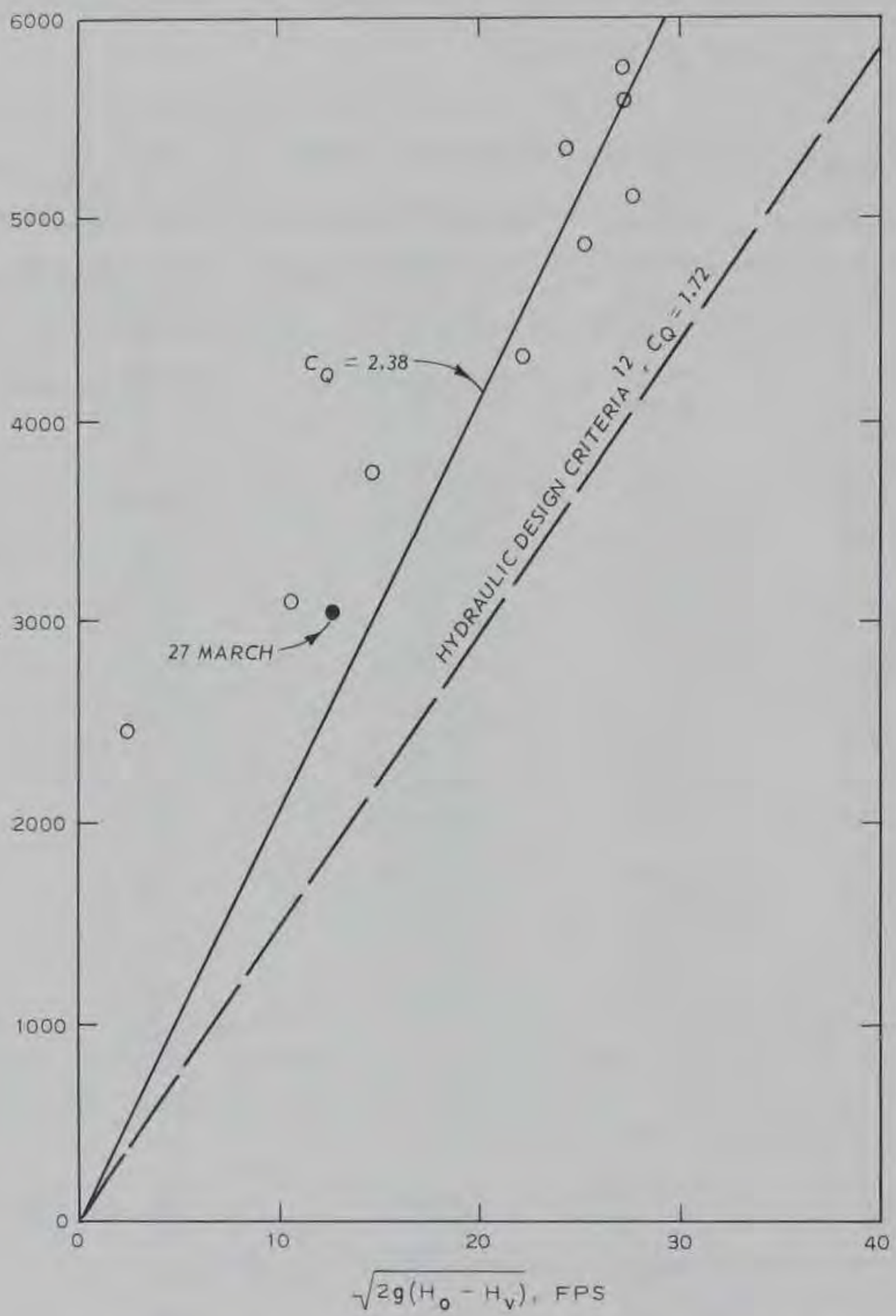


Fig. 12. Fully open butterfly valve discharge (29 March)

(a) the measured losses attributed to the butterfly valve actually include losses due to the reducer, the 9-ft-diam conduit, and the entrance to the Howell-Bunger valve; and (b) the piezometric head downstream from the

contracted flow section at the butterfly valve and reducer has not recovered to its uniform flow value at the measuring locations in the Howell-Bunger valve.

33. Howell-Bunger valve discharge coefficient. Flow through a Howell-Bunger valve is expressed as

$$Q = A_v C_D \sqrt{2gH} \qquad (5)$$

in which $A_v$ is the full cross-sectional area at the valve inlet, $C_D$ is a discharge coefficient, and $H$ is the total head in the flow entering the valve as measured above the valve center line. Equation 5 is evaluated using values listed in table 1 as follows:

| Date March | Dial Reading % | Q cfs | $\sqrt{2g(H_o - 1393.7)}$ fps | $C_{D_o}$ * | $\sqrt{2g(H_v - 1393.7)}$ fps | $C_D$ ** |
|---|---|---|---|---|---|---|
| 27 | 30 | 2430 | 124.4 | 0.314 | 124.4 | 0.314 |
| | 40 | 3010 | 123.6 | 0.392 | 122.9 | 0.394 |
| | 50 | 3800 | 122.5 | 0.500 | 123.5 | 0.495 |
| | 60 | 4410 | 121.7 | 0.585 | 123.0 | 0.577 |
| | 70 | 4990 | 120.4 | 0.668 | 122.7 | 0.654 |
| | 75 | 5210 | 119.9 | 0.701 | 121.7 | 0.689 |
| | 80 | 5380 | 119.4 | 0.727 | 120.4 | 0.719 |
| | 85 | 5590 | 119.2 | 0.757 | 120.4 | 0.747 |
| | 90 | 5830 | 118.5 | 0.794 | 120.1 | 0.781 |
| | 95 | 5790 | 118.6 | 0.788 | 120.8 | 0.771 |
| 29 | 30 | 2470 | 125.5 | 0.317 | 125.4 | 0.317 |
| | 40 | 3110 | 124.5 | 0.402 | 123.9 | 0.404 |
| | 50 | 3710 | 123.7 | 0.483 | 122.8 | 0.486 |
| | 60 | 4320 | 122.6 | 0.568 | 120.4 | 0.577 |
| | 70 | 4870 | 121.8 | 0.645 | 118.9 | 0.659 |
| | 75 | 5090 | 121.2 | 0.677 | 117.8 | 0.695 |
| | 80 | 5350 | 120.4 | 0.716 | 117.9 | 0.730 |
| | 85 | 5560 | 120.1 | 0.747 | 116.8 | 0.766 |
| | 90 | 5760 | 119.5 | 0.778 | 116.2 | 0.798 |

* $C_{D_o} = \dfrac{Q}{A_v \sqrt{2g(H_o - 1393.7)}}$ ; $A_v = 62.16$ sq ft; 1393.7 is the elevation of the valve center line in ft msl; velocity head based on $Q_T$ .

** $C_D = \dfrac{Q}{A_v \sqrt{2g(H_v - 1393.7)}}$ ; velocity head based on $Q$ .

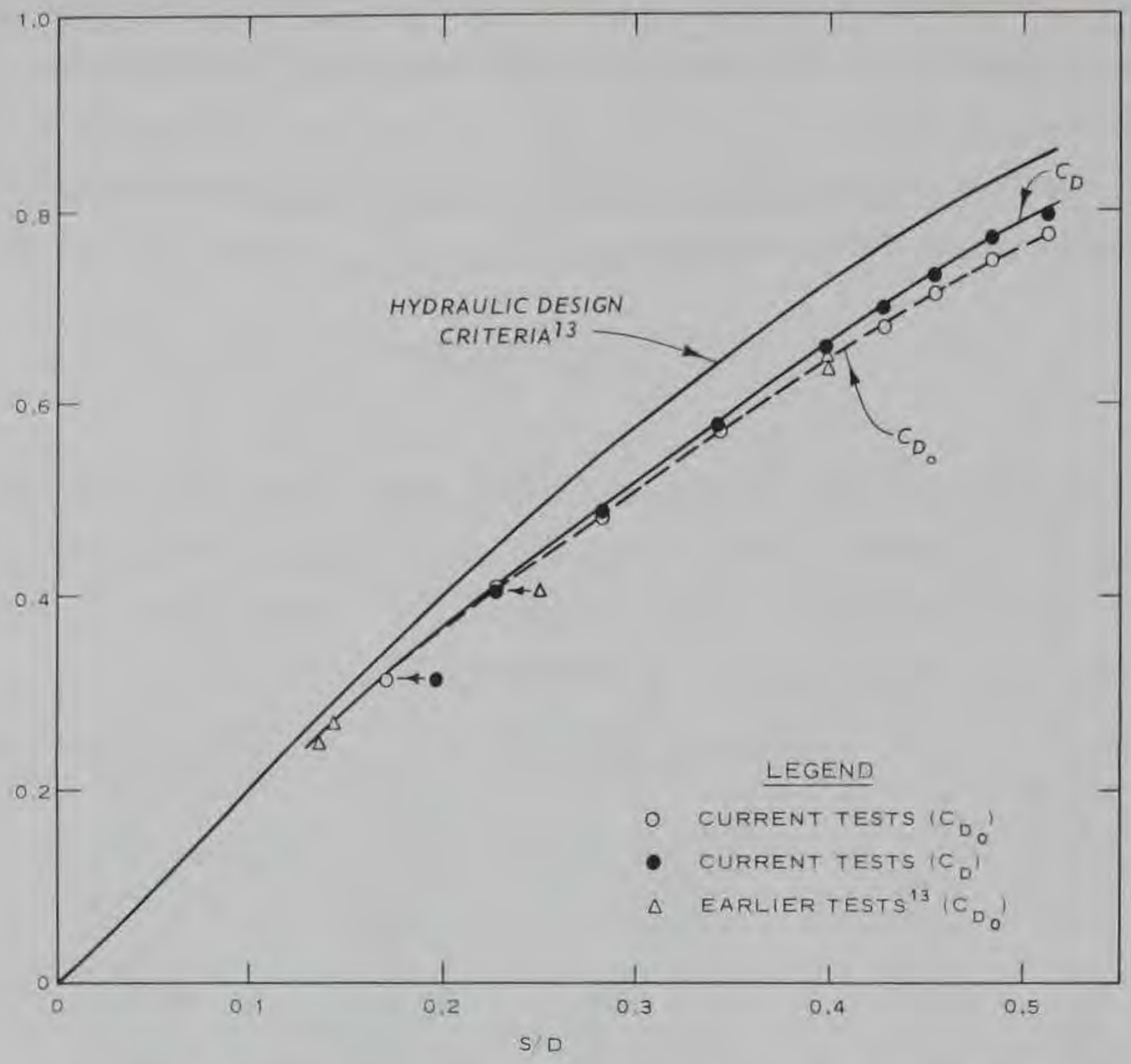


Fig. 13. Howell-Bunger valve discharge coefficient (29 March)

34. Discharge coefficients from the 29 March data are plotted in fig. 13. The Hydraulic Design Criteria[13] design curve and previous[11] observations on the same valve are also shown in fig. 13. As for the butterfly valve loss coefficient, values of $C_D$ using 27 March data are inconsistent and are not shown. Values of the ratio of sleeve travel to valve diameter, $S/D$, computed using original valve sleeve travel[11] data and new valve diameter (106.75 in.) are as follows:

| Dial Reading % | Sleeve Travel, S in. | $\frac{S}{D}$ | Dial Reading % | Sleeve Travel, S in. | $\frac{S}{D}$ |
|---|---|---|---|---|---|
| 30 | 18.26 | 0.171 | 75 | 45.66 | 0.428 |
| 40 | 24.35 | 0.228 | 80 | 48.70 | 0.456 |
| 50 | 30.44 | 0.285 | 85 | 51.74 | 0.485 |
| 60 | 36.53 | 0.342 | 90 | 54.79 | 0.513 |
| 70 | 42.61 | 0.399 | 95 | 57.83 | 0.542 |
| | | | 100 | 60.88 | 0.570 |

35. Outlet works rating curves. The rating curve for the tested conduit and outlet works is obtained by combining equations 1, 4, and 5; that is,

$$Q = C_D A_V \sqrt{2g\left(Z_R - \frac{K_L Q^2}{2gA_o^2} - \frac{Q^2}{gD_o^4 C_Q^2} - 1393.7\right)} \qquad (6)$$

Letting $K_L = 0.46$, $C_Q = 2.4$, $A_o/A_V = 1.529$, and rewriting equation 6 results in the discharge rating equation

$$Q = \frac{C_D A_V}{\left(1 + 0.288C_D^2\right)^{1/2}} \sqrt{2g(Z_R - 1393.7)} \qquad (7)$$

36. Rating curves, developed by means of equation 7 for flow from conduit 1 (with no flow through conduits 2 and 3 and the bypass line), are shown in plate 10. Data supplied by Huntington District* for measurements on 19 and 20 November 1968 are also shown. These data, which apply to a lower lake elevation, are tabulated below along with the error (as a percent of measured discharge) between the predicted and measured rates of flow.

| Date 1968 | Dial Reading % | Reservoir Elevation ft msl | Measured Discharge cfs | Computed Discharge cfs | Error % |
|---|---|---|---|---|---|
| 19 Nov | 30 | 1566.4 | 2080 | 2090 | +0.5 |
| | 45 | 1567.1 | 2980 | 2900 | -2.7 |
| | 60 | 1568.2 | 3780 | 3710 | -1.9 |
| 20 Nov | 75 | 1566.2 | 4550 | 4310 | -5.3 |
| | 90 | 1566.2 | 5030 | 4900 | -2.6 |

Since the maximum listed error, 5.3 percent, is within the probable accuracy of the discharge measurement and the dial setting, the developed rating (equation 7) is considered satisfactory for the evaluation of discharges during the subject tests.

Cavitation

37. The cavitation number $\sigma_c$ is an index used in the study of cavitation phenomena and is defined[14] as

---

* Unpublished.

$$\sigma_c = \frac{\frac{P_o}{\gamma} - \frac{P_v}{\gamma}}{V_o^2/2g} \qquad (8)$$

in which $P_v$ is the vapor pressure of the flowing liquid and $P_o$ and $V_o$ are a reference pressure and velocity, respectively. For water at 39 F the value of $P_v$ is 0.11 psia.[14] Using this value and values of $P_o$ and $V_o$ at location US,* the cavitation numbers during the tests are computed as follows and are plotted relative to the corresponding discharges in fig. 14:

| Dial Reading % | $\sigma_c$ 27 March | $\sigma_c$ 29 March |
|---|---|---|
| 30 | 24.0 | 23.5 |
| 40 | 15.3 | 14.4 |
| 50 | 9.2 | 9.9 |
| 60 | 6.5 | 6.9 |
| 70 | 4.7 | 5.1 |
| 75 | 4.2 | 4.6 |
| 80 | 3.9 | 4.0 |
| 85 | 3.5 | 3.6 |
| 90 | 3.1 | 3.3 |

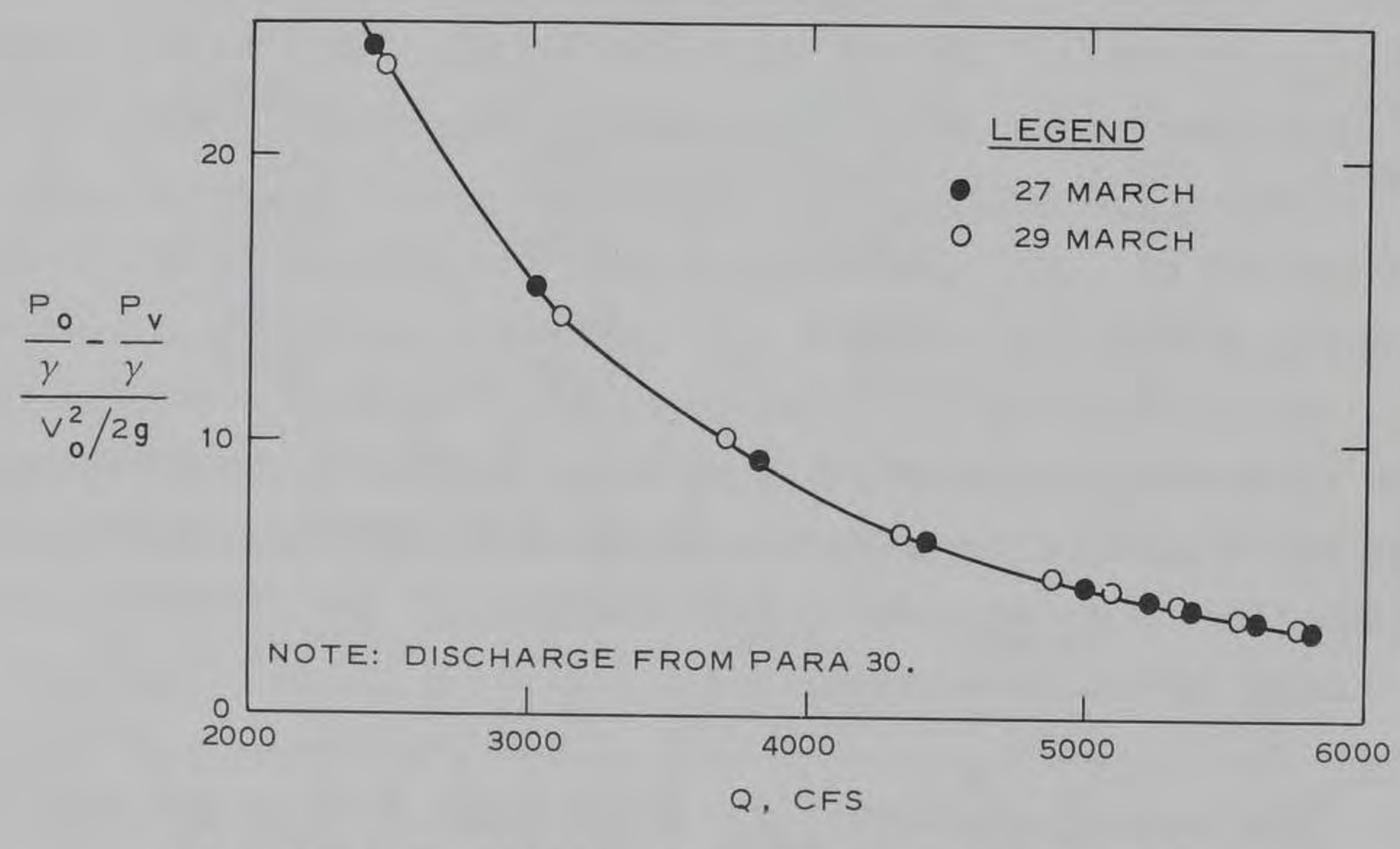


Fig. 14. Cavitation index (27 and 29 March)

* The elevation used in computing $P_o$ from gage readings US is 1399.2, i.e. the top of the conduit.

38. Since the cavitation index $\sigma_c$ decreases as the valve opening increases, the tendency toward cavitation in the conduit increases. Two consequences of cavitation occurring in the area immediately downstream from the butterfly valve would be as follows.

a. Excessive cavitation would cause a nonlinear relation to exist between Q and $\sqrt{Z_R - 1393.7}$. This condition did not occur to a measurable extent during the subject tests. However, the extrapolation of discharges (equation 7) to a condition having a cavitation index lower than the minimum value, 3.3, during the subject tests is tenuous.

b. An increase in pressure fluctuations in the flow downstream from the butterfly valve would occur if larger vapor cavities are created in the flow. Similar conditions, with regard to these cavities, occur at equal values of the cavitation index.

In view of these consequences, dashed lines are plotted in plate 10 corresponding to selected values of $\sigma_c$ computed by means of equation 8. The line $\sigma_c$, equal to 3.5, is near the limit to which the derived rating curve can be used with confidence. Each line of constant $\sigma_c$ corresponds to flow conditions at which cavitation conditions in the outlet conduit are similar.

Average pressures

39. Euler number. The Euler number, $\mathbb{E}$, is a dimensionless flow parameter involving fluid density $\rho$, a velocity $V$, and a difference in pressure intensity $\Delta P$, as follows:

$$\mathbb{E} = \frac{V}{\sqrt{\frac{2\Delta P}{\rho}}} \tag{9}$$

For a completely enclosed flow with similar boundary geometries the Euler number is of constant magnitude regardless of the boundary scale, the rate of flow, the density, and the absolute pressure as long as fluid properties such as weight and viscosity have no influence on the flow pattern.[15] In addition, when the motion is defined by solid boundaries, the sole effect of gravitational attraction is to change the pressure intensity from point to point in direct proportion to the change in elevation. The Euler number is used herein to assess changes in piezometric head at transducer locations near the conduit outlet.

40. Pressures. Following equation 9, the measured average pressures are reduced to the form

$$\mathbb{E}_1 = \frac{Z_R - \left(\frac{P}{\gamma} + Z\right)}{\frac{V_o^2}{2g}} \tag{10}$$

in which $V_o$ is the velocity of flow in the 11-ft-diam conduit based on $Q_T$, $g$ is the acceleration of gravity, $Z_R$ is the reservoir elevation, and $\left(\frac{P}{\gamma} + Z\right)$ is the piezometric head at the location being studied. Values of $\mathbb{E}_1$, computed by means of equation 10, are listed in table 2 and plotted in plate 11. Inasmuch as (a) the Reynolds number is large, and consequently, viscosity does not significantly alter the flow pattern and (b) the flow is enclosed by solid boundaries along the reach between the reservoir and the Howell-Bunger valve, the value of $\mathbb{E}_1$ will be constant[15] unless cavitation causes the flow pattern to change. The difference in Euler numbers between vanes 5 and 7, 3.29 compared with 3.67, means that the flow pattern entering the valve is not symmetrical about a vertical axis. The decrease in Euler numbers with increasing dial reading at transducers PUT and PUB shows that localized cavitation probably does occur at these locations. On the other hand, since the Euler numbers are not measurably altered (with increasing dial readings) at locations PDT, PS8, VG, PS4, P7L, P7R, P5L, and P5R, any localized cavitation is not of sufficient magnitude to alter the previously derived (equation 7) discharge rating curve.

Average strains and stresses

41. Stress $\sigma$ and strain $\Delta L/L$ are related by Hooke's law, $\sigma = E(\Delta L/L)$, in which $E$ is Young's modulus of elasticity. For an elastic material at low stress levels, such as exist in the shell and vanes of the subject valve, $E$ is constant. Hence the measured mean flexural strain $\overline{\Delta L/L}$ in paragraph 18 may be converted to mean flexural stress $\bar{\sigma}_f$ at the plate surface as follows.

$$\bar{\sigma}_f = E\left(\frac{\overline{\Delta L}}{L}\right) \tag{11a}$$

in which, for $\bar{\sigma}_f$ in psi and $\overline{\Delta L/L}$ in in./in., E equals $30 \times 10^6$ psi. Values of $\bar{\sigma}_f$ using the measured strain values in equation 11a are:

| Dial Reading % | Stress, 1000's of psi | | | | | | | |
|---|---|---|---|---|---|---|---|---|
| | S7L | S7R | V7B | V7T | S5L | S5R | V5B | V5T |
| 0 | -2.40 | 0.180 | 0.18 | -0.06 | -2.25 | -2.25 | 0.24 | 0.24 |
| 30 | -1.80 | -1.38 | 0.30 | 0.12 | -2.16 | -2.16 | 0.39 | 0.48 |
| 40 | -1.44 | -1.14 | 0.15 | 0.06 | -1.71 | -1.59 | 0.39 | 0.30 |
| 50 | -1.29 | -0.75 | 0.48 | 0.30 | -1.35 | -1.47 | 0.18 | 0.45 |
| 60 | -0.81 | -0.99 | 0.09 | 0.15 | -1.29 | -0.99 | 0.39 | 0.39 |
| 70 | -0.99 | -0.36 | 0.54 | 0.30 | -1.32 | -0.72 | 0.27 | 0.51 |
| 75 | -0.87 | -0.30 | 0.33 | 0.00 | -1.53 | -0.36 | 0.51 | -0.21 |
| 80 | -0.66 | -0.21 | 0.60 | 0.33 | -0.96 | -0.90 | 0.57 | 0.75 |
| 85 | -0.69 | 0.00 | 0.45 | 0.06 | -0.99 | -0.36 | 0.03 | 0.33 |
| 90 | -0.78 | 0.15 | 1.08 | 0.90 | -0.45 | -0.75 | 0.12 | 0.87 |
| 95 | -0.93 | 0.48 | 0.93 | 0.63 | -0.48 | -0.60 | -0.18 | 0.84 |

The commonly used flexure formula for computing bending stresses in a beam is

$$\bar{\sigma}_f = \frac{Mc}{I} \tag{11b}$$

in which M is the bending moment at the section, $\bar{\sigma}_f$ is the normal unit stress on a fiber a distance c from the neutral axis, and I is the moment of inertia of the beam cross section. Hence whenever two plates (vanes) of the same surface size, shape, and boundary conditions and made of the same material are subjected to the same static loadings, the fiber stresses are related by

$$\bar{\sigma}_{f_o} = \left(\frac{t}{t_o}\right)^2 \bar{\sigma}_f \tag{11c}$$

in which $t/t_o$ is the ratio of vane thicknesses. For example, the original Howell-Bunger valve vanes (t = 1.0 in.), when subjected to the same static loadings as the tested valve vanes ($t_o$ = 2.33 in.), would experience flexural stresses 5.42 times* as large as the values listed above.

---

* Since the distribution of the loading on the vanes is not known, the reduction in vane width (52.5 in. in the old valve to 50.375 in. in the new valve) has not been included in this ratio. Note that the change of vane width would increase the ratio slightly.

42. The positive and negative signs shown in the tabulation conform to the convention described in paragraph 18. The change in sign and magnitude of stress shows that the valve deformed into the shapes* shown below (fig. 15). Note that the sketches exaggerate the deformation and that the deformed shape is relative to the unloaded, or dry, shape. Changes in the

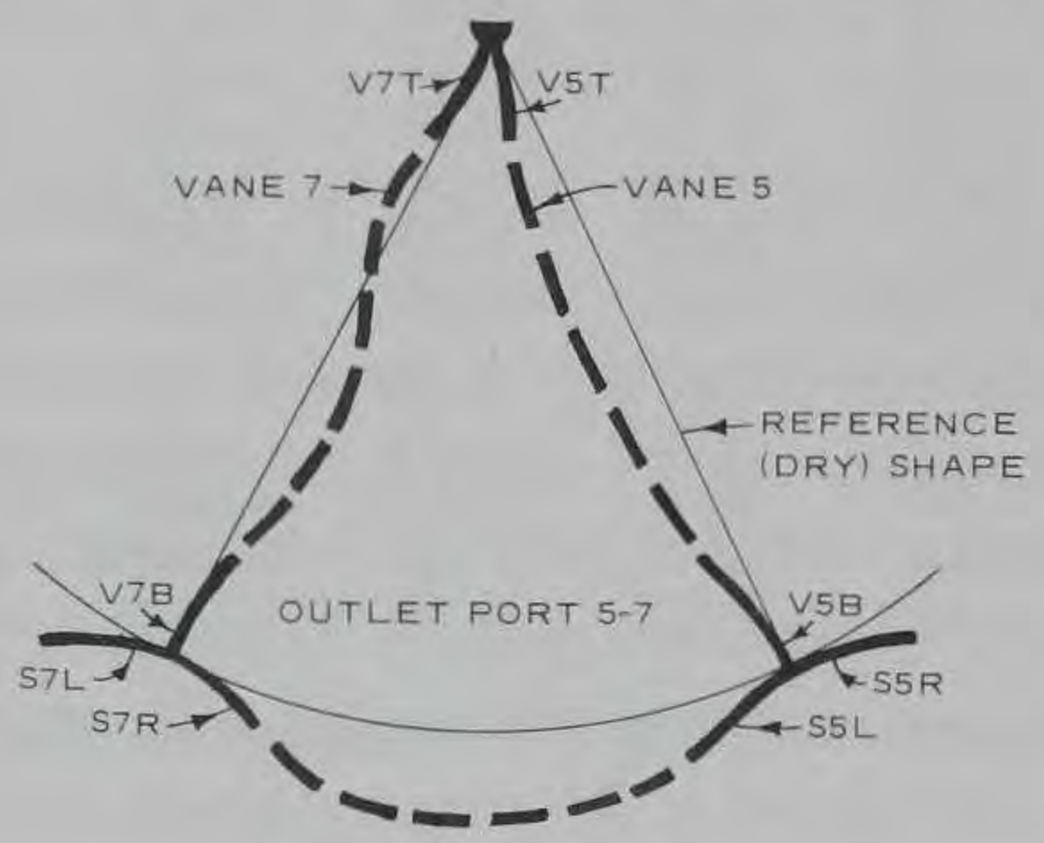


a. DIAL READING = 0%

b. DIAL READING = 75%

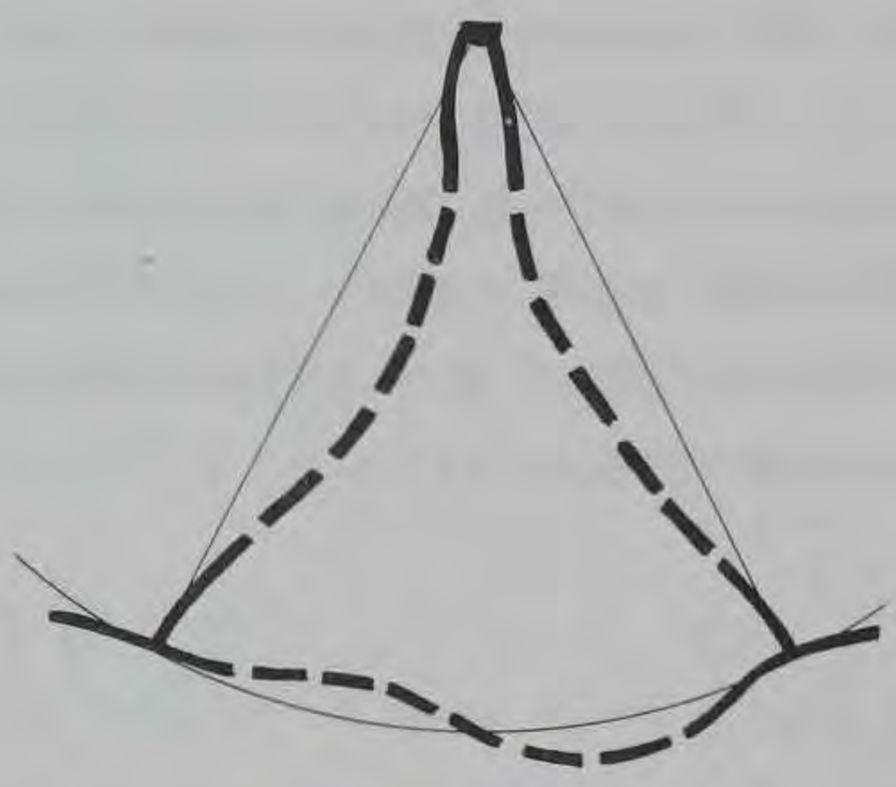

c. DIAL READING = 90%

Fig. 15. Average valve shapes (not to scale, 29 March)

---

* Strain fluctuations (paragraph 20) are measured relative to time-averaged strains; the configurations shown in fig. 15 correspond to time-averaged strain values and are the shapes about which the vibratory motion takes place.

general shape are caused by changes in the loading on the valve. Each of the figures shows some nonsymmetrical features about a vertical axis. Nonsymmetry at zero dial reading is the consequence of nonsymmetrical construction of some aspect of the valve or initial loading at mounting or of the placement of strain gages. The changes in the shape at large dial readings are the consequence of a nonsymmetrical flow pattern entering the valve.

Pressure and strain fluctuations

43. Pressure fluctuations. The 29 March pressure fluctuations previously listed in paragraph 19 are presented in plate 12 and listed nondimensionally in table 3, in terms of the velocity head of the flow in the valve body, $(V_{VN})^2/2g$ . The data show that the pressure fluctuations in the flow near the wall of the reducer (PUT and PUB) are approximately expressed by

$$\frac{P_{max} - P_{min}}{\gamma} \approx 0.16 \frac{(V_{VN})^2}{2g} \qquad (12)$$

Equation 12, when compared with published information (given below) concerning pressure fluctuations in turbulent flows, shows that these fluctuations are increased by about one order of magnitude as the flow passes around the butterfly valve hub.

---

The estimate of the intensity of the turbulent velocity fluctuations and pressure fluctuations in the flow immediately upstream of the butterfly valve is based on Laufer's[16] experimental data and Batchelor's[17] isotropic turbulence flow model. Laufer's measurements[16] show that the turbulence intensity at the center line of a circular pipe ($R_e = 5 \times 10^5$) is essentially isotropic with

$$\frac{u'}{V_o} \approx \frac{v'}{V_o} \approx \frac{w'}{V_o} \approx 0.035 \qquad (a)$$

where u' , v' , and w' are root-mean-square (rms) values of three orthogonal velocity fluctuations. Batchelor[17] shows that in isotropic turbulence

$$\frac{P'}{\gamma} = 1.17 \frac{u'^2}{2g} \qquad (b)$$

or, combining (a) and (b),

$$\frac{P'}{\gamma} = 0.0143 \frac{V_o^2}{2g} \qquad (c)$$

where P' is the rms value of the static-pressure fluctuations in the flow. Successively multiplying the coefficient in (c) by (1/0.707), 2, and 0.36 to obtain a peak-to-peak value referenced to the velocity entering the Howell-Bunger valve yields

$$\frac{P_{max} - P_{min}}{\gamma} = 0.015 \frac{(V_{VN})^2}{2g} \qquad (d)$$

This estimate is only a rough approximation of the pressure fluctuations in the flow upstream of the butterfly valve; however, a comparison of equation (d) with the prototype test results (transducers PUB and PUT) shows that the magnitude of the turbulent pressure fluctuations increases significantly as the flow passes through the butterfly valve.

---

The pressure fluctuations in the flow near the wall of the valve body (PS4, PS6, PS8, and PDT) are approximately expressed by

$$\frac{P_{max} - P_{min}}{\gamma} \approx 0.050 \frac{(V_{VN})^2}{2g} \qquad (13)$$

Equations 12 and 13 apply over the entire range (30-95 percent dial readings) of the test conditions. On the other hand, the fluctuations measured by the vane pressure gages shifted from

$$\frac{P_{max} - P_{min}}{\gamma} \approx 0.050 \frac{(V_{VN})^2}{2g}$$

at small dial readings, to

$$\frac{P_{max} - P_{min}}{\gamma} \approx 0.075 \frac{(V_{VN})^2}{2g} \qquad (14)$$

at large dial readings. A comparison of equations 12 and 13 shows that the magnitudes of average pressure fluctuations along the wall of the flow passage are reduced between the butterfly valve and the Howell-Bunger valve by about 70 percent of the magnitude of the fluctuations at the reducer. Equations 13 and 14 pertain to conditions near the center of the mainstream flow along the surface of the vanes. These equations show that the magnitude of the pressure fluctuations along vanes 5 and 7 ranges from 1.0 to 1.5 times the magnitude at the wall. These larger fluctuations are expected inasmuch as (a) acceleration (vibration) of a vane tends to increase the magnitude of a pressure measurement whenever the motion of the vane tends to accelerate the adjacent mass of water, and (b) pressure measurements P7R, P7L, P5R, and P5L were made at locations nearer the center of the mainstream flow and consequently are located in a more turbulent region of the flow field than are the pressure measurements at the flow passage boundary. The vanes do not have an opportunity to stabilize the flow since the vane pressure cells are located near the upstream end of the vanes.

44. Strain and stress fluctuations. The 29 March measured fluctuations of flexural strain, paragraph 20, are converted into flexural stress fluctuations by means of equation 11a:

| Dial Reading % | Maximum Peak-to-Peak Fluctuation, psi | | | | | | | |
|---|---|---|---|---|---|---|---|---|
| | S7L | S7R | V7B | V7T | S5L | S5R | V5B | V5T |
| 30 | 300 | 300 | 420 | 420 | 480 | 450 | 510 | 420 |
| 40 | 480 | 450 | 570 | 570 | 600 | 600 | 840 | 660 |
| 50 | 570 | 480 | 930 | 750 | 680 | 690 | 1230 | 900 |
| 60 | 630 | 690 | 1260 | 1170 | 1170 | 1170 | 1980 | 1530 |
| 70 | 1020 | 1020 | 1530 | 1560 | 1530 | 1410 | 2610 | 1860 |
| 75 | 780 | 840 | 1500 | 1380 | 1530 | 1380 | 2790 | 2130 |
| 80 | 1050 | 1080 | 2010 | 1950 | 1770 | 1770 | 2850 | 2040 |
| 85 | 1200 | 1170 | 2520 | 2460 | 1620 | 1710 | 3090 | 2460 |
| 90 | 1200 | 1560 | 2400 | 2070 | 2070 | 2070 | 3930 | 2970 |
| 95 | 1500 | 1620 | 2640 | 1890 | 2250 | 1860 | 3540 | 2760 |

Comparing the magnitudes of temporal mean stress with the corresponding

peak-to-peak stress fluctuation in the two preceding tabulations, fully reversed bending stresses (tension to compression and vice versa) occurred for channels V7T, V7B, V5T, and V5B for all listed test conditions, whereas channels S7R, S5L, and S5R experienced fully reversed bending for valve openings greater than 60, 85, and 70 percent, respectively, and channel S7L does not necessarily experience reversed bending.

45. An analysis of flow-induced vibration of a complex elastic structure can be approached via a general relation as follows:

$$\text{Response} = \text{Transfer Function} \times \text{Input} \tag{15}$$

in which the response is a measure of the vibration and the input is a measure of the flow properties causing the vibration. A linear transfer function is independent of the input and response; that is, a linear transfer function for the Howell-Bunger valve is governed solely by the elastic characteristics of the valve. For example, assuming that the magnitude of the fluctuating stresses is a consequence of the magnitude of the fluctuating pressures in the flow entering the valve and that the transfer function is simply a constant, $k$, then, according to equation 15

$$(\sigma_{f\max} - \sigma_{f\min}) = k(P_{\max} - P_{\min}) \tag{16a}$$

Obviously, this is an extreme simplification of the vibratory phenomena of the valve. However, whenever (a) the amplitude of vibration is small, (b) the input is independent of the response, and (c) the frequencies involved are well below structural natural frequencies, equation 16a will be a reasonable approximation to the physical situation. For example, combining equation 13, which pertains to pressure fluctuations at the valve wall, and equation 16a

$$\sigma_{f\max} - \sigma_{f\min} = 0.05k\gamma \frac{(V_{VN})^2}{2g} \tag{16b}$$

or

$$k = \frac{\sigma_{fmax} - \sigma_{fmin}}{0.05\gamma \frac{(V_{VN})^2}{2g}} \qquad (16c)$$

46. Experimentally determined values of the transfer coefficients, k , evaluated by means of equation 16c for each of the eight strain gage channels are listed below and are plotted in plate 13. These data indicate that the assumption of a constant as a transfer coefficient in equation 16c is acceptable for channels S5L, S5R, S7L, and S7R.

| Dial Reading % | $(\text{Stress}_{max} - \text{Stress}_{min})/0.05\gamma \left[(V_{VN})^2/2g\right]$ | | | | | | | |
|---|---|---|---|---|---|---|---|---|
| | S7L | S7R | V7B | V7T | S5L | S5R | V5B | V5T |
| 30 | 476 | 466 | 666 | 666 | 761 | 714 | 809 | 666 |
| 40 | 481 | 451 | 471 | 571 | 601 | 601 | 841 | 661 |
| 50 | 401 | 338 | 654 | 528 | 549 | 486 | 866 | 633 |
| 60 | 327 | 358 | 654 | 607 | 606 | 607 | 1027 | 794 |
| 70 | 416 | 416 | 624 | 637 | 624 | 576 | 1065 | 759 |
| 75 | 292 | 314 | 561 | 516 | 572 | 516 | 1043 | 796 |
| 80 | 355 | 365 | 680 | 659 | 599 | 599 | 964 | 690 |
| 85 | 376 | 366 | 689 | 770 | 507 | 536 | 968 | 770 |
| 90 | 350 | 455 | 700 | 604 | 604 | 604 | 1147 | 867 |
| 95 | 438 | 473 | 770 | 552 | 657 | 543 | 1033 | 805 |
| Average values | 391 | 400 | 647 | 611 | 608 | 578 | 976 | 744 |

On the other hand the value of k based on equation 16c for channels V5T and V5B clearly increases as the gate opening is increased. This increase in k is too large to be attributed solely to experimental errors, although a large scatter is anticipated due to the relatively large possible scaling errors in strain data (see paragraph 20). The vane fluctuating stress values are plotted in fig. 16 as a function of the measured fluctuating pressures in the mainstream flow. Despite the scatter in the plotted points, fig. 16 appears to be a more valid representation than equation 16c. The data clearly show (a) the flexural stress fluctuations at the shell end of vane 5 are larger than at the hub end, and (b) the fluctuations at channel V5B are significantly greater than at any other measuring location.

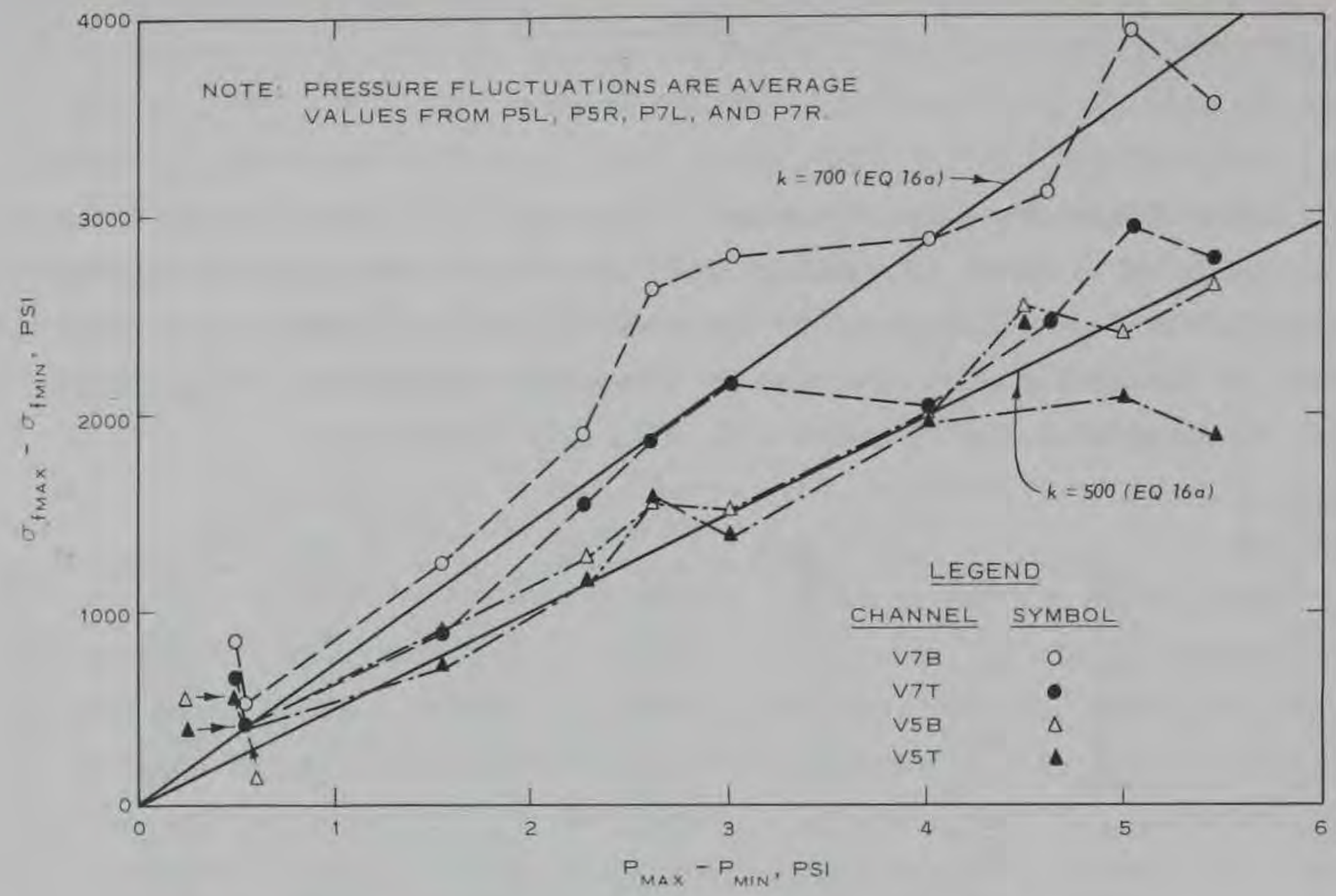


Fig. 16. Fluctuating stress in the vanes (29 March)

## Magnetic Tape Data

### Frequency considerations

47. A device that continuously measures a statistically stationary, dynamic quantity often produces a signal which is made up of many frequencies rather than being a simple harmonic. An oscillograph chart, which displays signal amplitude as a function of time, may not reveal which frequencies prevail in the data. On the other hand a display that shows the time-averaged amplitude of each frequency component in the signal provides specific information concerning the frequencies which prevail in the data. The linear spectral density diagram is this latter type of display and, consequently, is extremely useful in any study concerned with complex continuous signals. Since the subject tests are concerned with an elastic structure in which many resonant frequencies exist, the linear spectral

density diagrams are used to determine which structural frequencies are excited during the vibration.

48. Pertinent spectral diagrams obtained during the subject tests have been presented previously in plates 5, 6, and 7. The strain and acceleration data produced consistent and repeatable frequency spectra whereas only two of the pressure measuring channels (PUT and P7R) contained data of sufficient amplification so that spectral diagrams could be generated. In addition, the P7R diagrams in plate 5 contain false signals at about 15 cps and at higher harmonics of 15 cps. These false signals are caused by intermittent shifting of the signal zero level as the backup pressure regulator* operates.

49. The natural frequencies of vibration of the complete valve structure have not been evaluated by means of an elastic analysis. Instead, the three lower predominant frequencies that appear in the acceleration and strain spectra are considered as the consequence of natural vibration of sectional components of the valve. These apparent natural frequencies are listed below along with the spectra in which they appear and the particular vibration to which they are attributed. Each listed frequency is checked against approximate analytical solutions described briefly in the following paragraphs.

| Natural Frequency, Hz | Pertinent Spectra Plates 5 and 6 | Component Vibration |
|---|---|---|
| 75 | V7B, V7T, V5B, V5T, S7L, and S7R | Fundamental mode of vibration of a vane |
| 46 | AV, AP | Fundamental mode of transverse vibration of the cantilevered valve structure |
| 25 | AP | Fundamental mode of torsional vibration of the cone |

50. Fundamental mode of vibration of the vanes. The theory of the

---

* See paragraph 10c.

vibration of flat plates is described by Timoshenko,[6] Young,[18] etc. The fundamental natural frequency, $f_1$, of free vibration of a flat plate is

$$f_1 = \frac{\lambda_p}{2\pi L_v^2}\sqrt{\frac{D}{\mu}} \tag{17}$$

in which $\lambda_p$ is a coefficient that is a function of the geometry and boundary conditions of the plate, $D$ is the flexural rigidity of the plate and is equal to $Et^3/(12)(1 - \nu^2)$, and $\mu$ is the mass per unit area of the flat surface that is accelerated during the vibratory motion. For a plate vibrating in a vacuum, $\mu$ is equal to $\rho_s t$. In the above expressions, the modulus of elasticity $E$, Poisson's ratio $\nu$, and mass density $\rho_s$ are properties of the plate material, whereas length $L_v$ and thickness $t$ describe the plate geometry. Theoretically,* the value of $\lambda_p$ is 9.89 for a two-dimensional plate that is simply supported on each side and 22.4 for a two-dimensional plate that is clamped on each side.

51. To evaluate the reduced natural frequencies that occur when a structure vibrates in a dense fluid rather than in a vacuum, the value of $\mu$ must be increased to include the inertia of the fluid that is accelerated by the motion of the structure. A common analytical expedient is to represent the apparent increase in inertia by a mass of fluid displaced by the structure.[19] In the case of a thin, infinitely long lamina of breadth $L_v$ moving in the direction of its normal, the apparent mass as determined from a potential flow solution given by Lamb[20] is $\left(\pi\rho L_v^2\right)/4$ per unit length or $(\pi\rho L_v)/4$ per unit area. Hence, denoting the added mass per unit area as $K\rho L_v$, the value of $\mu$ in equation 17 is $\rho_s t + K\rho L_v$. Substituting the above expressions for $D$ and $\mu$ into equation 17 yields

$$f_1 = \frac{\lambda_p}{2\pi L_v^2}\sqrt{\frac{Et^3/(12)(1 - \nu^2)}{\rho_s t\left(1 + \frac{\rho K L_v}{\rho_s t}\right)}} \tag{17a}$$

---

* Timoshenko[6] beam theory values.

The two constant coefficients, K (which equals $\pi/4$ in Lamb's[20] potential flow situation) and $\lambda_p$, must be determined from experimental data. As shown in equation 17a, an evaluation of natural frequency is less sensitive to an error in the value of added mass coefficient than to an error in the value of the frequency coefficient. Hence an estimated value of K, based on experimental results by Abramson[21] who studied the vibration of various rectangular shapes of cantilever plates in air and water, is used along with the prototype Howell-Bunger valve data in computing $\lambda_p$.

52. Fig. 17 shows examples of Abramson's[21] data reduced to parameters

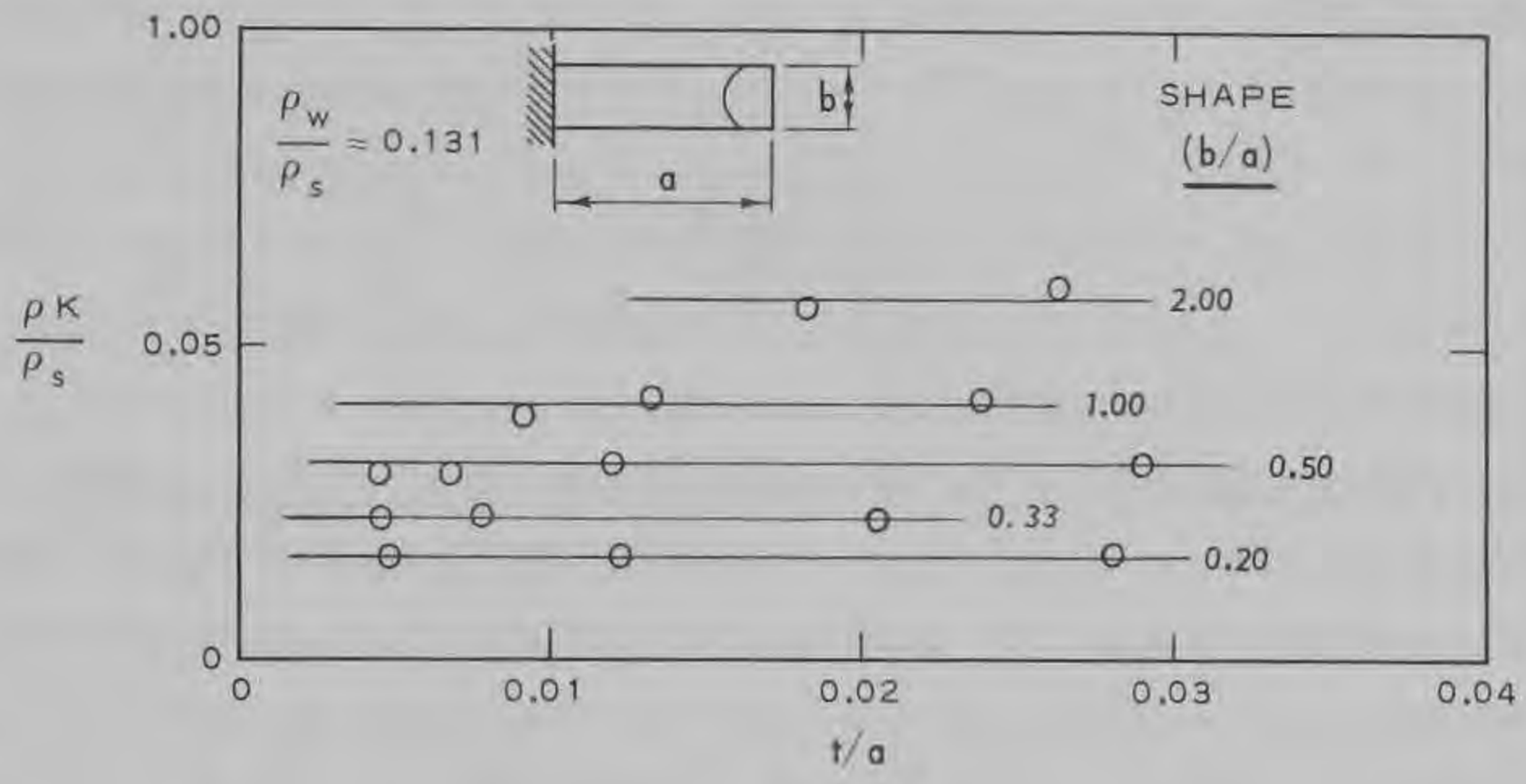


a. EFFECT OF PLATE THICKNESS (2ND LONGITUDINAL MODE)

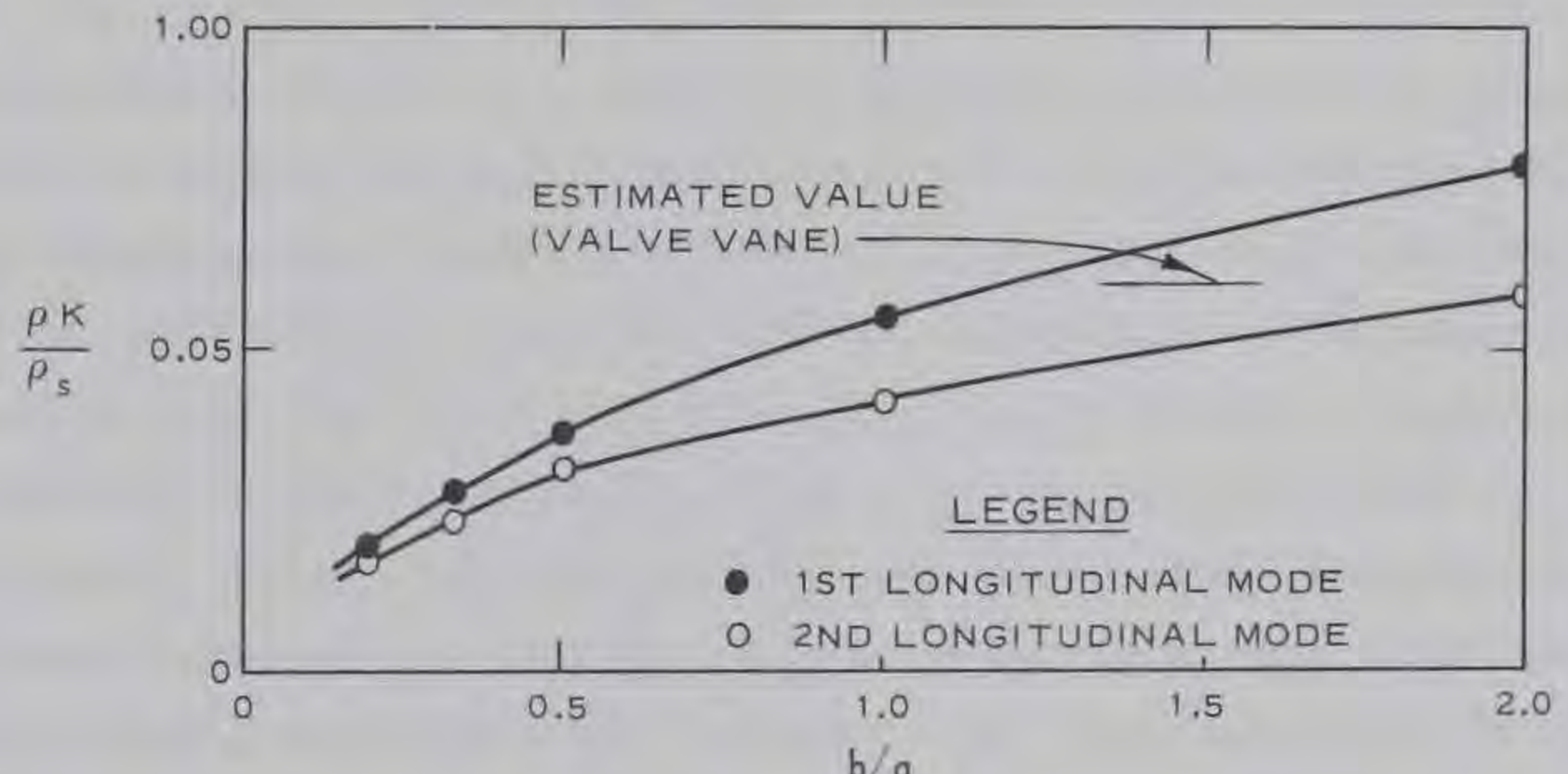


b. ADDED MASS COEFFICIENT (1ST AND 2ND LONGITUDINAL MODES)

Fig. 17. Added mass for a cantilevered flat steel plate in water (data from Abramson[21])

usable in equation 17a. Fig. 17a illustrates the fact that the added mass coefficient is indeed essentially constant for cantilevered rectangular plates of similar planar dimensions. Fig. 17b illustrates the variation in mean K values for various cantilevered rectangular plate dimensions in the first and second longitudinal modes of vibration. As shown in fig. 17b, a value of $\rho K/\rho_s$ equal to 0.06 is intermediate between values corresponding to the first ($\lambda_p \approx 3.51$*) and second ($\lambda_p \approx 22.0$*) longitudinal modes of vibration for a breadth-to-length ratio of 1.5. This value, $\rho K/\rho_s = 0.06$, is used in the following evaluation of $\lambda_p$.

53. Letting $L_v = 50.375$ in. and $t = 2.33$ in. (see plate 6), $\nu = 0.225$, $E = 30 \times 10^6$ psi, $\rho_s = 7.34 \times 10^{-4}$ lb-sec$^2$/in.$^4$, $\frac{\rho K}{\rho_s} = 0.06$, and $f_1 = 75$ Hz in equation 17a yields the value $\lambda_p = 13.00$. This computed value of $\lambda_p$ is intermediate between the clamped-clamped and simply supported values previously quoted.

54. Fundamental mode of transverse vibration of the valve. The transverse vibration of thin beams is described by Timoshenko,[6] Young,[18] etc. For a uniform beam, the fundamental natural frequency of free vibration is[6]

$$f_2 = \frac{\lambda_b}{2\pi}\sqrt{\frac{EIg}{WL^4}} \qquad (18)$$

in which $\lambda_b = 3.52$ for a cantilevered beam, W is the weight per unit length, L is the length of the beam, and I is the moment of inertia of the beam cross-sectional area about a horizontal axis passing through the beam center line. Letting $L = 13.2$ ft, $W = 10{,}000$ lb/ft, $g = 32.2$ ft/sec$^2$, $E = 30 \times 10^6$ psi, $I = 17.1$ ft$^4$, and $f_2 = 46$ Hz in equation 18 yields the value $\lambda_b = 3.27$. The value of I corresponds to the ribbed valve structure and does not include the shell. Despite the extreme simplification in applying equation 18 to the complex valve structure, the computed value of $\lambda_b$ compares favorably with the published value.

---

* Timoshenko beam theory[6] values.

55. Fundamental mode of torsional vibration of the valve. The fundamental natural frequency of torsional vibration of a vertical shaft with a disc attached is[6]

$$f_3 = \frac{1}{2\pi}\sqrt{\frac{K_t}{I_p}} \tag{19}$$

in which $K_t$ is the torsional stiffness of the shaft and $I_p$ is the mass polar moment of inertia at the disc. When the value of $K_t$ for the valve structure is approximated by $3(t^3DG/3L')$, which applies to the vanes and does not include the shell, and $I_p$ is approximated by $WD^2/8g$, which applies to the valve cone, the torsional stiffness of the valve is

$$f_3 = \frac{\lambda_t}{2\pi}\sqrt{\frac{8t^3Gg}{L'WD}} \tag{19a}$$

in which $\lambda_t$ is a coefficient (which should have a value near unity) and G is the modulus in shear of the valve material. Letting $t = 2.33$ in., $G = 12 \times 10^6$ psi, $g = 32.2$ ft/sec$^2$, $L' = 8.7$ ft (length from valve mounting flange to cone apex), $W = 2540$ lb (weight of cone plus interior cone supports), $D = 106.75$ in., and $F_3 = 25$ Hz in equation 19a, the value $\lambda_t = 1.22$ is obtained. This value is in reasonable agreement with the expected value of unity.

56. The spectral density diagrams for channels V7T, V7B, V5T, and V5B in plates 6 and 7 show that the maximum strain fluctuations occur at low frequencies, that is, frequencies well below the natural frequency of the vanes. The earlier valves at Summersville Dam were constructed of the same material as the current valve; however, the geometry was such that $L_v = 52.5$ in., $t = 1.00$ in., $L = 13.2$ ft, $w = 7400$ lb/ft, and $I = 7.59$ ft$^4$. Therefore, using equations 17a, 18, and 19a, with $\lambda_p = 13.00$, $\lambda_b = 3.27$, and $\lambda_t = 1.22$ and geometrical characteristics of the earlier valves, the natural frequencies of free vibration of the earlier valve are about $f_1 = 22.1$ Hz, $f_2 = 35.7$ Hz, and $f_3 = 7.0$ Hz, respectively. Note that the computed natural frequencies of free vibration of the earlier valve are much lower than the corresponding frequencies of the tested valve.

57. Strouhal number. The spectra for channels PUT and PUB shown in plate 5 show that the maximum pressure fluctuations occur near 2 cps; that is, at a frequency much less than the apparent structural resonant frequencies. A dimensionless parameter $S_t$, termed the Strouhal number, has been used[14] to describe the frequency of vortex shedding in the flow past submerged objects. The Strouhal number is defined as[14]

$$S_t = \frac{fL}{V} \tag{20}$$

in which $f$ is the frequency of vortex shedding, $L$ is a pertinent length dimension (i.e. the cylinder diameter), and $V$ is the mainstream flow velocity. For a circular cylinder, $S_t$ is essentially constant equaling 0.18 for Reynolds numbers in the range $10^3$ to $10^5$; for higher Reynolds numbers, the Strouhal number increases rapidly. Strouhal numbers computed from equation 20 for the flow past the butterfly valve, using $L = 3.0$ ft (the hub diameter) and $V = Q/71.0$ (where 71.0 is the flow-passage cross-sectional area at the center line of the butterfly), are tabulated below for a range of frequencies and discharges.

| | Discharge, cfs | | | |
|---|---|---|---|---|
| Frequency | 6000 | 5000 | 4000 | 3000 |
| 1 | 0.04 | 0.04 | 0.04 | 0.07 |
| 2 | 0.07 | 0.09 | 0.11 | 0.14 |
| 5 | 0.18 | 0.21 | 0.27 | 0.36 |
| 10 | 0.36 | 0.43 | 0.53 | 0.71 |
| 20 | 0.71 | 0.85 | 1.07 | 1.42 |
| 50 | 1.77 | 2.13 | 2.66 | 3.55 |

58. In view of the low-frequency limitations of the analog data reduction procedures (spectral peaks at near-zero frequencies are questionable), the precise frequency (between 0 and 5 Hz) of the peak in the pressure spectra cannot be specified. However, since this frequency range corresponds to reasonable values of $S_t$, as shown in the above listing, the butterfly valve may likely be the source of the fluctuations. If this is

the case, the value $S_t = 0.18$* , which applies to a circular cylinder at lower Reynolds numbers ($10^3$ to $10^5$), may be a reasonable estimate of $S_t$ for the butterfly valve hub at the test Reynolds numbers in the order of $10^7$ to $10^8$ (see paragraph 27).

Amplitude considerations

59. The frequency spectra discussed above do not provide information concerning the phase relations between the many frequency components in the data signal. Since the amplitude of the signal at any time is the summation of each component in the signal, the maximum possible signal would occur if all components were of the same polarity in phase and simultaneously at their maximum individual amplitudes; the minimum possible signal would occur if all components were of the same polarity and simultaneously at their minimum value. These extreme situations are infrequent occurrences in the subject data signals inasmuch as (a) the amplitude of each frequency component is highly time-dependent as indicated by the non-smoothed spectra in plate 7, and (b) each data signal is comprised of many frequency components (plates 5, 6, and 7). An electronic means of inspecting the variation of signal amplitude is provided by means of the amplitude density analyzer.

60. An amplitude density analyzer was used to inspect the amplitudes of the signals strain gage channels V7B, V5B, V7T, and V5T as a function of time. The three characteristics of the signal amplitudes previously presented (paragraph 24) are discussed in the following subparagraphs.

a. Number of zero crossings per second. The analyzer, in conjunction with a digital counter, was used to determine the average number of times per second the signal crossed the zero level. Hence this number (listed in paragraph 24) is the times per second that the amplitude of the flexural strain fluctuation changed sign. For example, the number of zero crossings of a sinusoidal signal is equal to twice the frequency of the signal. The results from this analysis converted to equivalent harmonic frequencies are as follows.

---

* The value of $S_t$ agrees with values obtained by Burkart and Macovsky[22] and Delaney and Sorenson[23] who studied the Strouhal variation in the wakes of various geometric models. For example, data[23] show $S_t = 0.12$ for a 2:1 ellipse and $S_t = 0.40$ for a 2:1 rectangular cylinder (parallel to the flow) for Reynolds numbers near $10^6$.

Note that the equivalent harmonic frequencies do not coincide with any natural frequency appearing in the spectral plots.

| Channel | Dial Reading % | Zero Crossings per Second | Equivalent Harmonic Frequency, Hz |
|---|---|---|---|
| V5T | 90 | 86.6 | 43.3 |
| V7T | 90 | 100.0 | 50.0 |
| V5B | 90 | 70.1 | 35.1 |
| | 80 | 56.5 | 28.3 |
| | 70 | 51.0 | 25.5 |
| | 60 | 47.2 | 23.6 |
| V7B | 90 | 86.1 | 43.1 |
| | 80 | 69.4 | 34.7 |
| | 70 | 60.5 | 30.3 |
| | 60 | 52.1 | 26.1 |

b. Probability density function. The analyzer electronically determined the statistical probability that the signal was at a particular amplitude level at a particular time. A small extent of amplitude, termed the window-width, and equaling one-tenth of the calibration step value (see plate 8) was inspected by the analyzer whose output is a measure of the percentage of time the signal is within the window. By ranging the window through the range of amplitudes that exist in the signal, probability distribution functions were obtained. The probability distribution functions for channels V5T, V7T, V5B, and V7B, as listed above, were previously presented in plate 8. The distribution curves in plate 8 show that the amplitudes of the strain fluctuations are essentially uniformly distributed with a near-zero mean value.

c. Cumulative density function. At any time, it is statistically (and physically) possible for the measured fluctuating flexural strains to have unusually high or unusually low values. Since the rare extreme values do not contribute significantly to the fatigue of the vane material, a means of determining a significant amplitude of strain (or stress) fluctuation is required. The probability that strain fluctuations were equal to or less than a particular amplitude was shown in the cumulative probability density diagrams in plate 8. The 99, 97.5, 95, and 90 percent levels (for maximum strains) and the corresponding 1, 2.5, 5, and 10 percent levels (for minimum strains) shown in plate 8 were converted to stress ($E = 30 \times 10^6$ psi) and are listed in table 4. As shown in the table, the peak-to-peak stress fluctuations measured from the oscillograph chart are roughly equivalent to the 5 to 95 percent $\Delta\sigma_f$ values determined by the amplitude density analyzer.

Correlograms

61. Three cross-correlation diagrams were previously presented in plate 9. The amplitude axes of the correlation curves were not calibrated with regard to the calibration steps placed on the relevant strain or pressure recordings. Hence the retrievable information in these diagrams pertains to (a) the sign product (+ or -) and the time delay for maximum correlation between two signals, and (b) phase relations of harmonic components that exist in both signals. General considerations in the interpretation of correlation functions are discussed by LuBow[24]; details of correlation analysis are available in texts such as Robson.[7] Inspection of these diagrams following LuBow[24] reveals the following information.

a. P7R cross-correlated with V7T. At zero time lag these two channels are opposite in sign. This is in general agreement with the strain sign convention shown previously in fig. 11. Note that since no operable magnetic tape data were obtained for channel P7L, the cross-correlation represents the loading on one side of the vane and not the net loading on the vane. A higher frequency time signal (74-96 Hz) occurs in channels P7R and V7T; the component of the pressure signal having this frequency lags the similar component in the strain signal by approximately 0.031 sec.

b. P7R cross-correlated with V7B. The above remarks also pertain to this correlogram. The higher order frequency that occurs in both signals is about 94 Hz and the lag time is 0.051 sec.

c. V7B cross-correlated with V5B. At zero time lag these two channels are opposite in sign. The vanes therefore tend to vibrate between the dashed and solid curves sketched in fig. 18. Note that considering a and b above, channels V7T and V7B are of the same sign at zero time lag. The common frequency component (ranging from about 67-83 Hz)

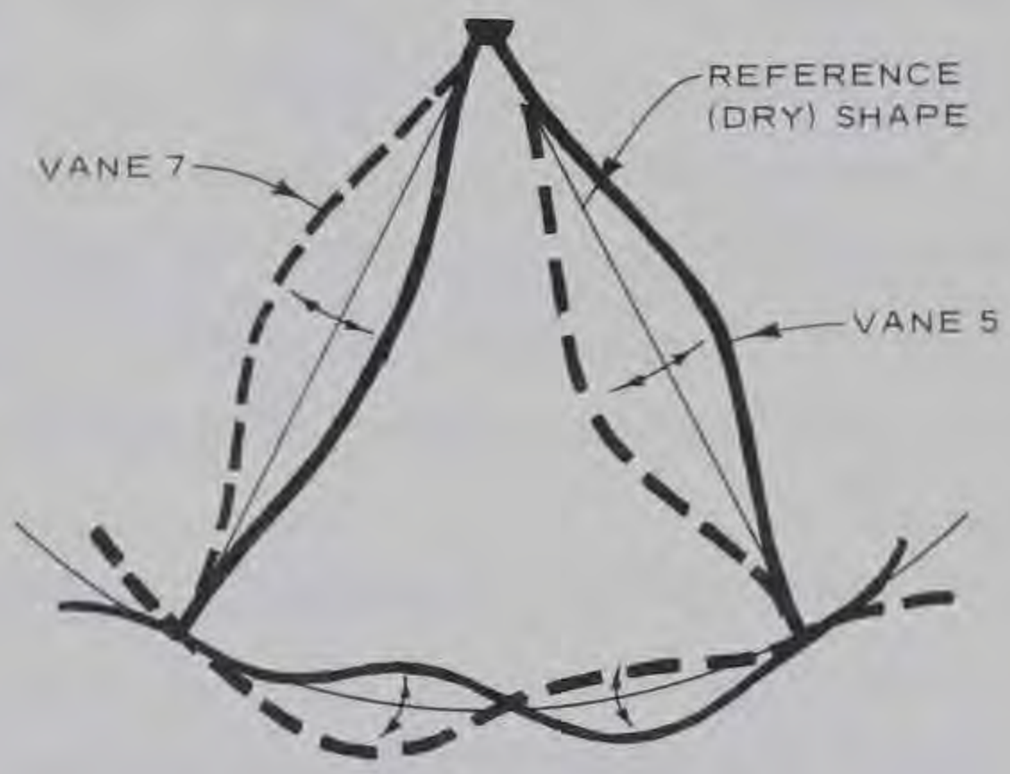


Fig. 18. Vibration of the valve (looking downstream and not to scale). Note that the shell is forced into its sixth natural mode shape[4]

appears to be a natural frequency of the valve structure; and the value 75 Hz previously observed in the linear spectral density diagrams is a reasonable average value.

62. An apparent tendency of the vanes toward self-excitation occurs at a frequency of about 95 Hz (see correlograms corresponding to a and b above). Self-excitation (at an extremely low stress level) is suggested since:

a. The harmonic in the strain signal precedes the same harmonic in the pressure signal. Whenever the vane is subjected to transverse forces due to vortices being shed from the mainstream flow at the leading edge of the vane and the shedding being triggered by the vibration, this sequence of signals will occur.

b. The apparent excitation frequency (about 95 Hz) is sufficiently greater than the natural frequency (about 75 Hz) of the vanes so that it is unlikely that the 95 Hz signal is the consequence of variations in the natural frequency of the vane.

63. Self-excited vibrations of flat plates, as described by Gongwer[25] and Ippen et al.,[26] result from periodic forces created as vortices are generated in the near wake of a flat plate. In particular, for a flat plate with a square trailing edge, Ippen et al.[26] show that the frequency of the periodic forces corresponds to a Strouhal number $S_t$ (see paragraph 55) of about 0.219-0.240. The pertinent length dimension in equation 20 is the thickness of the trailing edge; the velocity is the velocity normal to the trailing edge. Both studies[25,26] show that whenever the Strouhal frequency is near a natural frequency of the plate structure, resonant self-excited vibration occurs. In particular when the natural frequency of structural vibration is within the audible range and the resonant self-excited vibration condition exists, then vane "singing" may occur.[25]

64. The vane Strouhal number for $f = 95$ Hz, $L = 2.33$ in., and $V = 117.2$ fps* is, from equation 20, 0.157. Since the velocity normal to the trailing edge of the vane is less than the free jet velocity, due to

---

* $V$, the exit velocity from the valve, is approximately equal to $\sqrt{2g(H_V - 1390.1)}$ where 1390.1 is the elevation in ft msl of the exit edge of vanes 5 and 7 and $H_V$ is the total head in the flow in the valve as discussed in paragraph 30.

the geometry at the valve exit, this value of the Strouhal number is in reasonable agreement with published values[26] (i.e., $S_t \gtrsim \sqrt{2}(0.157) = 0.22$ which falls in the range 0.219-0.240 given above). Consequently, it is likely that this type of self-excitation does occur and is probably the primary reason for the amplification of the vane natural frequency (75 Hz) as shown in the spectral density plots (plates 6 and 7).

65. Knowing a vane natural frequency, the corresponding critical exit velocity $\left(V = \sqrt{2g(H_v - 1390.1)}\right)$ can be evaluated by means of equation 20 with $S_t = 0.157$. Thus the corresponding discharges can be computed (equation 5) for particular Howell-Bunger valve openings and the corresponding reservoir elevations for which self-excitation will occur can be evaluated from values given in plate 10. The results of these calculations are tabulated below.

| Valve | Mode | Natural Frequency* Hz | Critical Velocity $\sqrt{2g(H_v - 1390.1)}$ fps | Critical Reservoir Elevation $Z_R$, ft msl** Dial Reading 0% | Dial Reading 90% |
|---|---|---|---|---|---|
| New | 1 | 75 | 92.8 | 1521 | 1554 |
| | 2 | 206 | 254.8 | Above 1710 | Above 1710 |
| Original | 1 | 22.1 | 11.7 | Below 1464 | Below 1464 |
| | 2 | 60.8 | 32.3 | Below 1464 | Below 1464 |
| | 3 | 118.9 | 63.1 | Below 1464 | Below 1464 |
| | 4 | 196.2 | 104.1 | 1555 | 1591 |
| | 5 | 294 | 156.1 | Above 1710 | Above 1710 |

* The fundamental natural frequencies are multiplied by factors $(7.853/4.73)^2$, $(10.996/4.73)^2$, $(14.137/4.73)^2$, and $(17.279/4.73)^2$ to estimate the higher mode natural frequencies; these values correspond to a Timoshenko[6] clamped-clamped beam.

** Spillway crest el 1710 ft msl; intake el 1464 ft msl.

66. The following points should be recognized in considering self-excitation of the Howell-Bunger valve vane:

a. The fluctuating stresses produced in the vane at the self-excitation frequency are much lower in magnitude than the stresses produced at very low frequencies (see plates 6 and 7) and, consequently, were probably not a major factor in the earlier valve failure.

b. Amplification of the vibration at the structural natural

frequency occurs for a considerable range of Strouhal frequencies (see references 25 and 26), and consequently, audible self-excitation (singing) occurs in a range of reservoir elevations on either side of the critical reservoir elevations tabulated above.

## PART V: SUMMARY OF RESULTS

### General Hydraulic Considerations

Flow coefficients and discharge rating curves

67. The following relations, which are presented and evaluated in paragraphs 26-38, are applicable to Summersville Dam outlet works when operated in the same manner as during the subject tests (see paragraphs 11 and 12).

a. Head loss in between the reservoir and US:

$$H_L = 0.46 \frac{V_o^2}{2g} \tag{1}$$

b. Head loss between US and the Howell-Bunger valve (includes butterfly valve and reducer):

$$H_L = \frac{Q^2}{5.76gD_o^2} \tag{4}$$

c. Flow rate through the Howell-Bunger valve:

$$Q = C_D A_v \sqrt{2g(H_v - 1393.7)} \tag{5}$$

with $C_D$ values as shown in fig. 13.

d. Outlet works rating curve equation:

$$Q = \frac{C_D A_v}{\left(1 + 0.288C_D^2\right)^{1/2}} \sqrt{2g(Z_R - 1393.7)} \tag{7}$$

e. Cavitation index. The rating curve equation 7 is valid whenever the cavitation index, $\sigma_c$ in paragraphs 37 and 38,

is greater than or equal to 3.3; that is, whenever

$$\frac{\frac{P_o}{\gamma} - \frac{P_v}{\gamma}}{\frac{V_o^2}{2g}} \geq 3.3 \qquad (8)$$

Flow conditions between butterfly valve and Howell-Bunger valve

68. The following conditions pertain to the flow in the wake of the butterfly valve:

a. Cavitation. The Euler numbers presented in plate 11 show that:

(1) Localized cavitation occurs in the reducer immediately downstream from the butterfly valve.

(2) The cavitation does not measurably alter the mean flow pattern entering the valve.

b. Flow symmetry. The flow pattern entering the valve is non-symmetrical about a vertical axis as noted in paragraphs 40-42.

c. Pressure fluctuation peak-to-peak amplitude. The magnitudes of the pressure fluctuations along the wall of the conduit are expressed (paragraph 43) as:

(1) At the reducer

$$\frac{P_{max} - P_{min}}{\gamma} \approx 0.16 \frac{(V_{VN})^2}{2g} \qquad (12)$$

(2) In the valve

$$\frac{P_{max} - P_{min}}{\gamma} \approx 0.05 \frac{(V_{VN})^2}{2g} \qquad (13)$$

In other words, the pressure fluctuations are reduced by approximately 70 percent between the reducer and the

Howell-Bunger valve. Pressure fluctuations alongside the vanes are expressed as (paragraph 43):

(1) At small dial readings

$$\frac{P_{max} - P_{min}}{\gamma} \approx 0.05 \frac{(V_{VN})^2}{2g} \tag{13}$$

(2) At large dial readings (60-90% as shown in plate 12)

$$\frac{P_{max} - P_{min}}{\gamma} \approx 0.075 \frac{(V_{VN})^2}{2g} \tag{14}$$

d. Pressure fluctuation frequency. The dominant frequencies of the fluctuating pressure pulses are between 0 and 10 Hz (see paragraph 58) with a peak value occurring in the range 0.5-5 Hz (see plates 4 and 5).

e. Source of the pressure fluctuations. Consideration of the Strouhal number (paragraph 58) in conjunction with the PUT spectra (plate 5) and equations 12 and 13 above shows that the dominant pressure pulses probably originate at the butterfly valve.

## Howell-Bunger Valve Structural Considerations

### Steady-state stresses

69. The maximum steady-state flexural stress, equaling 2400 psi, occurred at channel S7L at zero dial reading (paragraph 41). The maximum time-averaged vane flexural stress of 1080 psi occurred at V7B at 90% dial reading.

### Natural frequencies

70. The three lowest natural frequencies observed in the linear spectral density diagrams occurred at about 25, 46, and 75 Hz (plates 5, 6, and 7). These were determined to be the fundamental frequencies of free torsional and transverse vibration of the cantilevered valve and of free transverse vibration of the vanes. The determination was based on pertinent frequency spectra and on the approximate analyses of the vibration of

valve components. The following relations are suggested to be used as estimates of natural frequencies in similar Howell-Bunger valves:

(1) Torsional vibration of the cantilevered valve (paragraph 55)

$$f_3 = \frac{1.22}{2\pi}\sqrt{\frac{8t^3Gg}{L'WD}} \tag{19a}$$

(2) Transverse vibration of the cantilevered valve (paragraph 54)

$$f_2 = \frac{3.27}{2\pi}\sqrt{\frac{EIg}{WL^4}} \tag{18}$$

(3) Transverse vibration of a vane (paragraphs 50-53)

$$f_1 = \frac{13.00}{2\pi L_v^2}\sqrt{\frac{Et^3/(12)(1-\nu^2)}{\rho_s t\left(1+\frac{\rho K L_v}{\rho_s t}\right)}} \tag{17a}$$

Equations 17a, 18, and 19a, above, do not supplant the need for a dynamic analysis of the valve vibration characteristics nor can their accuracy be determined unless further testing on geometrically different valves is performed. They are used herein, paragraph 56, only to estimate comparable frequencies in the original valve.

Comparison with the original valve

71. A comparison of the measured response characteristics of the new valve with the computed* characteristics of the original valve is as follows:

---

* The change in orientation of the two valves is not considered in this comparison.

| Response Characteristic | Paragraph No. | New Valve | Original Valve |
|---|---|---|---|
| 1. Maximum fluctuating stress, psi (neutral to peak, oscillograph data, fig. 16) | (41, 46) | 1770* | 9,600** |
| 2. Fluctuating stress, psi (neutral to peak, magnetic tape 2% greater or less than, table 4) | (41, 60) | 2750* | 14,900** |
| 3. $f_1$, Hz (vane in transverse motion) | (49, 56) | 75 | 22.1 |
| 4. $f_2$, Hz (valve in transverse motion) | (49, 56) | 46 | 35.7 |
| 5. $f_3$, Hz (valve in torsion) | (49, 56) | 25 | 7.0 |

* V5B at 90% dial reading.
** 5.42 times the comparable value in new valve.

72. The flow-induced vibrations in the original valve were of sufficient magnitude so as to cause initial fatigue failure of the vanes followed by more complete failure due to the large stagnation pressures of the high-velocity jets. For sustained valve operation a low-frequency stress reversal can be significant with regard to fatigue failure. For example, stress reversals at 1 Hz total about $2.4 \times 10^7$ stress reversals per year of continuous operation. With no structural resonance, the magnitude of the fluctuating stresses that occurred in the original vanes (tabulated above) due to low-frequency buffeting by pressure fluctuations (discussed in paragraph 63) in the flow were probably too large to tolerate in a climate amenable to fatigue failure. However, the original valve failure was unquestionably premature due to the tendency toward resonance at the relatively low natural frequencies of the earlier vanes. The new valve is a better design. First, the measured low-frequency stresses are well below the fatigue* limit of the vane material. Second, the natural frequencies of the valve ($f_1$, $f_2$, and $f_3$) are well separated and well above the frequency of the pressure fluctuations in the flow.

* Jacob Herman, unpublished communication to author, Sept 1968.

## Recommendations

### Periodic inspections of Summersville Howell-Bunger valve

73. Since the fluctuating stresses measured in the valve are well below the endurance limit of the valve metal, no structural modifications are deemed necessary; however, careful periodic inspections of regions in which stress concentrations are expected should be performed. If fatigue cracks appear, a suitable modification of the valve or of the immediate upstream flow passage should be developed by means of model tests.

### Future designs

74. Three dominant factors that probably contributed to the failure of the earlier valve are: (a) severe pressure fluctuations existed in the flow, (b) the valve vanes were structurally inadequate to withstand the large low-frequency pressure fluctuations, and (c) the vane and valve natural frequencies were low (i.e. the higher frequency pressure fluctuations were in resonance with the structural frequencies). These three factors should not exist at future installations provided (a) the flow passage upstream of the valve is well streamlined and convergent near the valve, and (b) the elastic properties of the valve and vanes are considered in the design. Ippen et al.[26] show that a reentrant trailing edge will reduce the amplitude of self-excited vibration; if a low-pitched sound accompanying valve operation is considered troublesome, then a change in vane trailing-edge geometry may be in order.

### Analytical studies

75. An analytical study, probably utilizing numerical methods, of the elastic properties of the Howell-Bunger valve is needed. In this regard the effect of the ratio of vane thickness to shell thickness, which has not been considered herein but which is an important design factor, should be evaluated.

### Additional prototype tests

76. A range of Howell-Bunger valve sizes (including 4-, 6-, and 8-vane valves) and geometries should be studied in the field. Note that most key vibration measurements, such as pressure and strain fluctuations in the valve, would be difficult to obtain from model tests whereas they are well

defined in the prototype data. In addition to data taken during such tests, a precise measurement of discharge is required in order to evaluate the change in discharge coefficient due to changes in interior valve geometry and to provide more precise rating values. Note that the prototype tests complement the above-suggested analytical study and that the analytical study would considerably reduce the number of field tests required to define the valve response.

# LITERATURE CITED


1. Elder, R. A. and Dougherty, G. B., "Characteristics of Fixed-Dispersion Cone Valves," Transactions, American Society of Civil Engineers, Vol 118, Paper No. 2567, 1953, pp 907-945; includes discussions by E. W. Murphy, R. E. Ballester, T. T. Siao, V. Gongwer, R. A. Elder, and G. B. Dougherty.

2. Davis, V. D. and Sorenson, K. E., editors, Handbook of Applied Hydraulics, 3d ed., McGraw-Hill, New York, 1969.

3. Kohler, W. H. and Ball, J. W., "High-Pressure Outlets, Gates, and Valves," Handbook of Applied Hydraulics, 3d ed., McGraw-Hill, New York, 1969, Section 22, pp 22-1 - 22-116.

4. Campbell, F. B., "Vibration Problems in Hydraulic Structures," Journal, Hydraulics Division, American Society of Civil Engineers, Vol 87, No. HY2, Paper No. 2772, Mar 1961, pp 61-77; discussions by D. W. Appel, A. L. Sanford, and H. L. Uppal, Vol 87, No. HY6, Nov 1961, pp 207-215.

5. Thomson, W. T., Vibration Theory and Applications, Prentice-Hall, Englewood Cliffs, N. J., 1965.

6. Timoshenko, S. and Young, D. H., Vibration Problems in Engineering, 3d ed., Van Nostrand, New York, 1955.

7. Robson, J. D., An Introduction to Random Vibration, Elsevier, Amsterdam, N. Y., 1964.

8. Flügge, W., ed., Handbook of Engineering Mechanics, McGraw-Hill, New York, 1962.

9. Toebes, G. H., "Flow-Induced Structural Vibrations," Journal, Engineering Mechanics Division, American Society of Civil Engineers, Vol 91, No. EM6, Paper No. 4564, Dec 1965, pp 39-66.

10. Heller, S. H., "Hydro-elasticity," Advances in Hydroscience, V. T. Chow, ed., Vol 1, Academic Press, New York, 1964.

11. Hart, E. D., "Pressure Tests in Flood-Control Conduits, Summersville Dam, Gauley River, West Virginia," Miscellaneous Paper No. 2-988, Apr 1968, U. S. Army Engineer Waterways Experiment Station, CE, Vicksburg, Miss., April 1968.

12. U. S. Army Engineer Waterways Experiment Station, CE, "Butterfly Valves; Discharge Coefficients, Valve in Pipe," Hydraulic Design Chart 331-1, Aug 1958, Hydraulic Design Criteria, Vol II, Vicksburg Miss.

13. _____, "Howell-Bunger Valves; Discharge Coefficients, Six Vanes," Hydraulic Design Chart 332-1/1, Feb 1954, Hydraulic Design Criteria, Vol II, Vicksburg, Miss.

14. Rouse, H., Engineering Hydraulics, Wiley, New York, 1950.

15. _____, Elementary Mechanics of Fluids, Wiley, New York, 1946.

16. Laufer, J., "The Structure of Turbulence in Fully Developed Pipe Flow," NACA 1174, 1954, National Aeronautics and Space Administration, Washington, D. C.

17. Batchelor, G. K., The Theory of Homogeneous Turbulence, Cambridge Press, New York, 1956.

18. Young, D., "Continuous Systems," Handbook of Engineering Mechanics, W. Flügge, ed., McGraw-Hill, New York, 1962, Chapter 61.

19. Dryden, H. L., Murnaghan, F. D., and Bateman, H., Hydrodynamics, Dover, New York, 1956, pp 97-101.

20. Lamb, H., Hydrodynamics, 6th ed., Dover, New York, 1945, pp 84-85.

21. Abramson, H. N., "Hydroelasticity--Some Problems and Some Solutions," Fluid Solid Interaction, J. E. Greenspan, ed., 1967, pp 187-222.

22. Burkart, M. P. and Macovsky, M. S., "Study of Hydrodynamic Parameters for Design of a Strut Suitable for Electromagnetic Rodmeter," Report No. 1027, Mar 1956, David W. Taylor Model Basin, Washington, D. C.

23. Delaney, N. K. and Sorenson, N. E., "Low-Speed Drag of Cylinders of Various Shapes," NACA Technical Note 3038, Nov 1953, National Advisory Committee for Aeronautics, Washington, D. C.

24. LuBow, B., "Correlation Entering New Fields with Real-Time Signal Analysis," Electronics, Vol 39, No. 22, 31 Oct 1966, pp 75-81.

25. Gongwer, C. A., "A Study of Vanes Singing in Water," Journal of Applied Mechanics, Transactions, American Society of Mechanical Engineers, Vol 19, No. 4, Dec 1952, pp 432-438.

26. Ippen, A. T., Toebes, G. H., and Eagleson, P. S., "The Hydroelastic Behavior of Flat Plates as Influenced by Trailing Edge Geometry," Technical Report No. 36, Apr 1960, Massachusetts Institute of Technology, Hydrodynamics Laboratory, Cambridge, Mass.

Table 1

Temporal Mean Pressures

| Dial Reading % | Pressure, psi | | | | | |
|---|---|---|---|---|---|---|
| | US | PUT | PUB | PDT* | PS8* | VG |
| | 27 March 1968, Reservoir El 1368.8 | | | | | |
| 0 | 98.0 | 104.0 | 108.0 | 105.0 | 107.0 | 97.5 |
| 30 | 91.0 | 93.5 | 93.5 | 90.0 | 93.5 | 84.2 |
| 40 | 87.5 | 85.5 | 85.5 | 81.0 | 83.5 | 76.0 |
| 50 | 81.5 | 77.0 | 78.5 | 71.5 | 73.5 | 65.0 |
| 60 | 76.0 | 70.0 | 70.5 | 61.0 | 62.0 | 53.5 |
| 70 | 70.0 | 57.5 | 58.5 | 48.5 | 50.0 | 42.5 |
| 75 | 67.5 | 50.5 | 54.0 | 40.0 | 45.0 | 37.5 |
| 80 | 65.5 | 47.5 | 49.0 | 36.0 | 37.0 | 32.0 |
| 85 | 63.0 | 43.5 | 47.0 | 32.0 | 32.0 | 26.5 |
| 90 | 60.0 | 37.0 | 40.0 | 23.5 | 27.5 | 21.0 |
| Piez el | 1413.3** | 1398.3 | 1389.2 | 1395.9 | 1391.4 | 1413.3** |

| | Pressure, psi | | | | | | | | |
|---|---|---|---|---|---|---|---|---|---|
| | US | PUT | PUB | PS4 | PS6 | P5L | P5R | P7L | P7R |
| | 29 March 1968, Reservoir El 1642.7 | | | | | | | | |
| 0 | 99.5 | 106.0 | 110.0 | 109.0 | 111.0 | 108.5 | 108.5 | 108.5 | 108.5 |
| 30 | 92.5 | 90.5 | 85.5 | 96.5 | 96.5 | 95.0 | 95.0 | 93.0 | 89.0 |
| 40 | 88.5 | 84.5 | 79.5 | 85.5 | 87.5 | 85.0 | 84.0 | 83.5 | 81.0 |
| 50 | 84.0 | 76.0 | 71.5 | 75.5 | 76.0 | 72.0 | 73.0 | 80.0 | 68.0 |
| 60 | 78.5 | 66.5 | 66.5 | 63.5 | 65.5 | 60.0 | 60.0 | 56.0 | 55.5 |
| 70 | 73.0 | 55.5 | † | 50.5 | 52.5 | 48.0 | 46.5 | 42.0 | 44.0 |
| 75 | 70.5 | 51.0 | 51.0 | 45.0 | 48.5 | 42.5 | 40.5 | 32.0 | 37.0 |
| 80 | 67.5 | 45.5 | 43.0 | † | 42.0 | 35.5 | 36.5 | † | 28.0 |
| 85 | 65.0 | 40.0 | † | † | 36.5 | 29.0 | 30.0 | † | 20.5 |
| 90 | 62.5 | † | 36.0 | † | 32.0 | 23.5 | † | † | 15.0 |
| Piez el | 1413.3** | 1398.3 | 1389.2 | 1391.4 | 1389.2 | 1391.7 | 1391.7 | 1391.7 | 1391.7 |

Note: All elevations are in feet referred to mean sea level.
* Channels PDT and PS8 became inoperable during testing.
** Gage elevation.
† Data not recoverable.

Table 2

Euler Numbers

| Dial Reading % | $\frac{V_o^{2*}}{2g}$ ft | Values of $E_1 = \frac{Z_R - h}{V_o^2/2g}$ | | | | | |
|---|---|---|---|---|---|---|---|
| | | US** | PUT | PUB | PDT | PS8 | VG |
| | | | 27 March | | | | |
| 30 | 10.8 | 1.46 | 2.29 | 3.13 | 3.26 | 2.93 | 2.97 |
| 40 | 16.3 | 1.46 | 2.65 | 3.21 | 3.43 | 3.35 | 3.08 |
| 50 | 25.8 | 1.46 | 2.43 | 2.65 | 3.02 | 3.01 | 2.93 |
| 60 | 34.5 | 1.46 | 2.29 | 2.52 | 2.96 | 3.02 | 2.96 |
| 70 | 44.0 | 1.46 | 2.45 | 2.60 | 2.98 | 3.00 | 2.90 |
| 75 | 47.9 | 1.46 | 2.59 | 2.61 | 3.14 | 3.00 | 2.90 |
| 80 | 51.1 | 1.46 | 2.56 | 2.67 | 3.13 | 3.17 | 2.97 |
| 85 | 55.1 | 1.46 | 2.54 | 2.56 | 3.07 | 3.15 | 2.98 |
| 90 | 59.9 | 1.46 | 2.59 | 2.63 | 3.15 | 3.07 | 2.96 |
| | Mean values | 1.46 | 2.49 | 2.73 | 3.13 | 3.08 | 2.96 |

| Dial Reading % | Values of $E_1 = \frac{Z_R - h}{V_o^2/2g}$ | | | | | | | | |
|---|---|---|---|---|---|---|---|---|---|
| | US | PUT | PUB | PS4 | PS6 | P5L | P5R | P7L | P7R |
| | | | 29 March | | | | | | |
| 30 | 11.1 | 1.46 | 3.20 | 5.06 | 2.68 | 2.77 | 2.86 | 2.76 | 3.28 | 4.11 |
| 40 | 17.4 | 1.46 | 2.84 | 4.02 | 3.10 | 2.96 | 3.15 | 3.28 | 3.35 | 3.68 |
| 50 | 24.5 | 1.46 | 2.82 | 3.61 | 3.14 | 3.19 | 3.46 | 3.37 | 3.56 | 3.84 |
| 60 | 33.1 | 1.46 | 2.75 | 3.02 | 3.16 | 3.09 | 3.40 | 3.40 | 3.68 | 3.71 |
| 70 | 42.0 | 1.46 | 2.77 | -- | 3.21 | 3.15 | 3.34 | 3.42 | 3.67 | 3.56 |
| 75 | 45.8 | 1.46 | 2.77 | 2.96 | 3.22 | 3.09 | 3.34 | 3.44 | 3.87 | 3.62 |
| 80 | 50.5 | 1.46 | 2.76 | 3.05 | -- | 3.10 | 3.34 | 3.30 | -- | 3.69 |
| 85 | 54.5 | 1.46 | 2.79 | -- | -- | 3.11 | 3.35 | 3.34 | -- | 3.74 |
| 90 | 58.4 | 1.46 | -- | 2.92 | -- | 3.08 | 3.38 | -- | -- | 3.71 |
| | Mean values | 1.46 | 2.84 | 3.52 | 3.09 | 3.06 | 3.29 | 3.29 | 3.57 | 3.74 |

* $V_o = Q_T/A_o$ .
** $E_1$ at US = $K_L = 1$ .

Table 3

Nondimensional Pressure Fluctuations

29 March

| Dial Reading % | $\frac{(V_{VN})^2}{2g}$ ft | $\frac{(P_{max} - P_{min})/\gamma}{(V_{VN})^2/2g}$ | | | | | | | | | |
|---|---|---|---|---|---|---|---|---|---|---|---|
| | | PUT | PUB | PS4 | PS6 | P5L | P5R | P7L | P7R | PDT | PS8 |
| 30 | 29.1 | 0.198 | 0.222 | 0.0555 | 0.0476 | 0.0793 | 0.0952 | 0.0000 | 0.0000 | 0.0818 | 0.0409 |
| 40 | 46.1 | 0.175 | 0.165 | 0.0451 | 0.0651 | 0.0501 | 0.0501 | 0.0000 | 0.0000 | 0.1015 | 0.0427 |
| 50 | 65.6 | 0.141 | 0.116 | 0.0422 | 0.0493 | 0.0633 | 0.0528 | 0.0493 | 0.0528 | 0.0805 | 0.0268 |
| 60 | 89.0 | 0.143 | 0.148 | 0.0519 | 0.0441 | 0.0519 | 0.0493 | 0.0596 | 0.0752 | 0.0598 | 0.0299 |
| 70 | 113.1 | 0.133 | 0.145 | 0.0551 | 0.0408 | 0.0469 | 0.0531 | 0.0653 | 0.0490 | 0.0564 | 0.0194 |
| 75 | 123.5 | 0.198 | 0.150 | 0.0505 | 0.0411 | 0.0430 | 0.0430 | 0.0673 | 0.0729 | 0.0519 | 0.0285 |
| 80 | 136.5 | 0.179 | 0.159 | 0.0524 | 0.0490 | 0.0710 | 0.0845 | -- | 0.0485 | 0.0418 | -- |
| 85 | 147.4 | 0.174 | -- | -- | 0.0470 | 0.0767 | 0.0705 | 0.0705 | -- | 0.0449 | 0.0418 |
| 90 | 158.2 | 0.147 | -- | -- | 0.0438 | 0.0744 | -- | 0.0729 | -- | 0.0484 | 0.0399 |
| 95 | (158.2) | -- | -- | -- | 0.0496 | 0.0861 | -- | 0.0729 | -- | 0.0708 | 0.0462 |
| Average values | | 0.165 | 0.158 | 0.0504 | 0.0477 | 0.0643 | 0.0623 | 0.0509 | 0.0426 | 0.0638 | 0.0351 |

Table 4

Comparison of Magnetic Tape and Oscillograph Stress Results

| Channel | Dial Reading % | Oscillograph* (Peak-to-Peak) | Stress Fluctuations, psi | | | | | | | | | | | |
|---|---|---|---|---|---|---|---|---|---|---|---|---|---|---|
| | | | 2% Level | | | 5% Level | | | 10% Level | | | 20% Level | | |
| | | | 99 (Max) | 1 (Min) | $\Delta\sigma_f$** | 97.5 (Max) | 2.5 (Min) | $\Delta\sigma_f$ | 95 (Max) | 5 (Min) | $\Delta\sigma_f$ | 90 (Max) | 10 (Min) | $\Delta\sigma_f$ |
| V7T | 90 | 2070 | 1890 | 1890 | 3780 | 1510 | 1430 | 2930 | 1130 | 860 | 1990 | 760 | 590 | 1350 |
| V5T | 90 | 2970 | 2160 | 2020 | 4180 | 1620 | 1620 | 3240 | 1290 | 1130 | 2420 | 760 | 810 | 1570 |
| V7B | 90 | 2400 | 2130 | 1950 | 4080 | 1640 | 1620 | 3260 | 1300 | 1300 | 2600 | 810 | 810 | 1620 |
| | 80 | 2010 | 1750 | 1860 | 3610 | 1350 | 1350 | 2700 | 1000 | 920 | 1920 | 590 | 540 | 1130 |
| | 70 | 1530 | 1460 | 1300 | 2760 | 1130 | 920 | 2050 | 960 | 760 | 1730 | 590 | 490 | 1080 |
| | 60 | 1260 | 1130 | 1080 | 2210 | 890 | 1130 | 2020 | 730 | 760 | 1490 | 460 | 490 | 950 |
| V5B | 90 | 3930 | 2750 | 2750 | 5500 | 2220 | 2190 | 4410 | 1840 | 1670 | 3510 | 1110 | 1080 | 2190 |
| | 80 | 2850 | 2290 | 2210 | 4500 | 1840 | 1890 | 3730 | 1350 | 1570 | 2920 | 810 | 1030 | 1840 |
| | 70 | 1980 | 1620 | 1400 | 3020 | 1350 | 1080 | 2430 | 1030 | 810 | 1840 | 590 | 490 | 1080 |

* From paragraph 44.
** $\Delta\sigma_f$ is the peak-to-peak stress fluctuation.

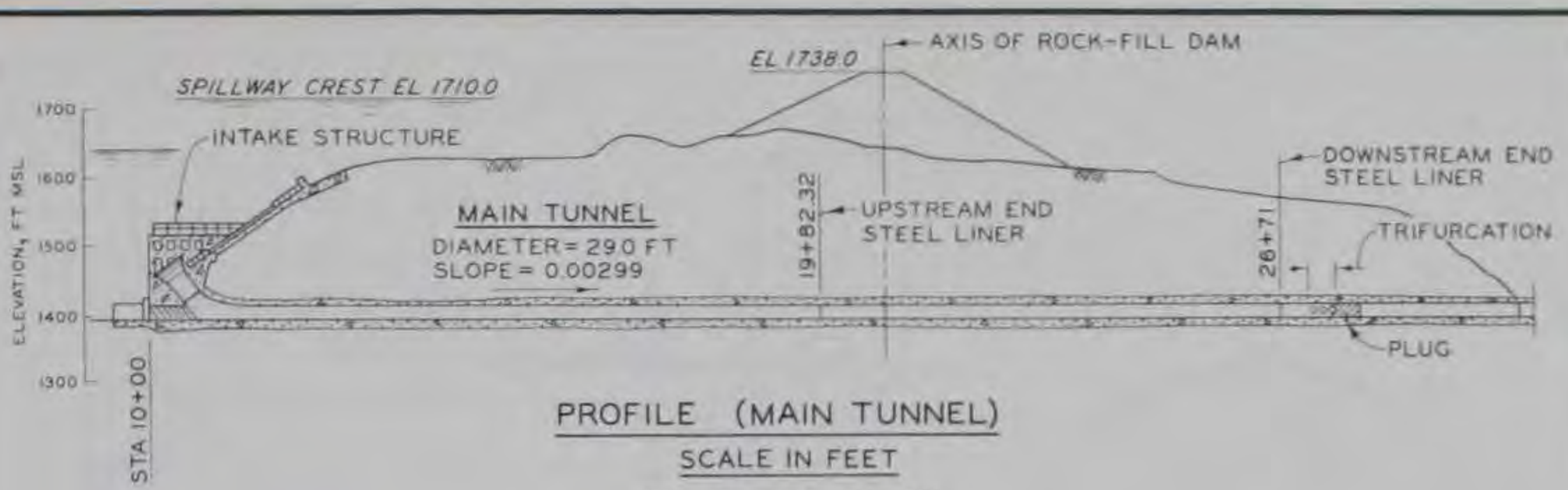


PROFILE (MAIN TUNNEL)

SCALE IN FEET

100 0 100 200 300

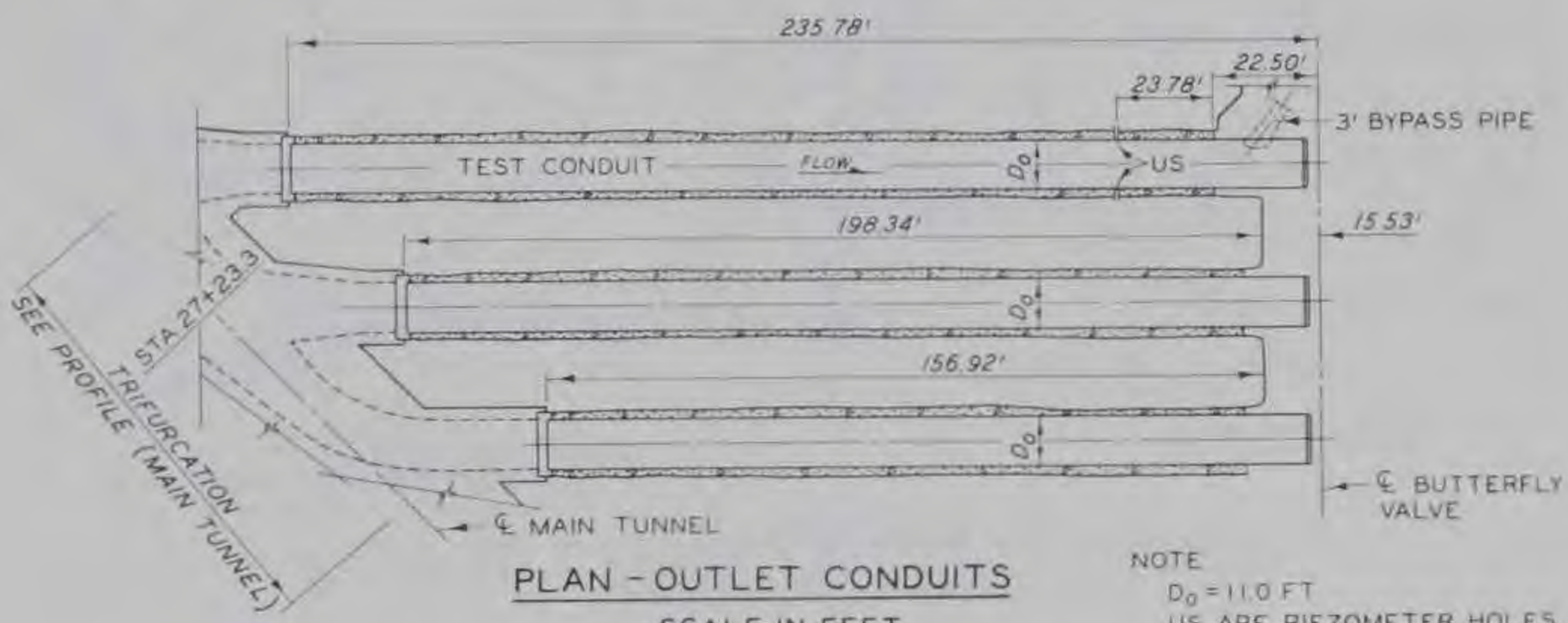


PLAN - OUTLET CONDUITS

SCALE IN FEET

20 0 20 40

NOTE
$D_o$ = 11.0 FT
US ARE PIEZOMETER HOLES

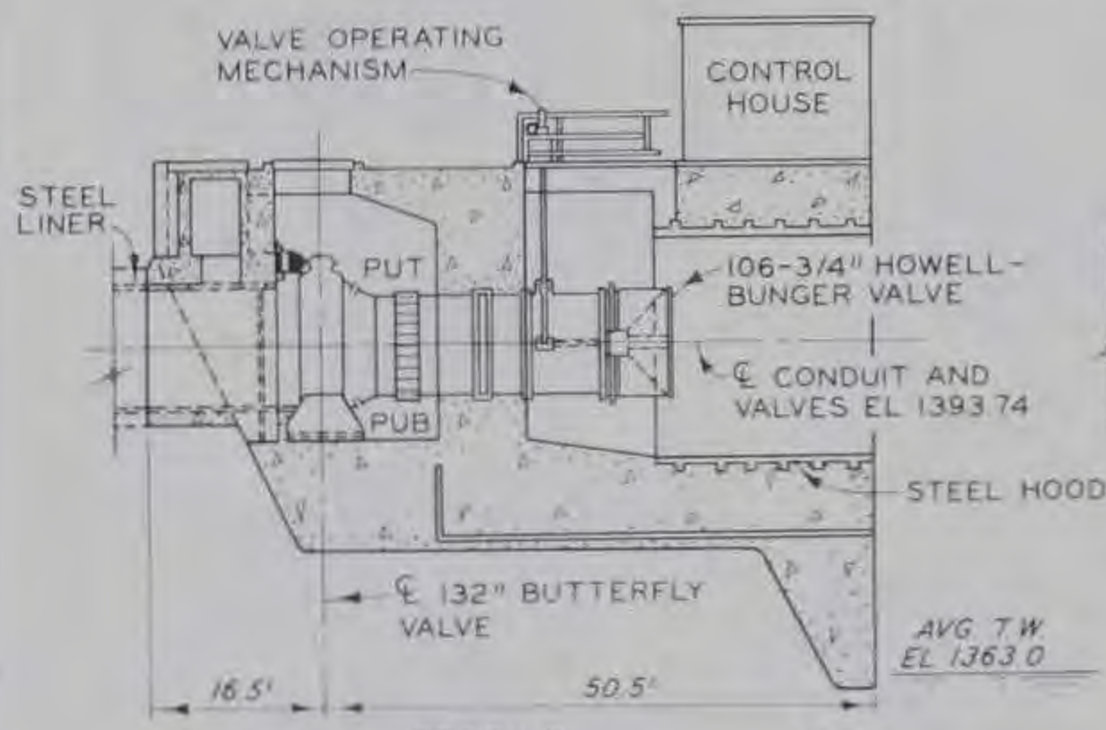


PROFILE

NOTE:
PUT AND PUB ARE PRESSURE TRANSDUCER LOCATIONS

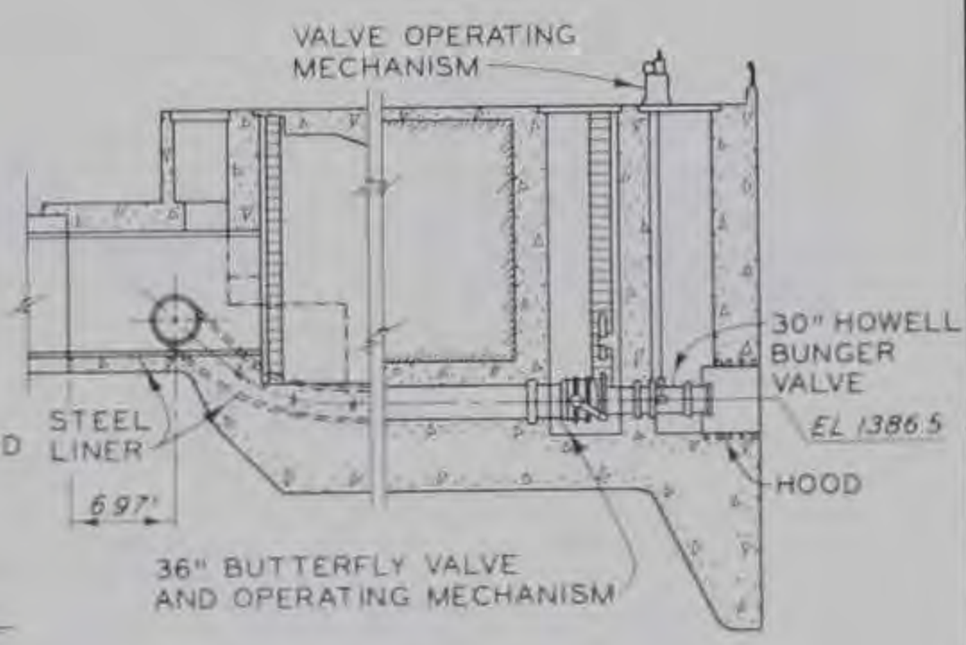


3-FT BYPASS PIPE

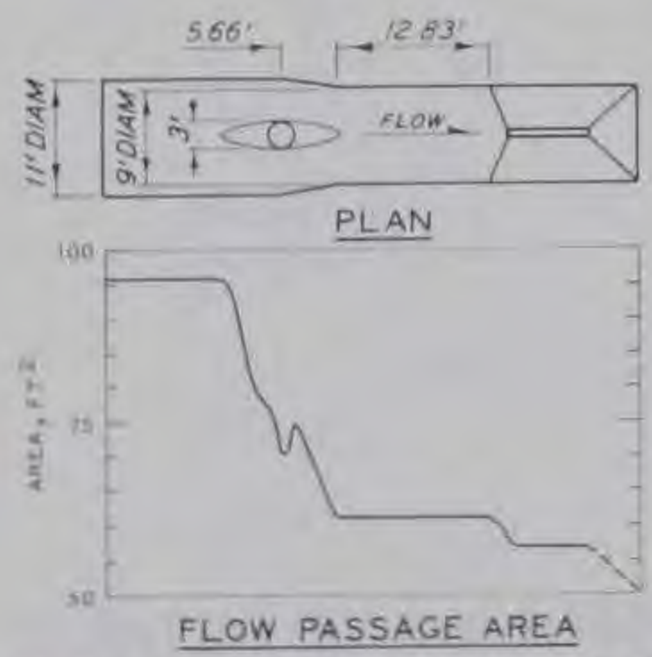


11-FT CONDUIT OUTLET DETAILS

SCALE IN FEET

10 0 10 20 30

# GENERAL OUTLET WORKS DETAILS

PLATE I

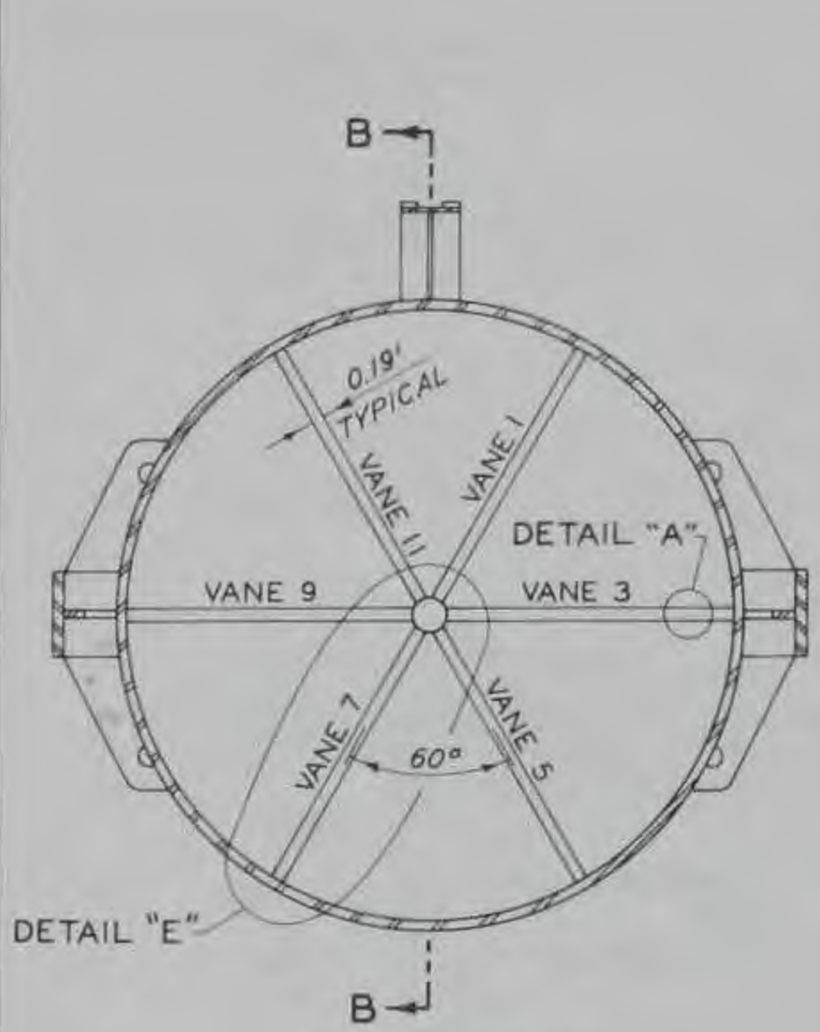


SECTION A-A

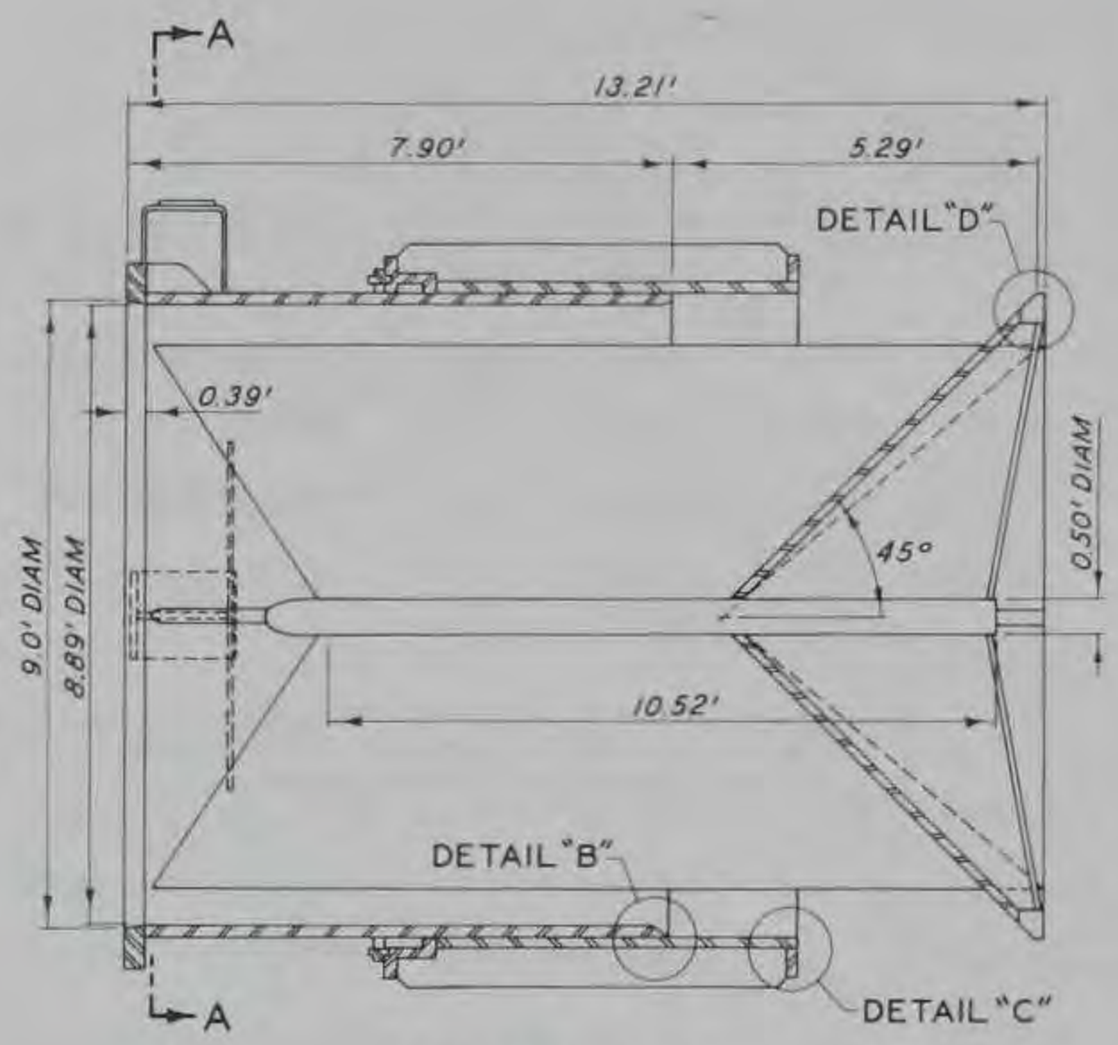


SECTION B-B

SCALE IN FEET

2 0 2 4 6

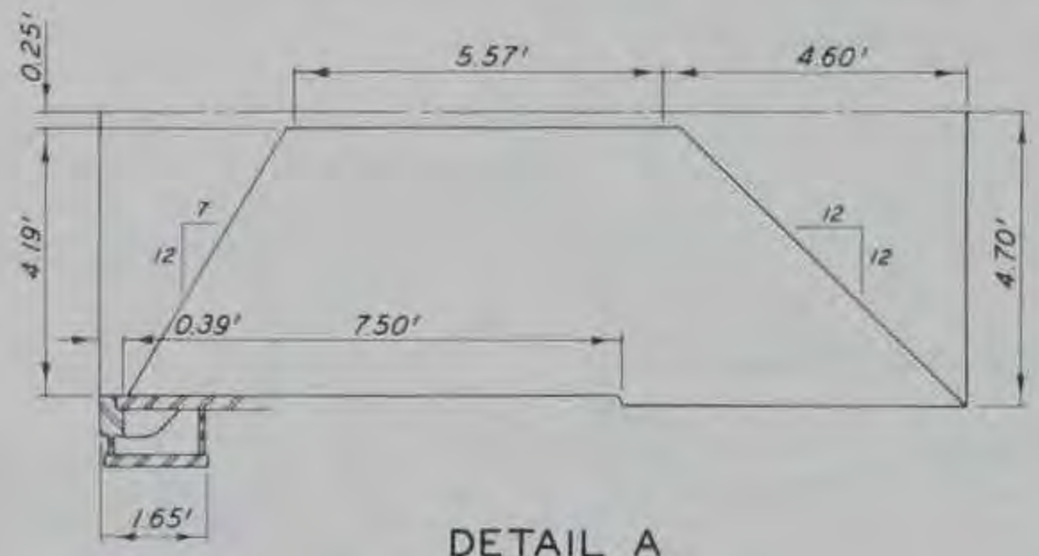


DETAIL A

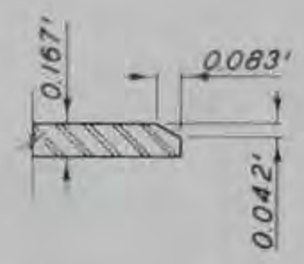


DETAIL B

NOT TO SCALE

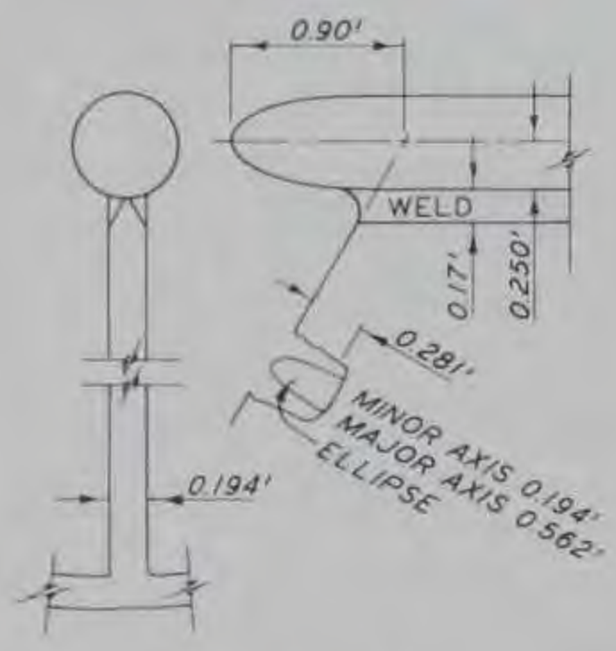


DETAIL E

NOT TO SCALE

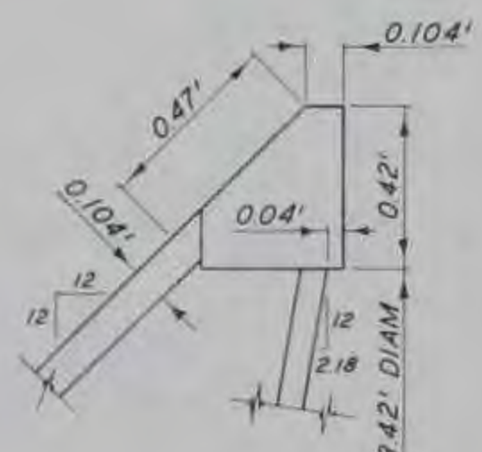


DETAIL D

NOT TO SCALE

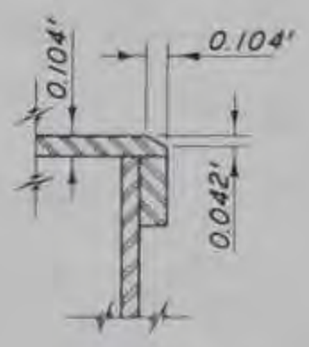


DETAIL C

NOT TO SCALE

HOWELL-BUNGER VALVE DETAILS

PLATE 2

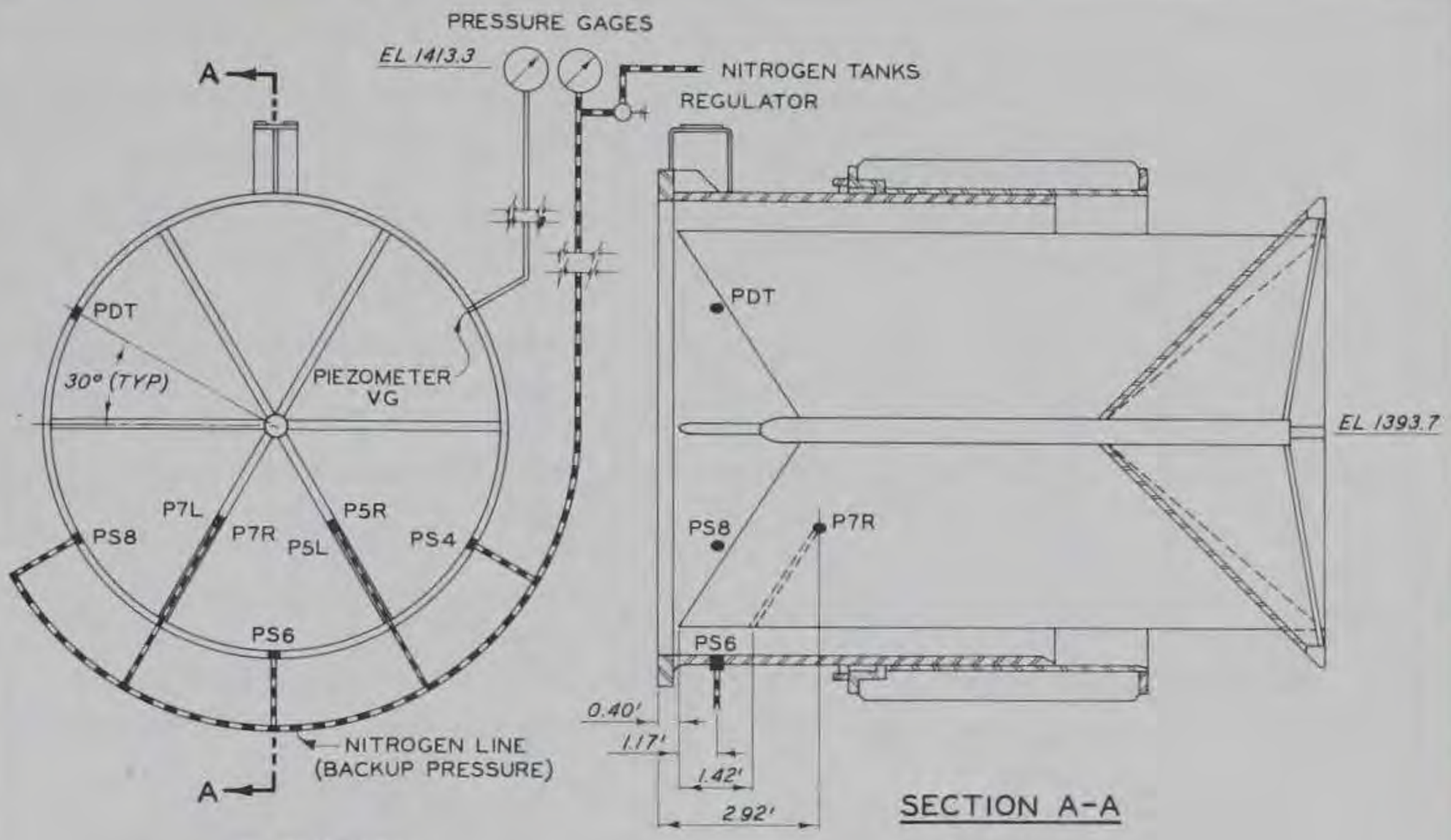


ELEVATION
(LOOKING DOWNSTREAM)

SECTION A-A

## PRESSURE TRANSDUCERS AND PIEZOMETER

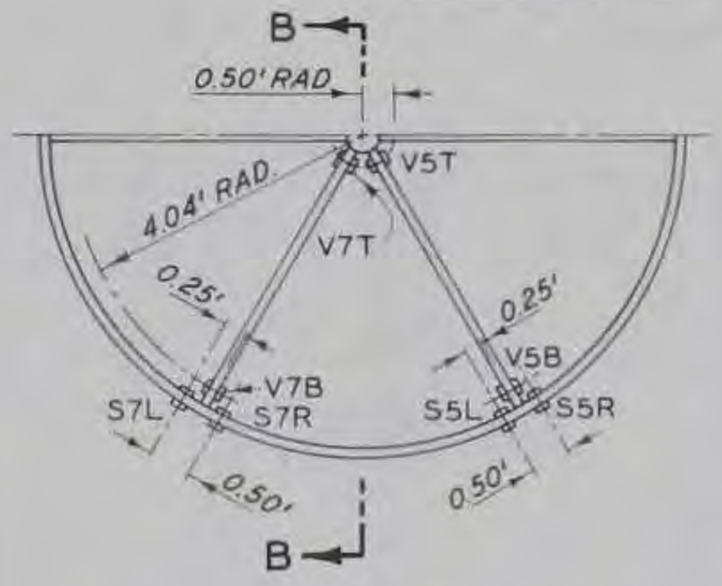


ELEVATION
(LOOKING DOWNSTREAM)

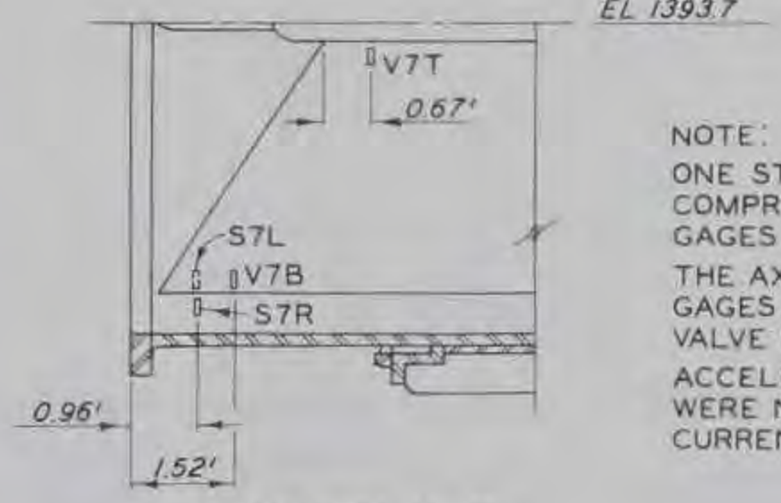


SECTION B-B

NOTE:
ONE STRAIN GAGE CHANNEL IS COMPRISED OF TWO STRAIN GAGES (SEE TEXT).
THE AXES OF THE STRAIN GAGES ARE NORMAL TO THE VALVE CENTER LINE
ACCELEROMETERS AV AND AT WERE NOT OPERATED CONCURRENTLY.

## STRAIN GAGE PAIRS

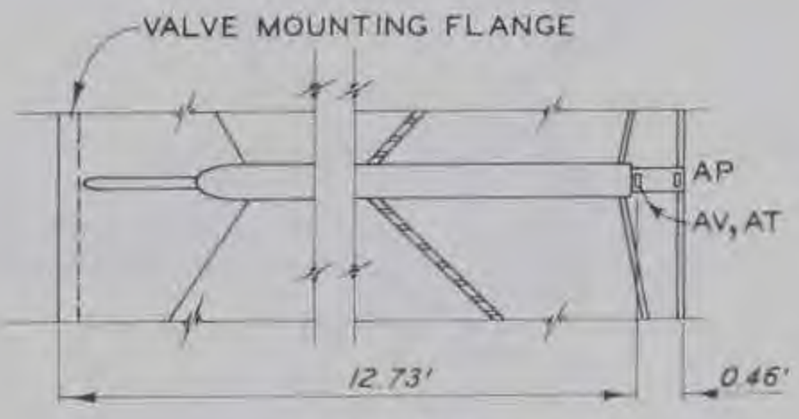


SECTION C-C

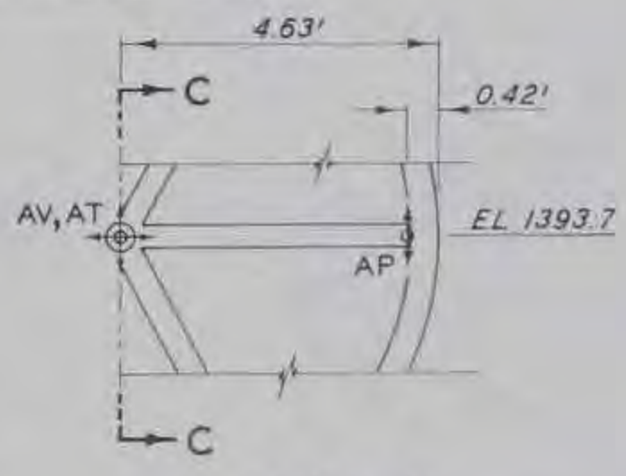


ELEVATION
(LOOKING UPSTREAM)

## ACCELEROMETERS

## TRANSDUCER LOCATIONS

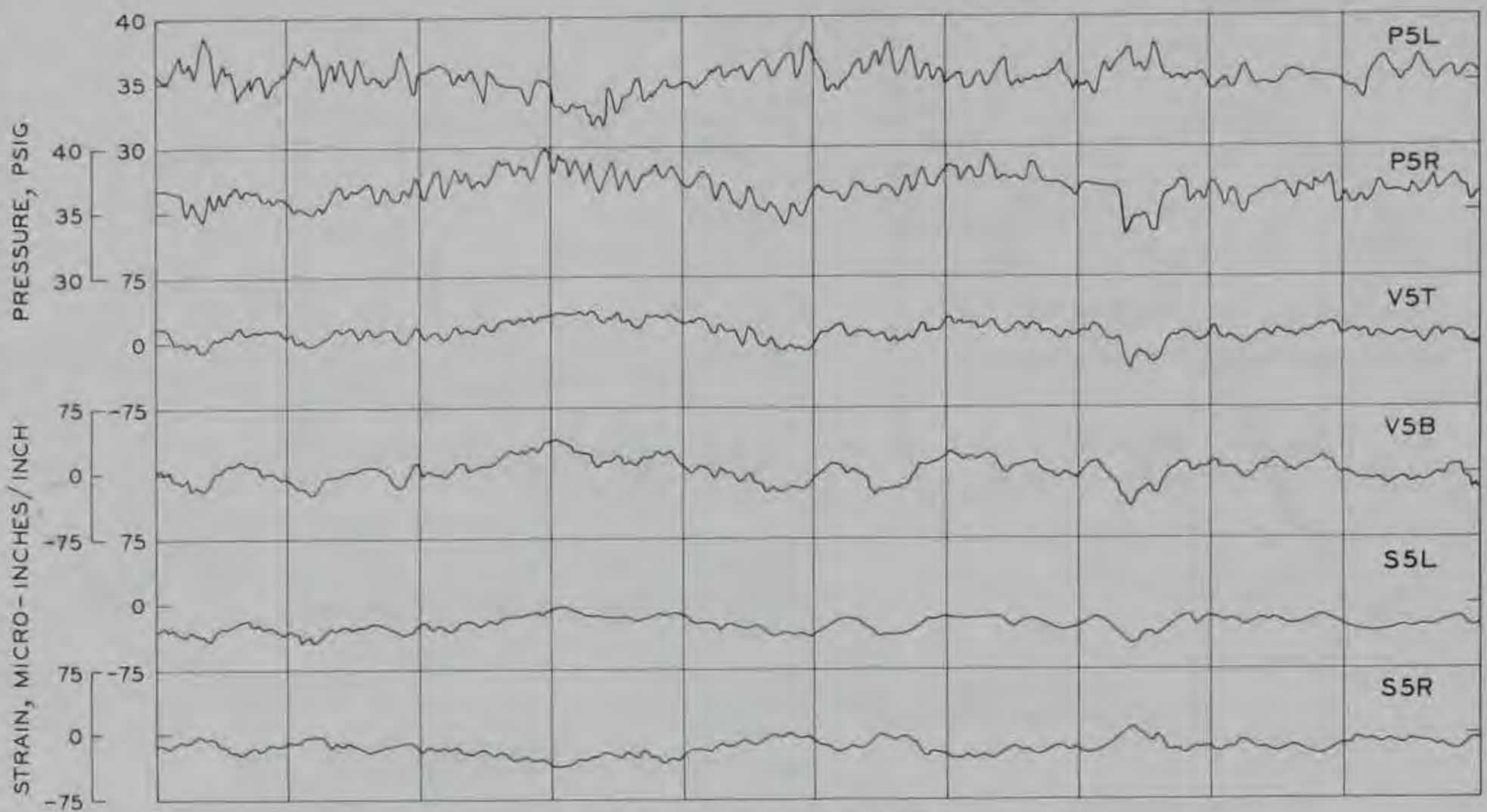


OSCILLOGRAPH DATA

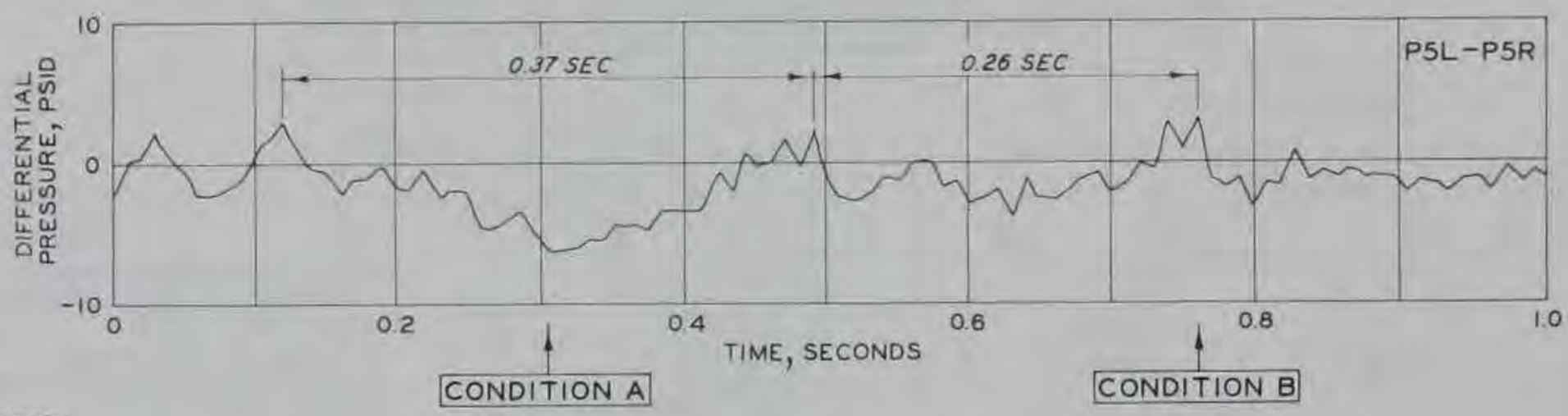


NOTES:

1. DATA TRACED FROM RECORDER CHARTS
2. 0.01 SECOND DIGITAL PLOT
3. DIAL READING EQUAL 80 PER-CENT
4. TESTS OF 29 MARCH 1968

COMPUTED NET PRESSURE LOADING ON VANE

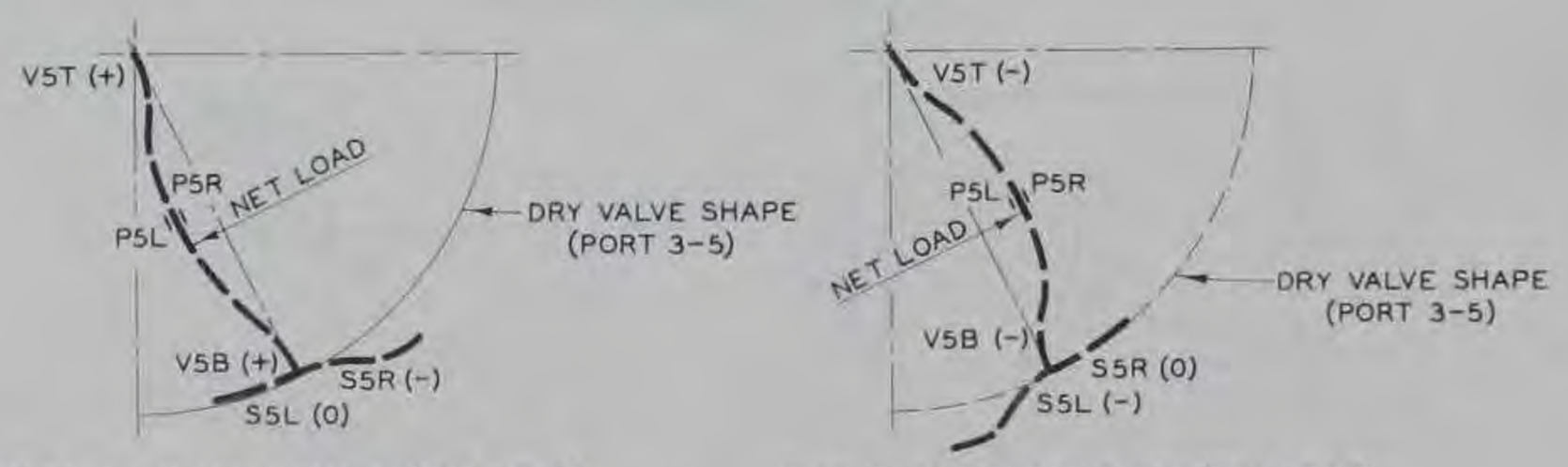


SHAPE AT CONDITION A (P5L<P5R)

SHAPE AT CONDITION B (P5L>P5R)

DEFORMATION OF VANE

OSCILLOGRAPH VIBRATION DATA
VANE 5

PLATE 4

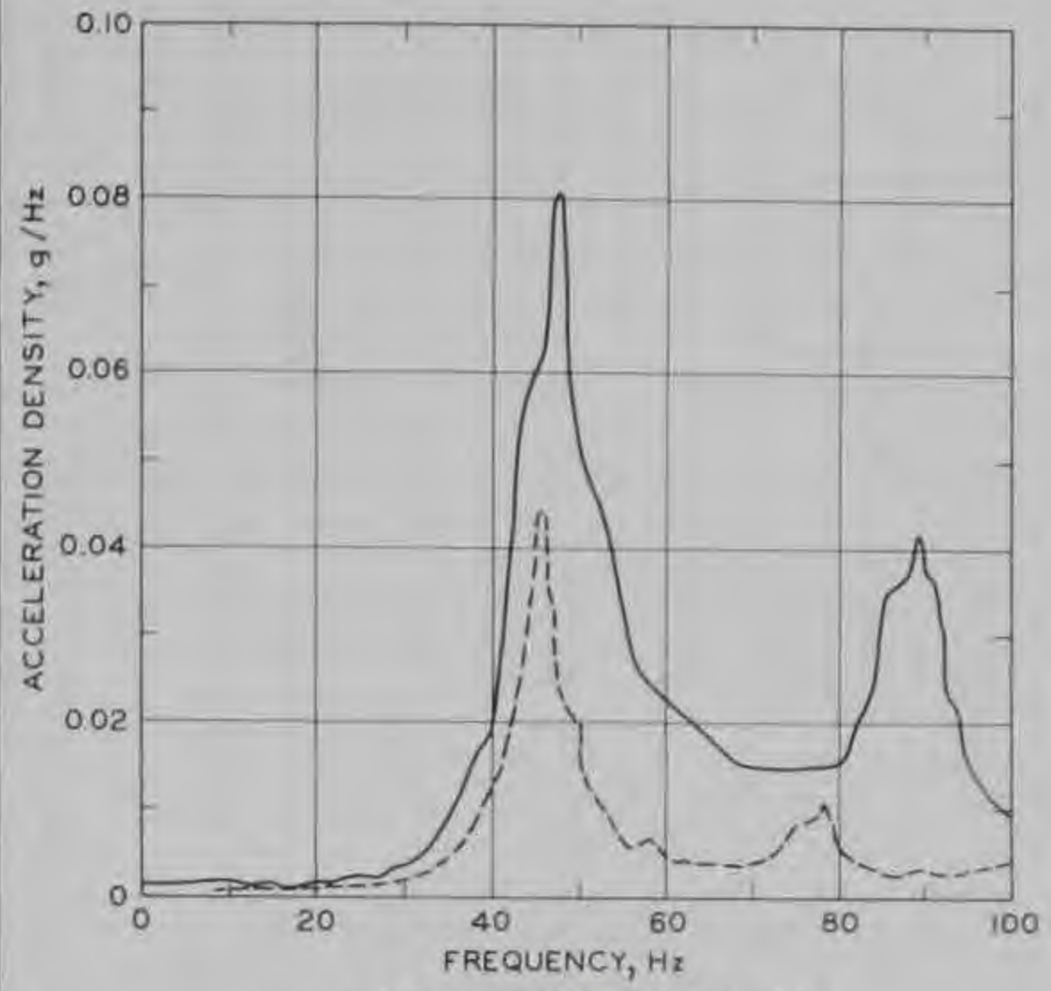


ACCELEROMETER AV

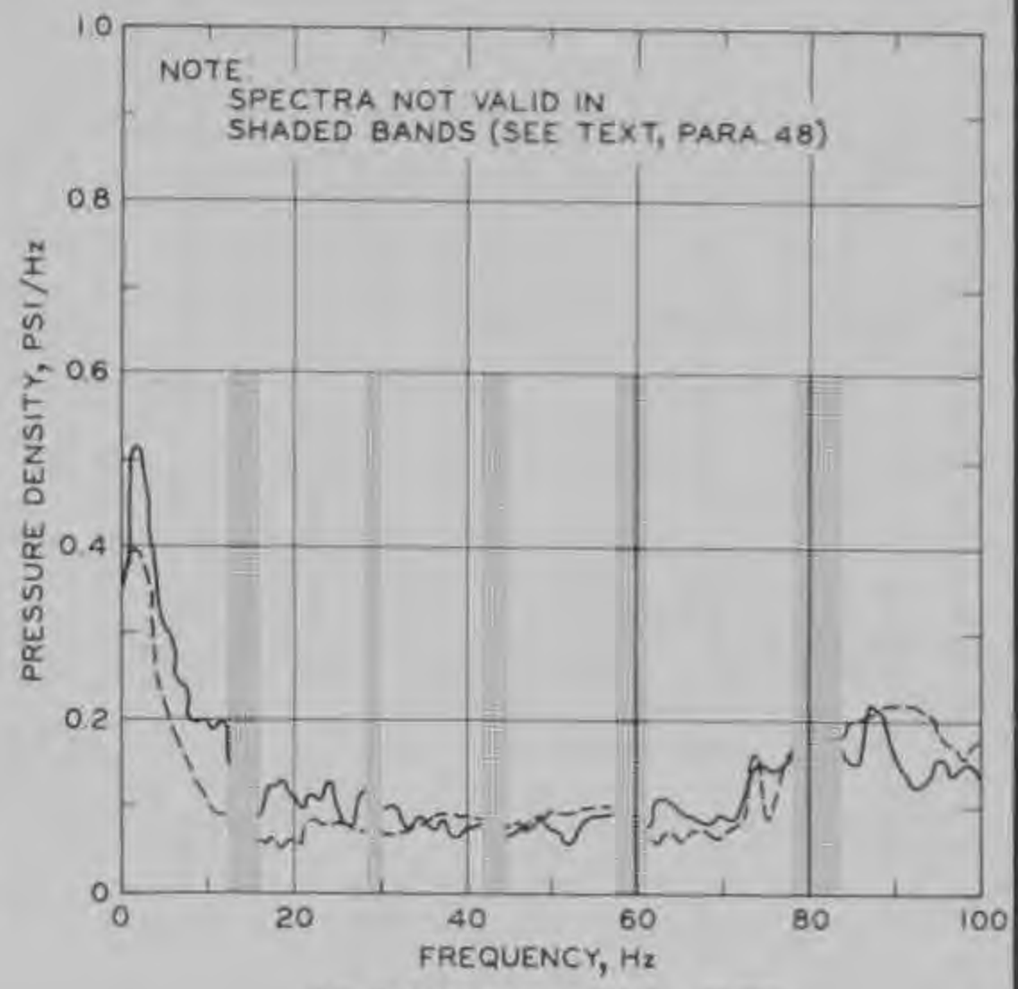


PRESSURE CELL P7R

NOTES:

1. GATE OPENING IS INDICATED BY DIAL READING.
2. TESTS OF 29 MARCH 1968.

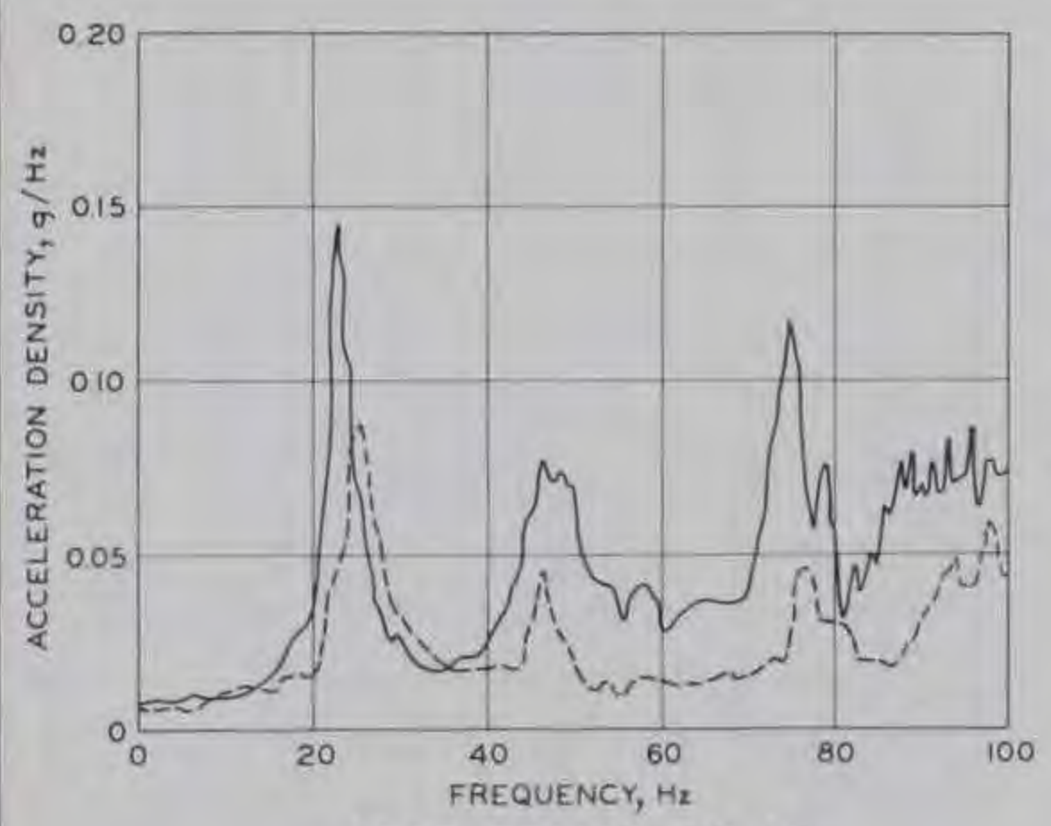


ACCELEROMETER AP

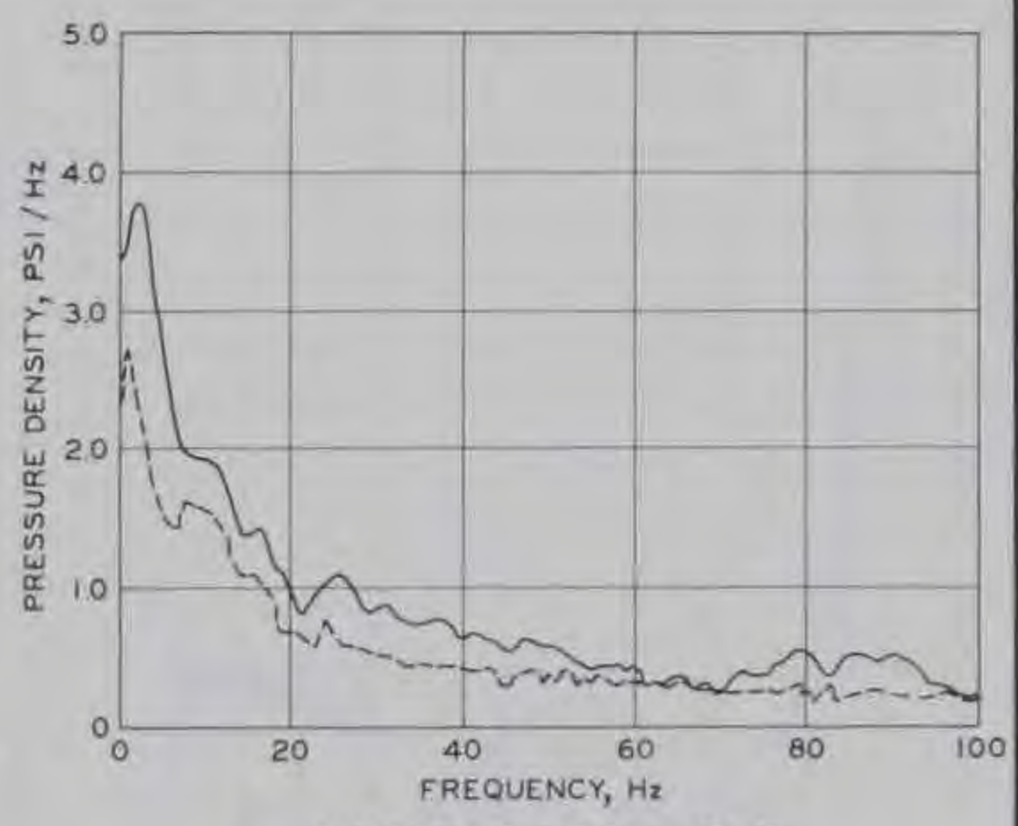


PRESSURE CELL PUT

## ACCELERATION SPECTRA

## PRESSURE SPECTRA

LEGEND

—— 90 % DIAL READING
---- 70 % DIAL READING

# LINEAR SPECTRAL DENSITY ENVELOPES

ACCELERATIONS AND PRESSURES

PLATE 5

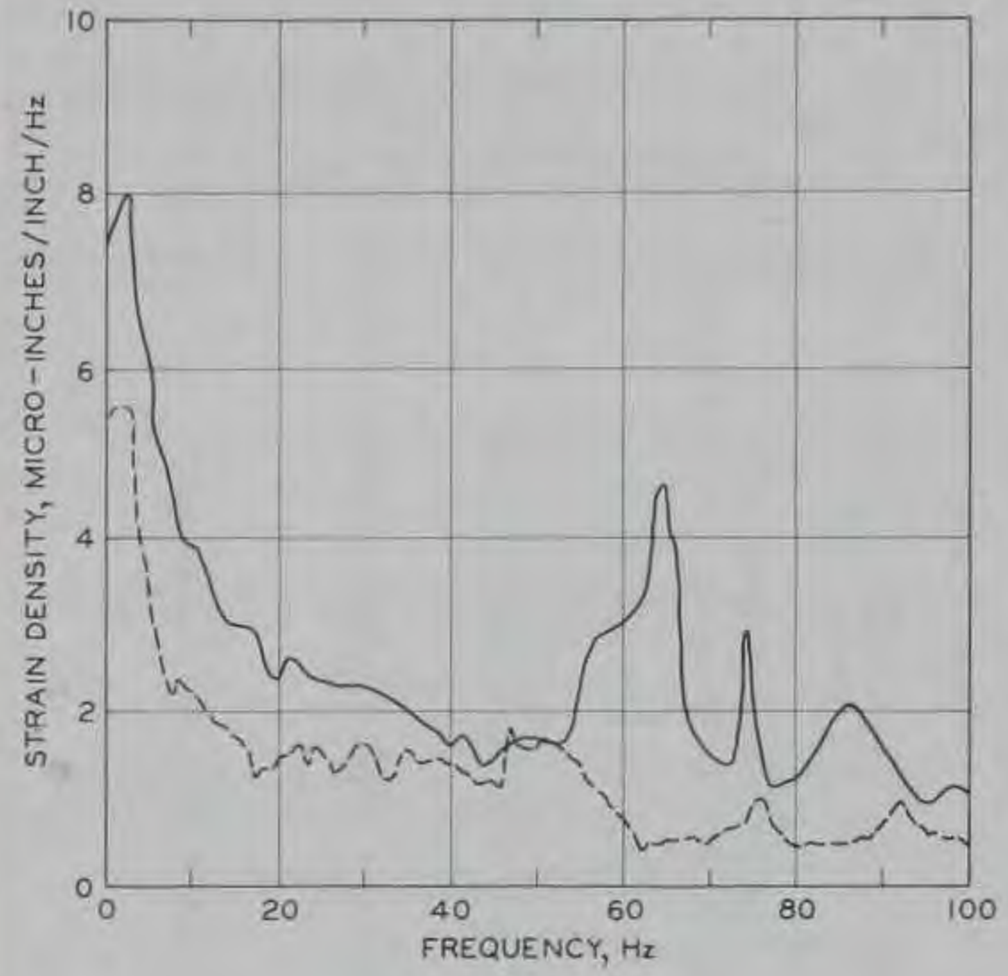


GAGE V7T

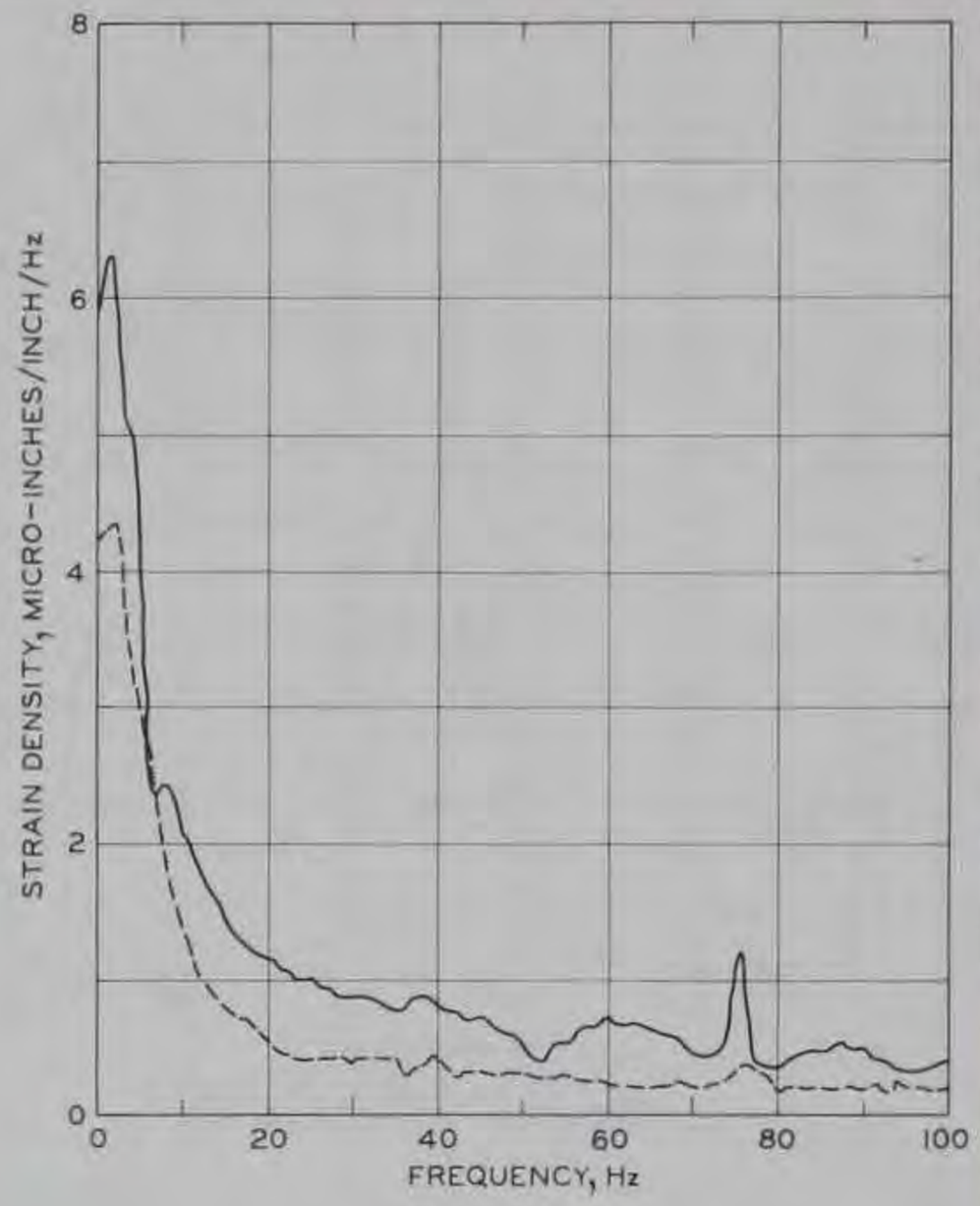


GAGE S7L

NOTES:
1. SEE PLATE 5
2. TESTS OF 29 MARCH 1968

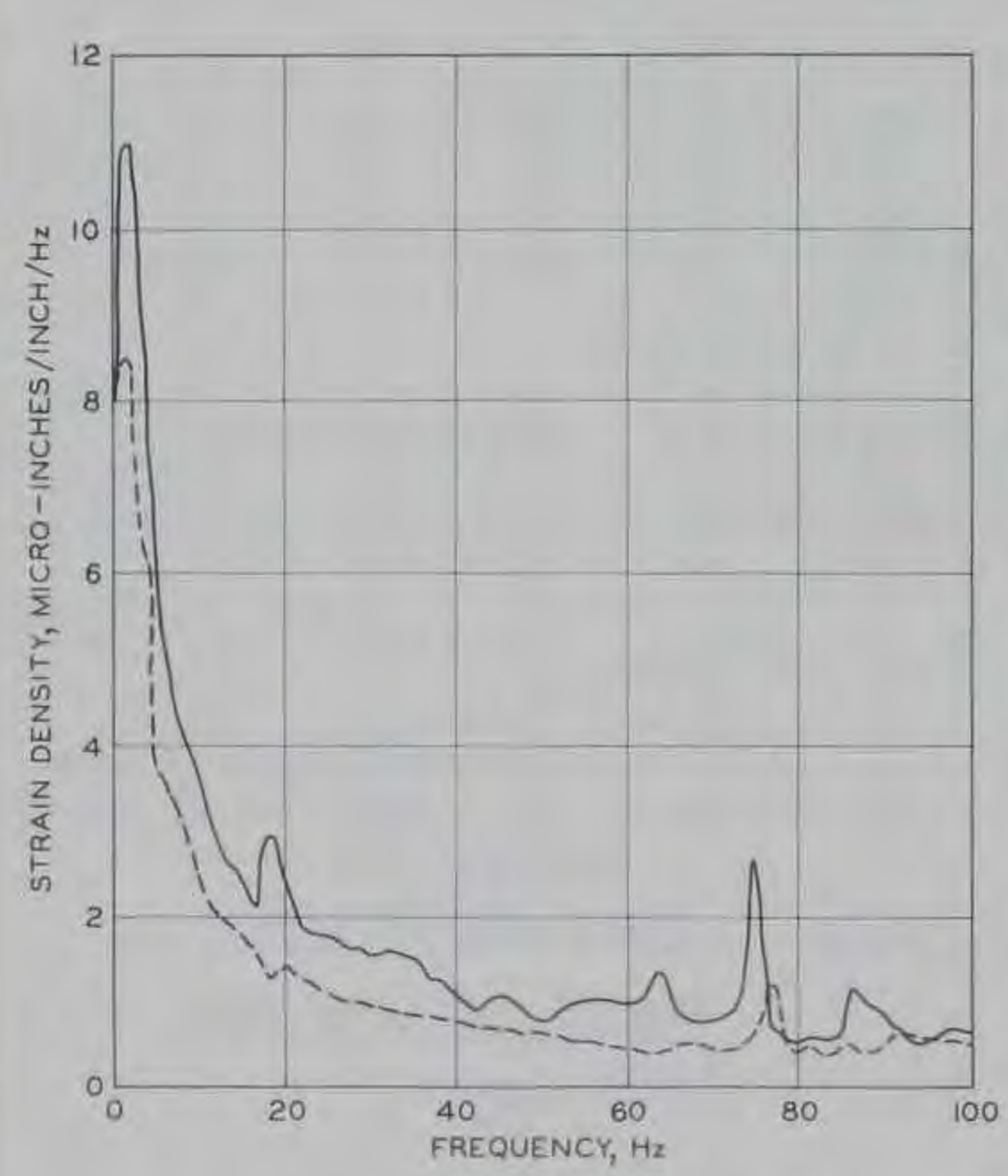


GAGE V7B

VANE STRAIN GAGES

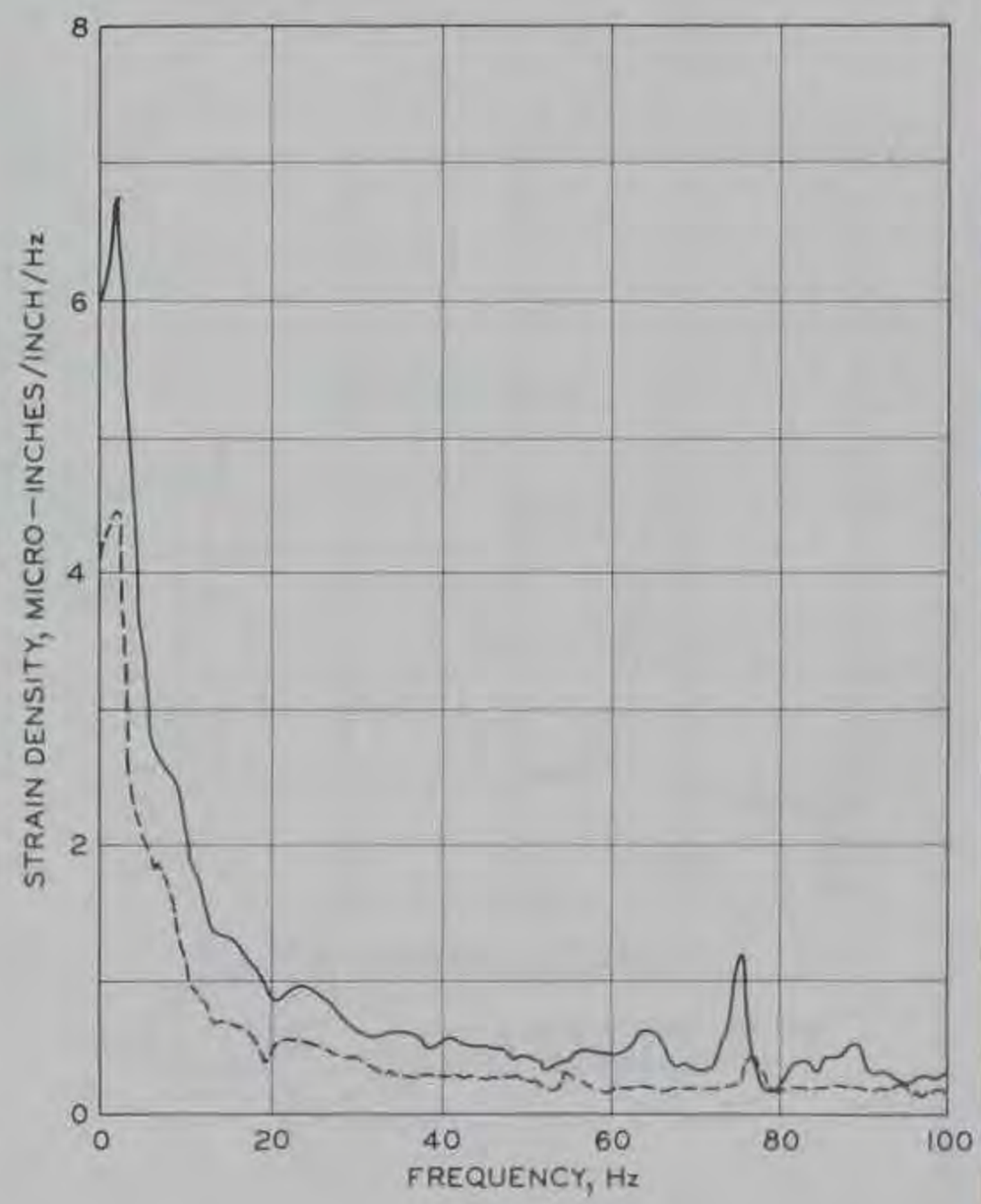


GAGE S7R

SHELL STRAIN GAGES

LEGEND

—— 90% DIAL READING
---- 70% DIAL READING

LINEAR SPECTRAL DENSITY ENVELOPES

STRAIN GAGES AT VANE 7

PLATE 6

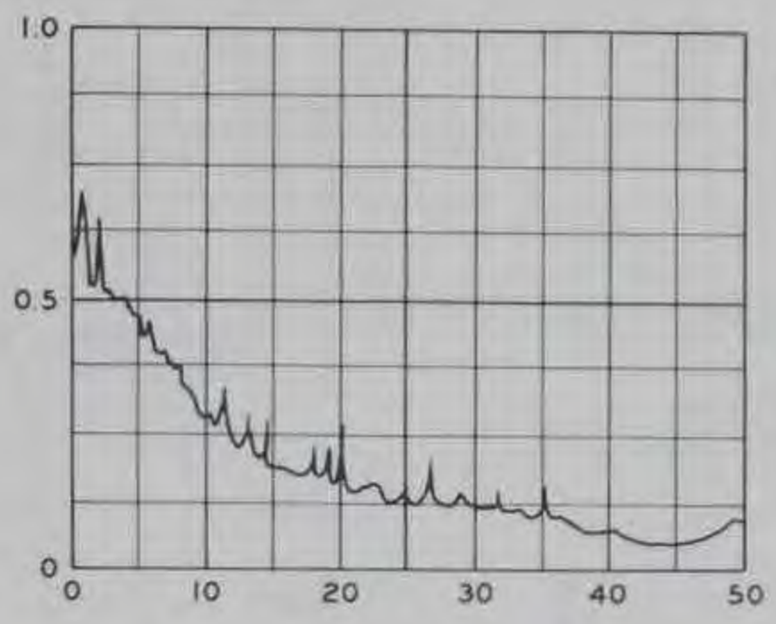


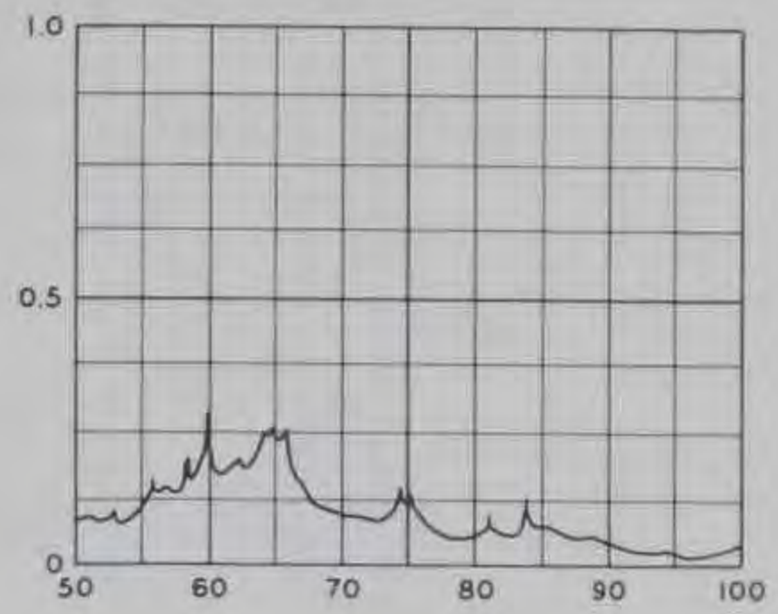


V7T

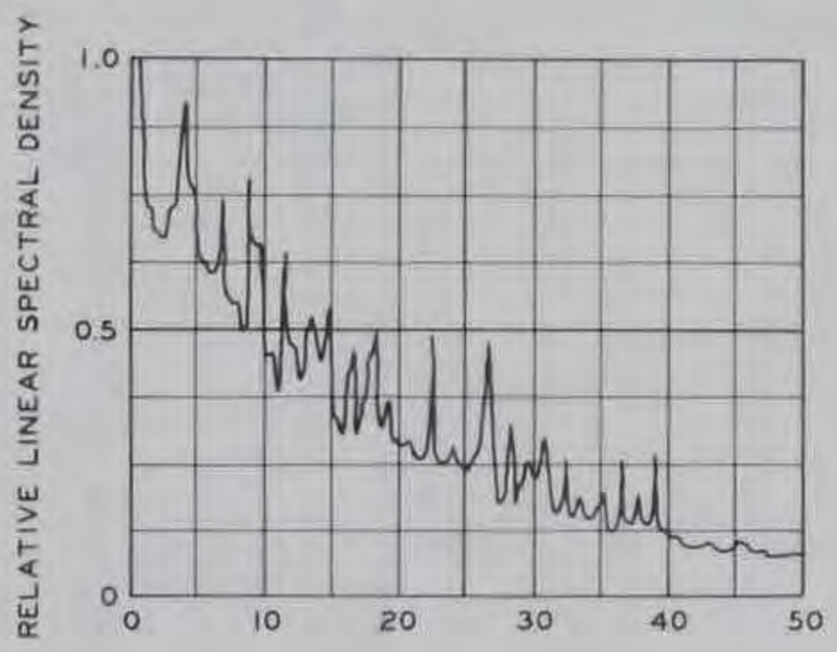


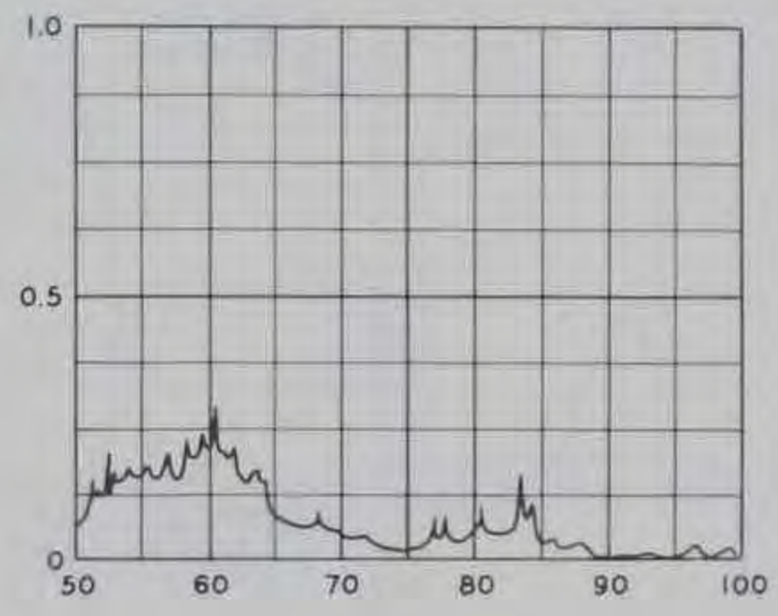


V5T

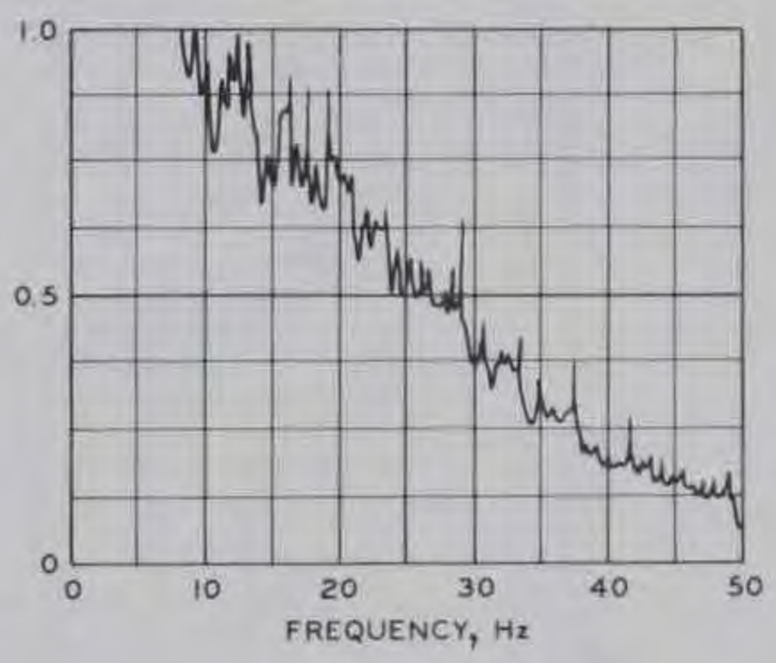


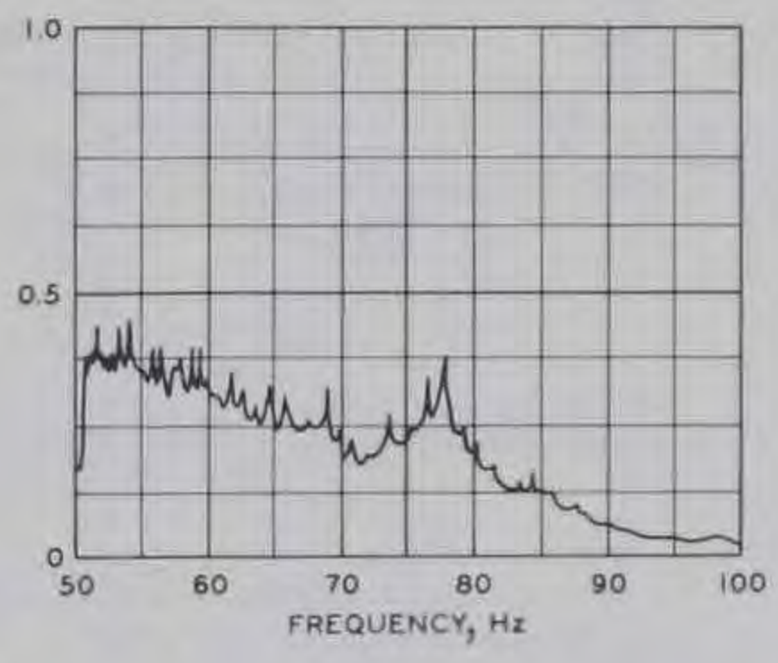


V5B

NOTE:
DIAL READING EQUAL 90 PERCENT
A RELATIVE DENSITY OF 1.0 IS APPROXIMATELY EQUAL TO 20 MICRO-INCHES/INCH/Hz. (COMPARE RELATIVE V7T WITH PREVIOUSLY CALIBRATED V7T SPECTRUM ON PLATE 6.)
TESTS OF 29 MARCH 1968

# RELATIVE LINEAR SPECTRAL DENSITIES

## STRAIN GAGES V5T, V5B, AND V7T

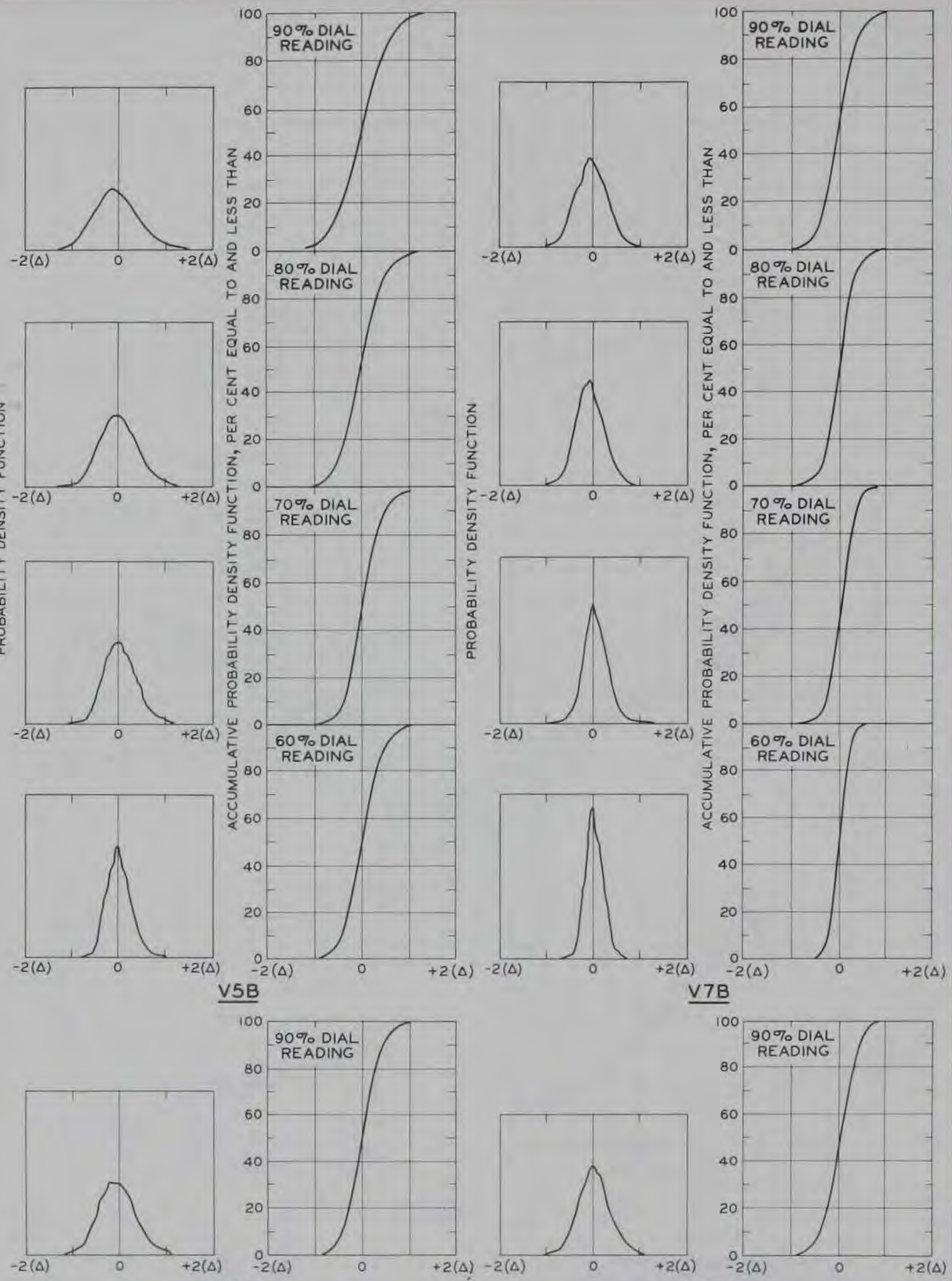


NOTE
Δ IS THE CHANNEL CALIBRATION STEP AND EQUALS 90 MICROIN./IN. FOR ALL DIAGRAMS.
DIAL READINGS AS NOTED
TESTS OF 29 MARCH 1968

# AMPLITUDE DISTRIBUTION FUNCTIONS (CHANNELS V5B, V5T, V7B, V7T)

PLATE 8

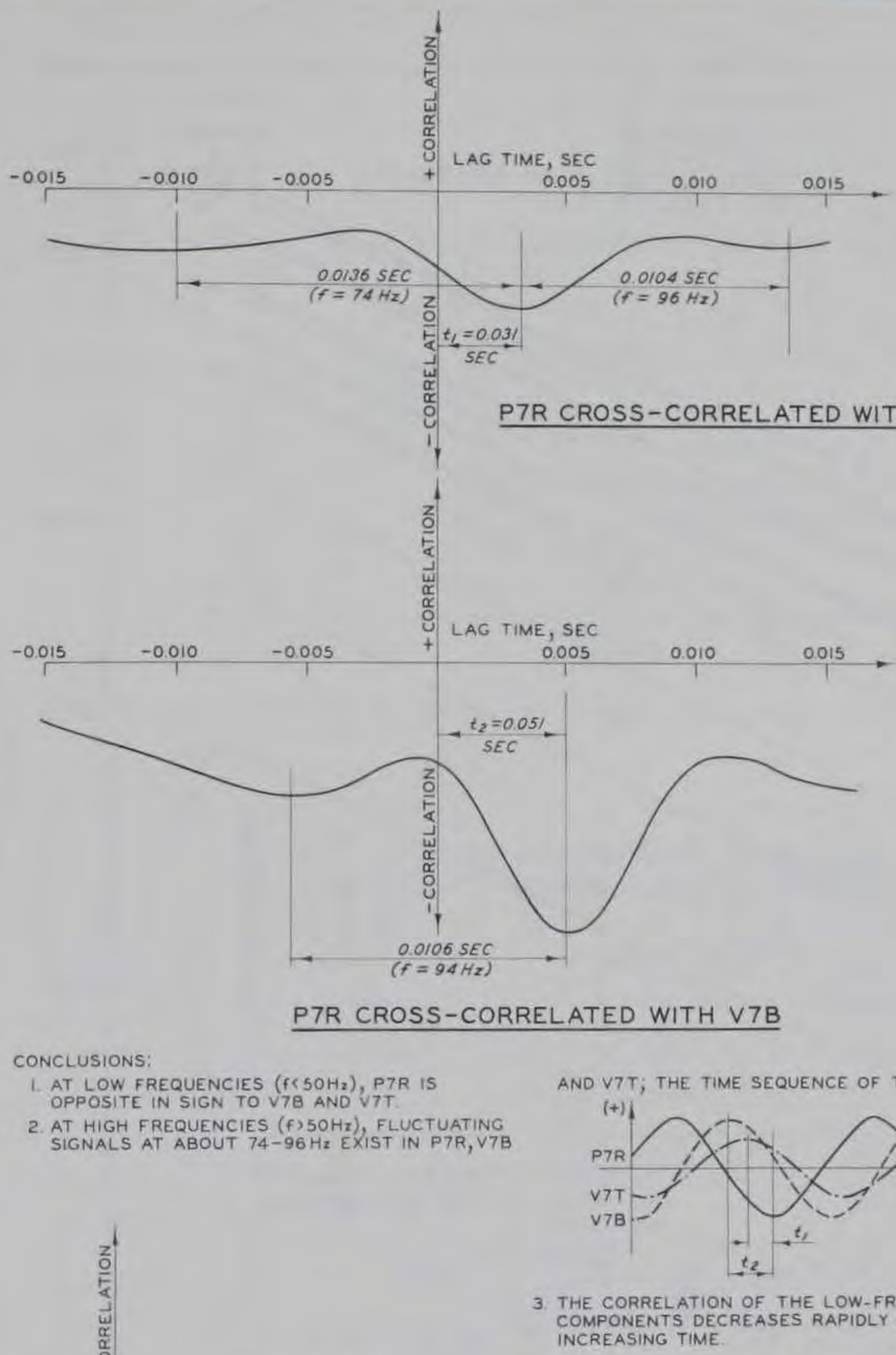


P7R CROSS-CORRELATED WITH V7T




P7R CROSS-CORRELATED WITH V7B

CONCLUSIONS:

1. AT LOW FREQUENCIES (f<50Hz), P7R IS OPPOSITE IN SIGN TO V7B AND V7T.
2. AT HIGH FREQUENCIES (f>50Hz), FLUCTUATING SIGNALS AT ABOUT 74-96Hz EXIST IN P7R, V7B AND V7T; THE TIME SEQUENCE OF THESE SIGNALS IS:




3. THE CORRELATION OF THE LOW-FREQUENCY COMPONENTS DECREASES RAPIDLY WITH INCREASING TIME.

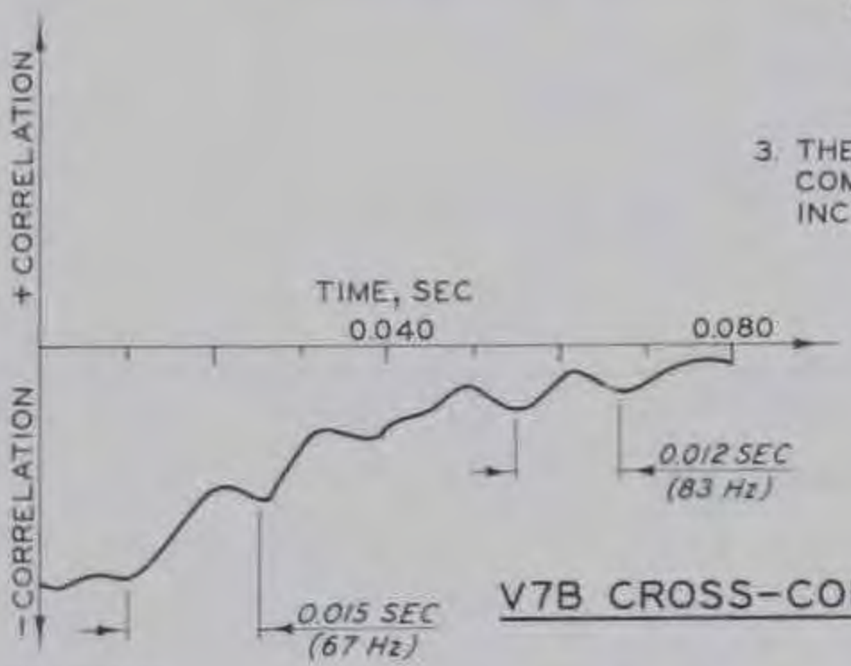


V7B CROSS-CORRELATED WITH V5B

NOTES:

1. ALL DIAL READINGS ARE 90%
2. TESTS OF 29 MARCH 1968

CONCLUSIONS:

1. AT LOW FREQUENCIES (f<50 Hz), V7B IS OPPOSITE IN SIGN TO V5B.
2. AT HIGH FREQUENCIES (f>50 Hz), PERIODIC SIGNALS AT ABOUT 67-83 Hz EXIST IN V7B AND V5B.

# CROSS-CORRELATIONS
## V7T & V7B WITH P7R AND V7B WITH V5B

PLATE 9

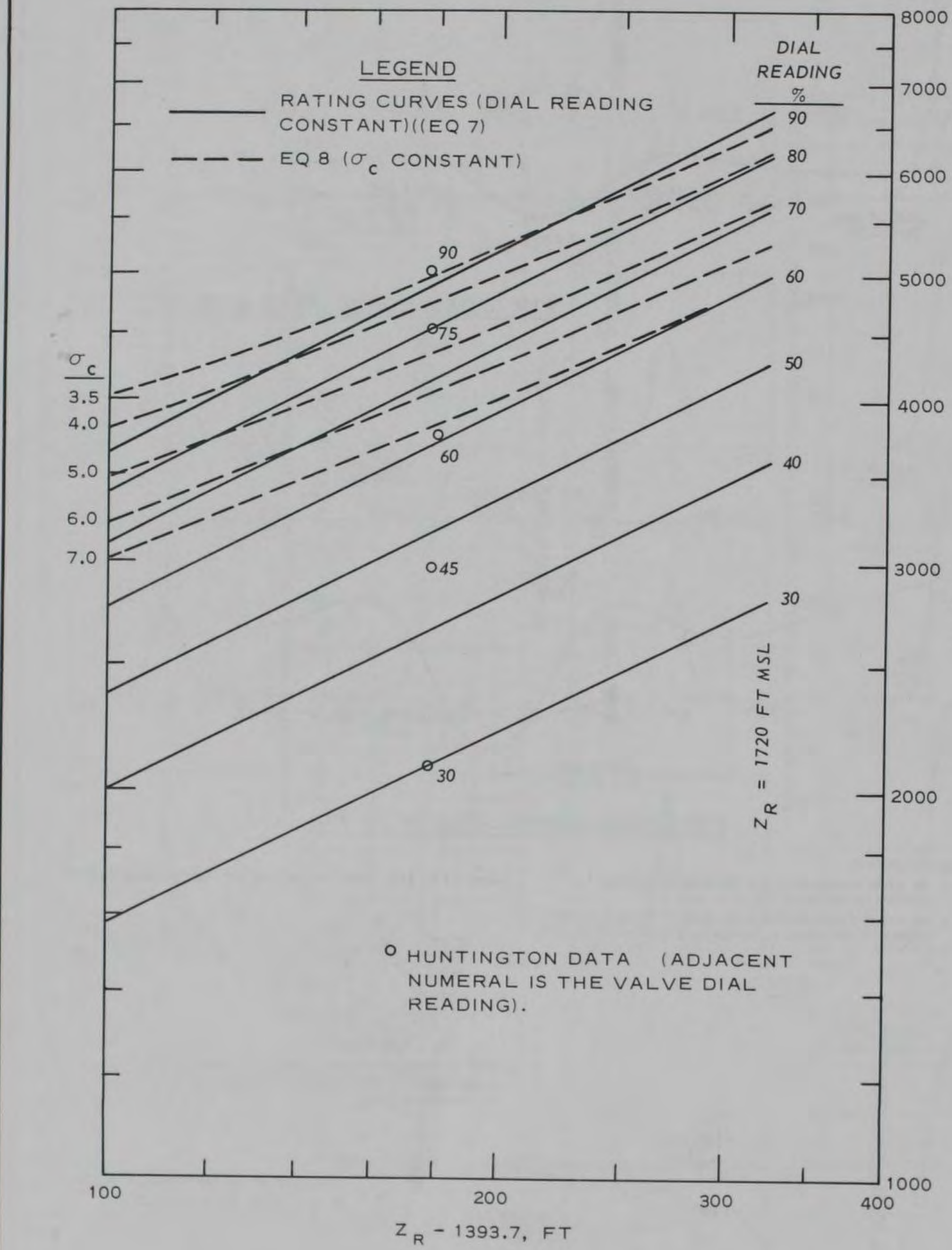


DISCHARGE RATING CURVES

PLATE 10

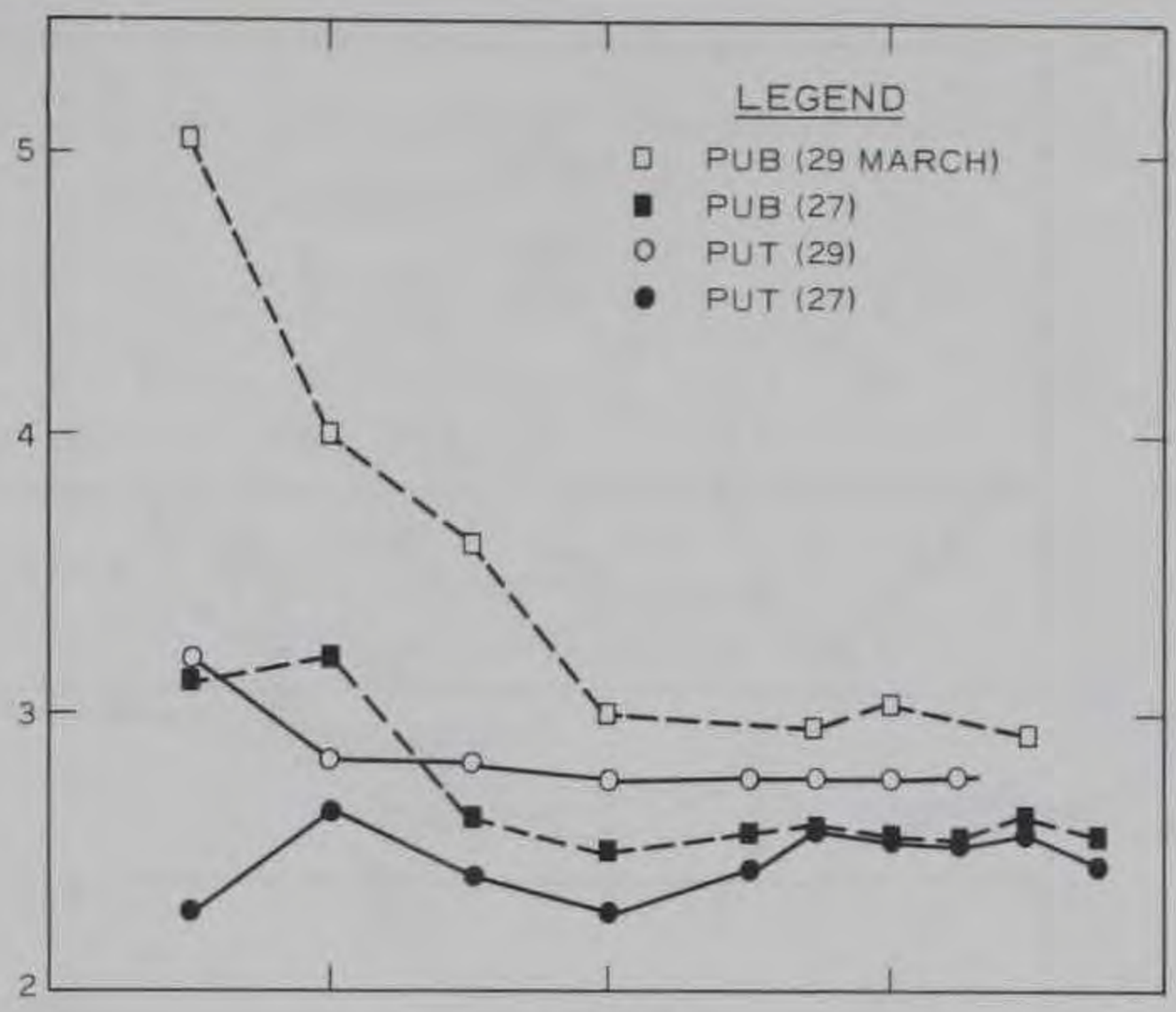


REDUCER

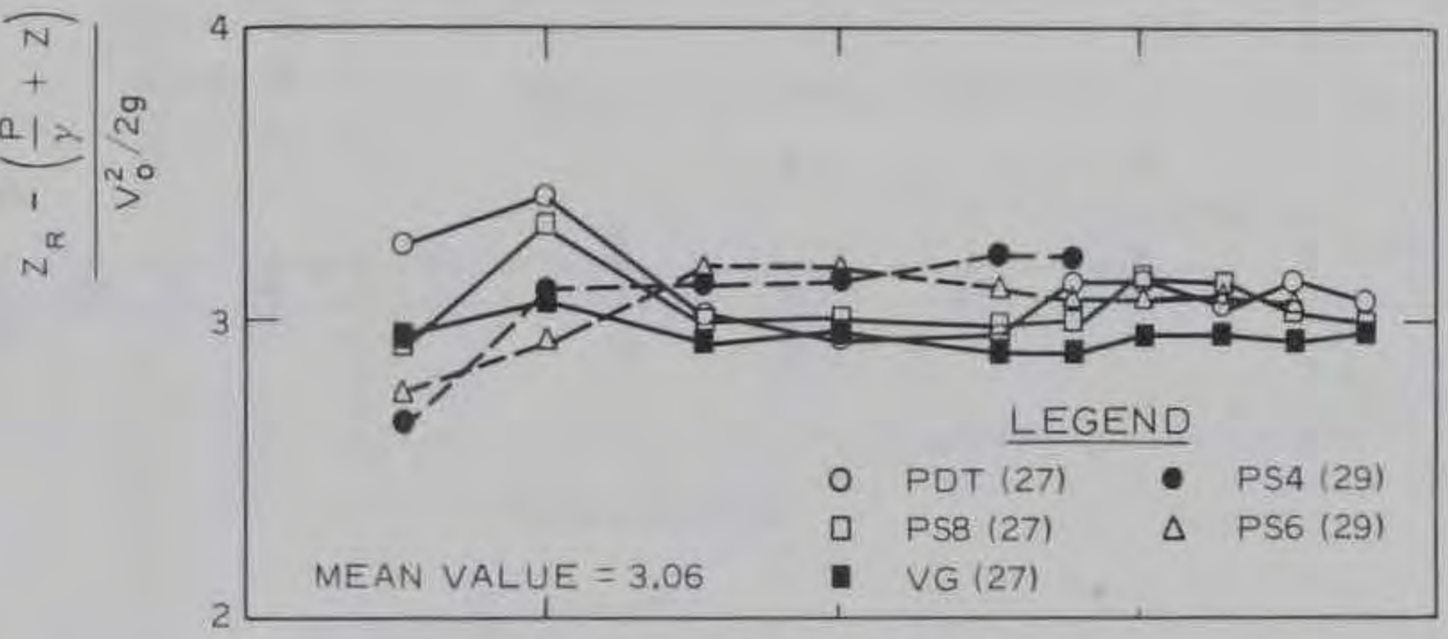


VALVE SHELL

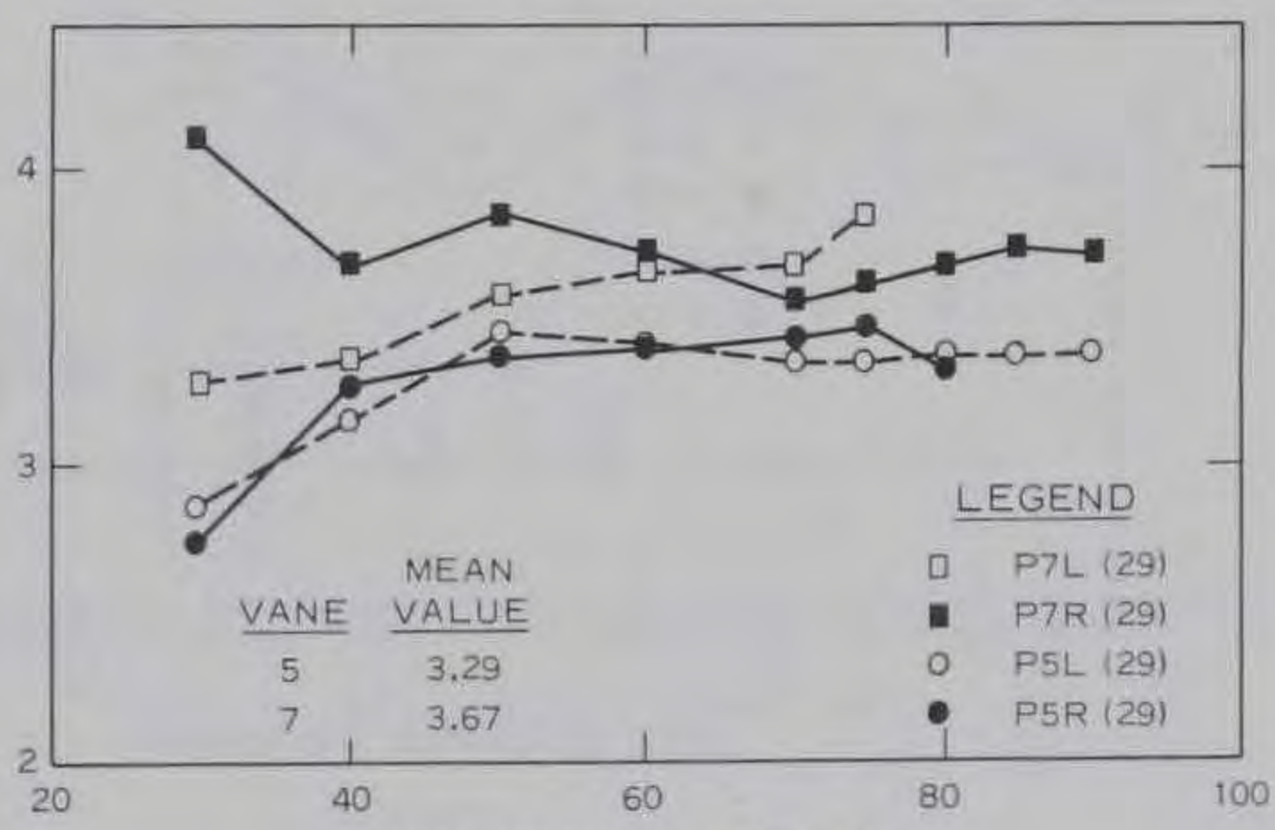


VANES

EULER NUMBERS

PLATE II

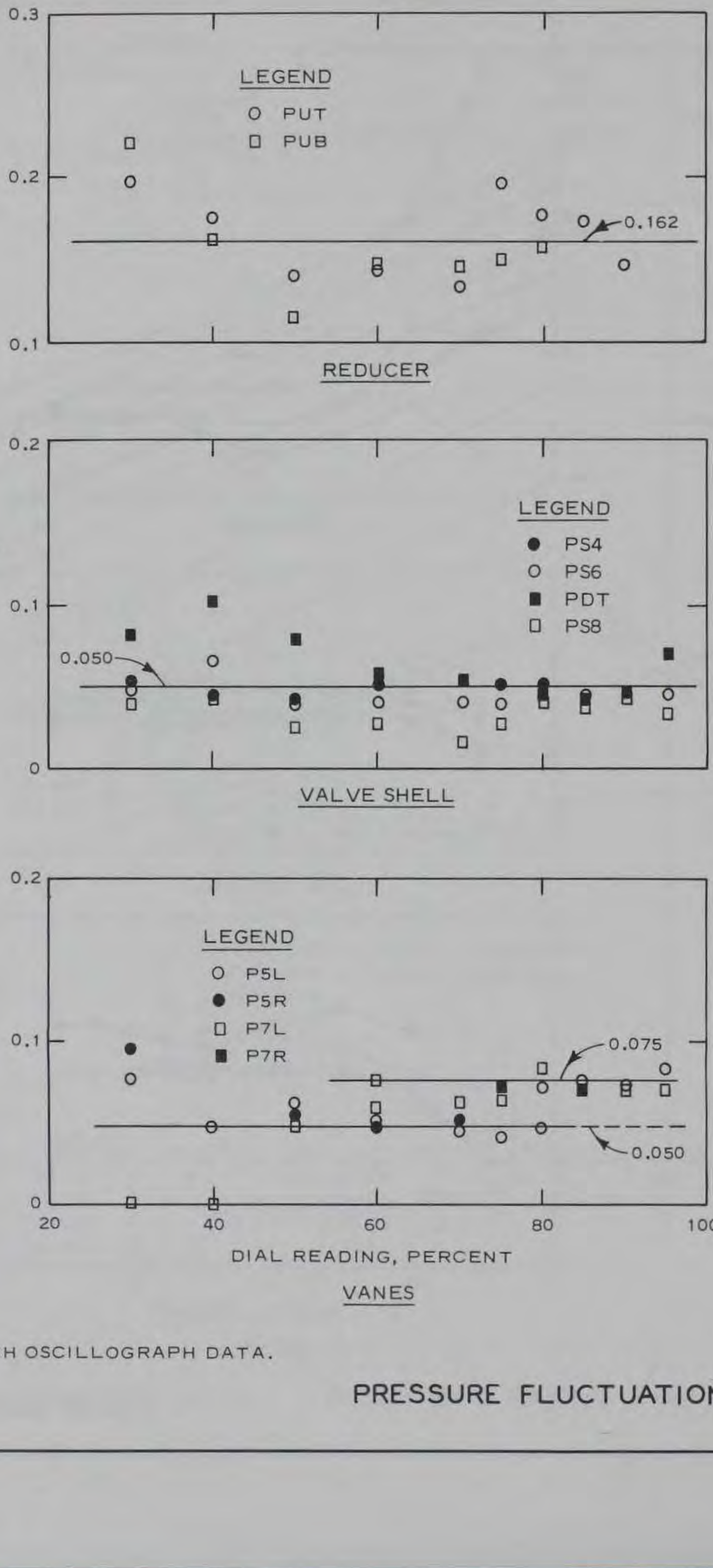


NOTE:

29 MARCH OSCILLOGRAPH DATA.

# PRESSURE FLUCTUATIONS

PLATE 12

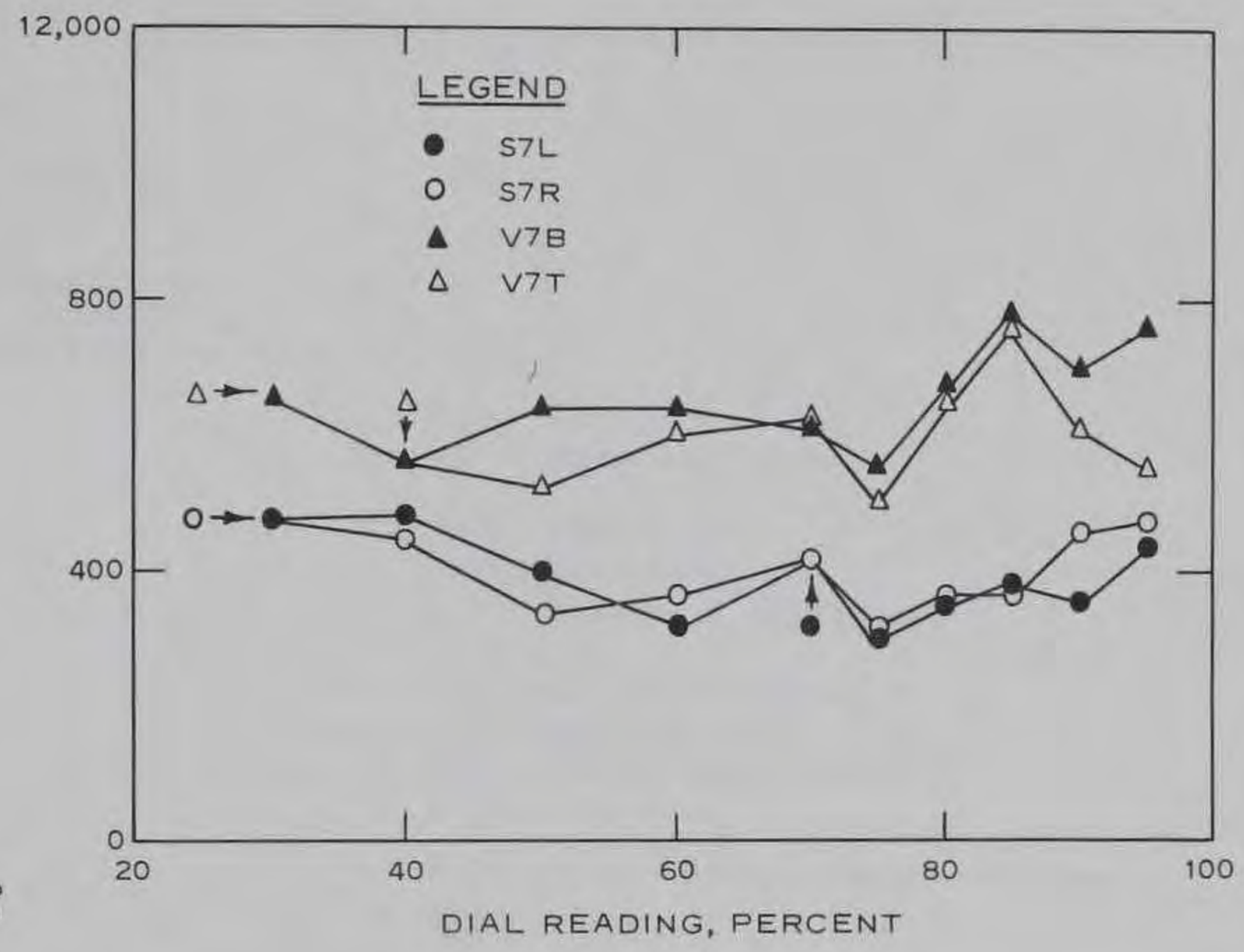


$$\frac{\sigma_{f\,MAX} - \sigma_{f\,MIN}}{0.05\gamma \dfrac{(V_{VN})^2}{2g}}$$

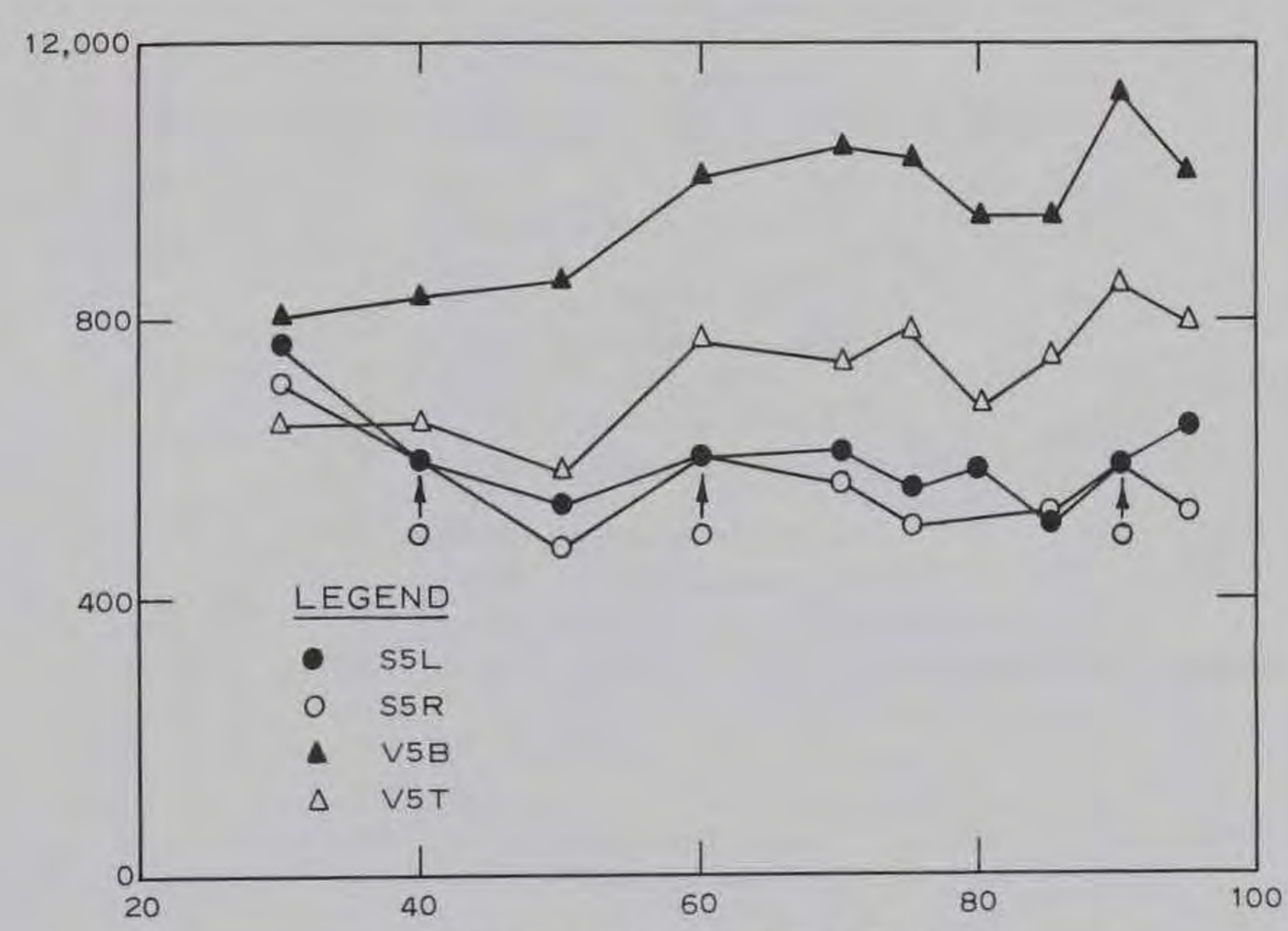


NOTE: 29 MARCH OSCILLOGRAPH DATA.

# STRESS FLUCTUATIONS

PLATE 13

# HYDRAULIC RESEARCH REPORTS DISTRIBUTION LIST

| Office | No. of Copies | Remarks |
|---|---|---|
| OCE (ENGCW) | 2 | |
| OCE (ENGCW-PC) | 1 | |
| OCE (ENGAS-I) | 1 | |
| OCE (ENGAS-I, Library) | 1 | |
| OCE (ENGSA) | 1 | |
| Bd of Engrs for Rivers & Harbors | 1 | |
| The Engr Center, Fort Belvoir, Va. | 1 | |
| Engr School Library, Fort Belvoir, Va. | 1 | |
| CERC | 1 | ATTN: Director |
| | 1 | ATTN: Chief, Design Branch |
| LMVD | 1 | ATTN: Library |
| Memphis | 1 | ATTN: Tech Library |
| New Orleans | 1 | ATTN: Hydraulics Br, Engrg Division |
| St. Louis | 1 | DE |
| | 1 | Chief, Hydraulics Br (LMSED-H) |
| Vicksburg | 1 | ATTN: Hydraulics Branch |
| | 1 | ATTN: River Stabilization Section |
| | 1 | ATTN: Design Branch |
| MRD | 4 | ATTN: Office of Administrative Services (Library) |
| Kansas City | 3 | ATTN: Library |
| NAD | 1 | ATTN: Engineering Division |
| | 1 | ATTN: Mr. A. G. Distefano |
| | 1 | ATTN: Mr. Otto Reyholec |
| | 1 | ATTN: Planning Division |
| | 1 | ATTN: Mr. L. J. Mauriello |
| | 1 | ATTN: Civil Works Br, Constr-Oper Div |
| | 1 | ATTN: Mr. Morris Colen |
| | 1 | ATTN: Mr. Morris Colen |
| Baltimore | 1 | DE<br>Abstract of report to DE |
| New York | 1 | DE |
| | 1 | ATTN: Mr. Frank L. Panuzio |
| | 1 | ATTN: Mr. Jacob Gelberman |
| | 1 | ATTN: Mr. Jesse Rosen |
| Norfolk | 1 | ATTN: Engineering Division |
| Philadelphia | 1 | ATTN: Engineering Division, NAPEN-H |
| NCD | 1 | ATTN: Hydraulics Branch |
| Buffalo | 1 | ATTN: Chief, Engineering Division |
| Chicago | 1 | ATTN: Hydraulics Branch Engineering Division<br>Abstract of report to Chief, Construction-Operations Division<br>Abstract of report to Chief, Engrg Div |
| Detroit | 1 | ATTN: Library |
| Rock Island | 1 | DE |
| St. Paul | 1 | ATTN: Engineering Division |
| | 1 | ATTN: Hydraulics Branch |
| NED | 1 | ATTN: Hydrologic Engineering Branch |

| Office | No. of Copies | Remarks |
|---|---|---|
| NPD | 1 | ATTN: Technical Engineering Branch |
| | 1 | ATTN: Division Hydraulic Laboratory |
| Alaska | 1 | ATTN: Foundations and Materials Branch |
| | 1 | ATTN: District Library |
| | 1 | ATTN: Planning and Reports |
| | 1 | ATTN: Hydraulics and Waterways Section |
| Portland | 2 | ATTN: District Library |
| Seattle | 1 | DE |
| | 1 | ATTN: Chief, Hydraulics Section |
| Walla Walla | 1 | DE |
| ORD | 1 | DE |
| | 1 | ATTN: Mr. W. H. Browne, Jr. |
| Huntington | 15 | DE |
| Louisville | 1 | ATTN: Hydraulics Branch |
| Nashville | 1 | ATTN: Hydraulics Branch, Engrg Div |
| Pittsburgh | 1 | ATTN: Office of Administrative Services, Tech Library |
| | 1 | ATTN: Engineering Div, Hydraulics Br |
| POD | 1 | ATTN: Chief, Technical Review Branch |
| | 1 | ATTN: Chief, Civil Works Branch |
| SAD | 1 | ATTN: Engineering Division |
| | 1 | ATTN: Planning Division |
| Charleston | 1 | ATTN: Chief, Engineering Division |
| | 1 | ATTN: Chief, Project Planning Branch |
| | 1 | ATTN: Coastal Engineering Branch |
| Jacksonville | 1 | DE |
| | 1 | ATTN: Hydraulics Section |
| Mobile | 1 | ATTN: SAMEN-DV |
| | 1 | ATTN: SAMEN-H |
| | 1 | ATTN: District Library |
| Savannah | 1 | ATTN: Library |
| | 1 | ATTN: Planning Branch |
| Wilmington | 1 | ATTN: Engineering Division |
| SPD | 1 | ATTN: Chief, Technical Engineering Branch |
| Los Angeles | 1 | ATTN: Library<br>Abstract of report:<br>Mr. Robert S. Perkins<br>Mr. Albert P. Gildea<br>Mr. Frederick R. Cline<br>Mr. A. Robles, Jr.<br>Mr. A. V. Potter |
| Sacramento | 2 | ATTN: District Library |
| | 1 | ATTN: Hydrologic Engineering Center |
| San Francisco | 2 | ATTN: Library |
| SWD | 1 | ATTN: Library |
| Albuquerque | 2 | ATTN: Engineering Division Library<br>Abstract of report to Engineering Division Librarian |
| Fort Worth | 1 | ATTN: Librarian |
| Galveston | 1 | ATTN: Librarian |
| | 1 | ATTN: Project Planning Branch |
| Little Rock | 1 | DE |
| | 1 | ATTN: Mr. J. T. Clements, Jr. |
| Tulsa | 1 | DE |
| | 1 | ATTN: Hydraulics Branch |
| DDC | 12 | ATTN: Mr. Myer Kahn |

| | No. of Copies |
|---|---|
| Automatic: | |
| Engineering Societies Library, New York, N. Y. | 1 |
| Library, Div of Public Doc (NO CLASSIFIED REPORTS TO THIS AGENCY), U. S. Govt Printing Office, Washington, D. C. | 1 |
| Library of Congress, Doc Expd Proj, Washington, D. C. | 3 |
| COL C. T. Newton | 1 |
| U. S. Naval Academy, Library, Serial Div, Annapolis, Md. | 1 |
| COL Alex G. Sutton, Jr. (USA, Ret), 2431 Dryden Road, Houston, Texas 77025 | 1 |
| U. S. Department of Commerce, National Oceanic and Atmospheric Administration, National Ocean Survey, Lake Survey Center, 630 Federal Bldg & U. S. Courthouse, Detroit, Michigan 48226 | 2 |
| Library, U. S. Geological Survey, Room 1033, G. S. A. Bldg, 18th & F Streets, N. W. Washington, D. C. 20242 | 1 |
| Exchange Basis: | |
| Foreign: | |
| HOUILLE BLANCHE, Grenoble, France (ENG-63) | 1 |
| The Library, National Research Council, Ottawa, Canada (ENG-17) | 1 |
| The Librarian, Hydraulics Research Station, Wallingford, Berk, England (ENG-46) | 1 |
| The Inst of Civil Engineers, London, England (ENG-47) | 2 |
| Inst of Engineers, Sydney, Australia (ENG-162) | 1 |
| Electricite de France, Chatou, France (ENG-62) | 1 |
| McGill University, Montreal, Quebec, Canada (ENG-271) | 1 |
| Director, Public Works Research Inst, Ministry of Constr, Bunkyo-ku, Tokyo, Japan (ENG-324) | 1 |
| International Commission on Irrigation and Drainage, New Delhi-21, India (ENG-337) | 1 |
| River and Harbour Research Laboratory, Technical Univ of Norway, Trondheim, Norway (ENG-338) | 1 |
| Western Canada Hydraulic Laboratories, Ltd, 1186 Pipeline Road, Port Coquitlam, B. C., Canada (ENG-351) | 1 |
| Federal Bureau for Highway Engineering, Cologne, West Germany (ENG-366) | 1 |
| Director, Institut fur Wasserbau und Wasserwirtschaft, Technische Universitat Berlin, Postfach 320, 1 Berlin 10, Germany (ENG-354) | 1 |
| Laboratorio de Hidraulica, Escola Politecnica, Universidade de Sao Paulo, Sao Paulo, Brazil (ENG-357) | 1 |
| National Mechanical Engineering Research Institute (NMERI), P. O. Box 395, Pretoria, South Africa (ENG-371) | 1 |
| Domestic: | |
| APPLIED MECHANICS REVIEWS, San Antonio, Tex. | 2 |
| Dept of Civil Engineering, The Univ of Arizona, Tucson, Ariz. | 1 |
| Head Professor, Civil Engineering Department, Auburn University, Auburn, Ala. | 1 |
| Library, Bureau of Reclamation, Denver, Colo. | 1 |
| Engrg Lib, Institute of Eng Research, Univ of California, Berkeley, Calif. | 1 |
| Central Records Library, Dept of Water Resources, Sacramento, Calif. | 1 |
| W. M. Keck Lab of Hydraulics & Water Resources, Calif. Inst of Tech, Pasadena, Calif. | 1 |
| Associate Head, Engineering Division, Case Institute of Technology, University Circle, Cleveland, Ohio | 1 |
| Central Serial Record Dept, Cornell Univ Lib, Ithaca, N. Y. | 1 |
| Office of the Editor, Engineering and Industrial Experiment Station, University of Florida, Gainesville, Fla. | 1 |
| Price Gilbert Memorial Library, Georgia Inst of Tech, Atlanta, Ga. | 1 |
| Gordon McKay Library, Harvard Univ, Cambridge, Mass. | 1 |
| Gift & Exchange Div, Univ of Illinois Library, Urbana, Ill. | 1 |
| Library, Iowa State Univ of Science & Tech, Ames, Iowa | 1 |
| Engrg Experi Sta, Kansas State Univ of Agric & Applied Science, Manhattan, Kans. | 1 |
| Documents Room, Univ Lib, Univ of Kansas, Lawrence, Kans. | 1 |
| Fritz Engineering Lab, Lehigh Univ, Bethlehem, Pa. (also 1 to Chief, Hydraulics Div) | 2 |
| Hydrodynamics Laboratory, MIT, Cambridge, Mass. | 1 |
| Engrg Librarian, Univ of Michigan, Ann Arbor, Mich. | 1 |
| Engineering & Ind Research Sta, State College, Miss. | 1 |
| College of Engineering, Univ of Missouri, Columbia, Mo. | 1 |
| Univ of Missouri, School of Mines & Metallurgy, Rolla, Mo. | 1 |
| Associate Director, Dept of Environmental and Water Resources Engineering, Vanderbilt University, Nashville, Tenn. | 1 |
| New York Univ, ATTN: Engrg Lib, University Heights, Bronx, N. Y. | 1 |
| Dept of Engrg Research, North Carolina State College, Raleigh, N. C. | 1 |
| Dept of Civil Engrg, Technological Inst, Northwestern Univ, Evanston, Ill. | 1 |
| Main Library, Ohio State Univ, Columbus, Ohio | 1 |
| Serials Acquisitions, Univ of Iowa Libraries, Iowa City, Iowa | 1 |
| Engrg Experiment Sta, Oregon State Univ, Corvallis, Oreg. | 1 |

Exchange Basis: (Continued)

| | |
|---|---|
| Domestic: (Continued) | |
| Engrg Library, Pennsylvania State Univ, University Park, Pa. | 1 |
| Periodicals Checking Files, Purdue Univ Libraries, Lafayette, Ind. | 1 |
| Engineering Library, Stanford Univ, Stanford, Calif. | 1 |
| Chief Engineer, Tennessee Valley Authority, Knoxville, Tenn. | 1 |
| Mr. Rex Elder, TVA, Norris, Tenn. | 1 |
| Dept of Civil Engrg, Texas A&M Univ, College Station, Tex. | 1 |
| The Trend in Engineering, 14 Loew Hall, University of Washington, Seattle, Wash. | 1 |
| Albrook Hydraulic Lab, Washington State Univ, Pullman, Wash. | 1 |
| Engrg Lib, Univ of Wisconsin, Madison, Wis. | 1 |
| College of Engrg, University of Arkansas, Fayetteville, Ark. | 1 |
| Lorenz G. Straub Memorial Library, St. Anthony Falls Hydraulic Laboratory, Univ of Minn., Minneapolis, Minn. | 1 |
| Professor Sandor Popovics, Northern Arizona University, Box 5753, Flagstaff, Arizona | 1 |

Consultants:

| | |
|---|---|
| Dr. George Bugliarello | 1 |
| Dr. A. T. Ippen | 1 |
| Professor J. W. Johnson | 1 |
| Dr. John F. Kennedy | 1 |
| Dr. Vito A. Vanoni | 1 |
| Dr. Ray B. Krone | 1 |
| Dr. Basil W. Wilson | 1 |

Send with bill:

| | |
|---|---|
| Librarian, Dept of Public Works, Sydney, Australia | 1 |

Abstract of Report:

Princeton University River & Harbor Library, Princeton, N. J.
Duke University Library, Durham, S. C.
Princeton University Library, Princeton, N. J.
Louisiana State University, Baton Rogue, La.
The Johns Hopkins University Library, Baltimore, Md.
University of Kansas Libraries, Lawrence, Kans.
Laboratorio Nacional de Engenharia Civil, Lisboa, Portugal
Dept of Civil Engr, Univ of Tokyo, Bunkyo-ku, Tokyo, Japan
Mr. Shigematsu Suzuki, Civil Engr Res Inst, Hokkaido Development Bureau, Nakanoshima, Sopporo, Japan
Commandant, USAREUR Engineer-Ordnance School, APO New York
Mr. J. C. Harrold, 11720 Edgewater Dr., Lakewood, Ohio 44107
University of Arkansas, Reference Dept, University Library, Fayetteville, Ark.
Water Information Center, Inc., Port Washington, N. Y.
Duke University, College of Engineering Library, Durham, N. C.
Serials Record, Pennsylvania State University, University Park, Pa.
Northeastern Forest Experiment Station, Forestry Sciences Lab, Morgantown, W. Va.
Mrs. Virginia K. Blatcher, U. S. Geological Survey, Washington, D. C.
Director, Instituto di Idraulica e Construzioni Idrauliche del Politecnico di Milano, Milano, Italy
Director, Coastal Studies Institute, Geology Building, Louisiana State University, Baton Rogue, La.
Commanding Officer & Director, U. S. Naval Civil Eng Lab, Port Hueneme, Calif. 93041
ATTN: Code L31
Mr. L. A. Pardee, City Engineer, Department of Public Works, Bureau of Engineering, Los Angeles, Calif. 90012

Announcement of Availability by Public Affairs Office:

CIVIL ENGINEERING
THE MILITARY ENGINEER
ENGINEERING NEWS-RECORD

Unclassified

Security Classification

## DOCUMENT CONTROL DATA - R & D

*(Security classification of title, body of abstract and indexing annotation must be entered when the overall report is classified)*

1. ORIGINATING ACTIVITY *(Corporate author)*

U. S. Army Engineer Waterways Experiment Station
Vicksburg, Mississippi

2a. REPORT SECURITY CLASSIFICATION

Unclassified

2b. GROUP

3. REPORT TITLE

HOWELL-BUNGER VALVE VIBRATION, SUMMERSVILLE DAM PROTOTYPE TESTS

4. DESCRIPTIVE NOTES *(Type of report and inclusive dates)*

Final report

5. AUTHOR(S) *(First name, middle initial, last name)*

Frank M. Neilson

| 6. REPORT DATE | 7a. TOTAL NO. OF PAGES | 7b. NO. OF REFS |
|---|---|---|
| September 1971 | 86 | 26 |

| 8a. CONTRACT OR GRANT NO. | 9a. ORIGINATOR'S REPORT NUMBER(S) |
|---|---|
| b. PROJECT NO. | Technical Report H-71-6 |
| c. | 9b. OTHER REPORT NO(S) *(Any other numbers that may be assigned this report)* |
| d. | |

10. DISTRIBUTION STATEMENT

Approved for public release; distribution unlimited.

| 11. SUPPLEMENTARY NOTES | 12. SPONSORING MILITARY ACTIVITY |
|---|---|
| | U. S. Army Engineer District<br>Huntington, West Virginia |

13. ABSTRACT

This report presents data obtained during prototype tests concerned with the vibration of a 106-3/4-in.-diam Howell-Bunger valve at Summersville Dam, Gauley River, W. Va. Prototype measurements include both dynamic and time-averaged values of pressures in the flow and strain at locations on the valve structure. Transverse, vertical, and peripheral accelerations were measured at the downstream end of the valve cone. The data were recorded simultaneously on analog magnetic tape and on oscillograph charts. Data reduction was by scaling the oscillograph traces and by using electronic analog equipment to perform linear spectral density, amplitude density, and cross-correlation analyses on the magnetic tape data. The results include information on (a) discharge characteristics of the Summersville outlet works, (b) evaluation of the nature of the pressure fluctuations in the flow, and (c) evaluation of the nature of the vibration (including approximate natural frequency values) of the valve at the strain gage and accelerometer locations. The primary conclusion regarding the vibration is that the significant strain fluctuations are caused by low-frequency pressure fluctuations buffeting the valve. These frequencies are well below the natural frequencies of the structure.

DD FORM 1 NOV 68 1473 REPLACES DD FORM 1473, 1 JAN 64, WHICH IS OBSOLETE FOR ARMY USE.

Unclassified

Security Classification

| 14. KEY WORDS | LINK A | | LINK B | | LINK C | |
|---|---|---|---|---|---|---|
| | ROLE | WT | ROLE | WT | ROLE | WT |
| Howell-Bunger valves | | | | | | |
| Prototypes | | | | | | |
| Summersville Dam | | | | | | |
| Valves | | | | | | |
| Vibration | | | | | | |
| Water flow | | | | | | |